



Cite this: *Chem. Soc. Rev.*, 2023, 52, 6031

Received 8th February 2023

DOI: 10.1039/d2cs00765g

rsc.li/chem-soc-rev

Development of flow battery technologies using the principles of sustainable chemistry

Ziming Zhao,^{†^ab} Xianghui Liu,^{†^a} Mengqi Zhang,^{†^a} Leyuan Zhang,^c Changkun Zhang,^{†^a} Xianfeng Li^{†^a} and Guihua Yu^{†^ac}

Realizing decarbonization and sustainable energy supply by the integration of variable renewable energies has become an important direction for energy development. Flow batteries (FBs) are currently one of the most promising technologies for large-scale energy storage. This review aims to provide a comprehensive analysis of the state-of-the-art progress in FBs from the new perspectives of technological and environmental sustainability, thus guiding the future development of FB technologies. More importantly, we evaluate the current situation and future development of key materials with key aspects of green economy and decarbonization to promote sustainable development and improve the novel energy framework. Finally, we present an analysis of the current challenges and prospects on how to effectively construct low-carbon and sustainable FB materials in the future.

1. Introduction

1.1. Renewable energy storage and FBs

Decarbonization of the energy system is an inevitable trend to achieve energy sustainable development and tackle climate change. The use of clean energy, renewables in particular, is

an important route for energy transformation.¹ On the other hand, it is a consensus that the intermittency, volatility and cyclicity of renewables need to be balanced by energy storage devices, especially with a long duration time. For this purpose, numerous methods including physical and chemical energy storage have been proposed,^{2–4} among which flow batteries (FBs) garner much interest mainly due to attractive features of high safety, flexible design, long cycle life, and not restricted by the geographical environment compared to other technologies such as pumped hydroelectric and thermal energy storage systems.⁵

A typical FB system consists of an electrochemical cell stack, electrolytes, and pumps, which are connected by pipelines (Fig. 1). The electrochemical cell is mainly composed of a

^a Division of Energy Storage, Dalian National Laboratory for Clean Energy, Dalian Institute of Chemical Physics, Chinese Academy of Sciences, 457 Zhongshan Road, Dalian 116023, China. E-mail: zhangchk17@dicp.ac.cn, lixfanfeng@dicp.ac.cn

^b University of Science and Technology of China, Hefei 230026, China

^c Materials Science and Engineering Program and Department of Mechanical Engineering, The University of Texas at Austin, Austin, Texas 78712, USA. E-mail: ghyu@austin.utexas.edu

† These authors contributed equally to this work.



Ziming Zhao

Ziming Zhao is a PhD student at Changchun Institute of Applied Chemistry, Chinese Academy of Sciences. He is presently studying at the Division of Energy Storage, Dalian Institute of Chemical Physics as an academic visitor. His work involves the research of organic redox-active materials and ion conductive membranes for flow batteries.



Xianghui Liu

Xianghui Liu is a postdoctoral fellow at the Chinese Academy of Sciences, Dalian Institute of Chemical Physics. After recently receiving her PhD degree (2021) in physical chemistry at the Chinese Academy of Sciences, Dalian Institute of Chemical Physics, with a special interest in organic chemistry, she is currently focused on the design and synthesis of organic redox-active materials for organic flow batteries.

membrane, electrodes, and bipolar plates. Electrolytes containing redox species are pumped into the stack anode and cathode chambers separated by the membrane and subsequently flow through the porous electrode where electron transfer reactions occur on the electrode surface and finally flow back to the tanks. Energy is continuously generated and stored while cycling. The whole system is managed by several control modules including a battery management system (BMS), a power conversion system (PCS), and an energy management system (EMS).

Based on the unique structure of an FB system, the power of the FB system is determined by the effective area of the electrodes and the number of cells in a stack, whereas the energy storage capacity is determined by the concentration and volume of the redox species in electrolyte, therefore, the power and energy capacity of an FB system can be independently designed and regulated. Also, the anolyte and catholyte are stored separately in two tanks, which can reduce the risk of self-discharge during battery storage. Besides, the modular structure facilitates access and replacement of faulty components,

extending service life and improving cost-effectiveness over the life cycle. In addition to the representative commercialized vanadium FB (VFB) technology, the possibility of more and more novel FB technologies has emerged as an exciting opportunity to expand upon. Electrolyte, membrane, and electrode as the key materials have a significant effect on the electrochemical performance of a FB system (energy density, power density, Coulombic efficiency (CE), voltage efficiency (VE), energy efficiency (EE) and durability)⁶ (Fig. 2).

1.2. Sustainability of FB key materials

Undoubtedly, a low-carbon sustainable grid with advanced energy storage systems should also be part of the electricity decarbonization. To be an inseparable part of a future low-carbon sustainable grid, the low-carbon and sustainable FB technology must be considered. However, the relationship between FBs and sustainable energy development from the perspective of a green economy and low carbon emissions is rarely covered in recently published reviews, and most reviews mainly summarize the progress in the key materials and



Mengqi Zhang

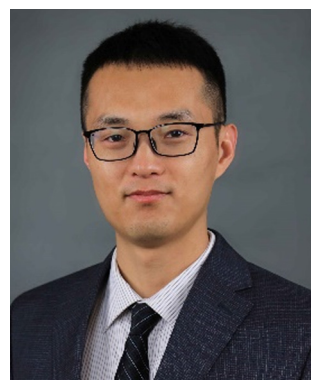
Mengqi Zhang received her bachelor's degree from Huazhong University of Science and Technology in 2020. She is currently pursuing a PhD degree in Dalian Institute of Chemical Physics (DICP), Chinese Academy of Sciences. Her research is mainly focused on molecular engineering of redox-active organic molecules for aqueous organic flow batteries.



Leyuan Zhang

and catalysts for energy storage applications.

Leyuan Zhang received his BS degree from Zhejiang University in 2012 and then his Master's degree from the University of Chinese Academy of Sciences in 2015. He completed his PhD degree at the University of Texas at Austin under the supervision of Prof. Guihua Yu in 2020. Now, he is working as a postdoctoral fellow at the University of California, Los Angeles. His research interests mainly focus on designing organic materials



Changkun Zhang

Changkun Zhang is a full professor at Dalian Institute of Chemical Physics, Chinese Academy of Science. He was a postdoctoral researcher at the University of Texas at Austin from 2016 to 2020. He received his BS in Chemical Engineering and Technology from Harbin Engineering University and PhD in Chemical Engineering from Dalian Institute of Chemical Physics, Chinese Academy of Science. His work is focused on novel key materials for next-generation energy storage, including redox-active molecules and electrolyte microstructures.



Xianfeng Li

and the industrial development and application demonstration of flow batteries.

Xianfeng Li received his PhD degree in Polymer Chemistry and Physics from Jilin University. He was appointed as a full professor at Dalian Institute of Chemical Physics (DICP), Chinese Academy of Science, in 2012. He is currently the vice-director of DICP and the head of the Energy Storage Division. His research interests include key materials and core technologies of flow batteries, innovation battery technologies,

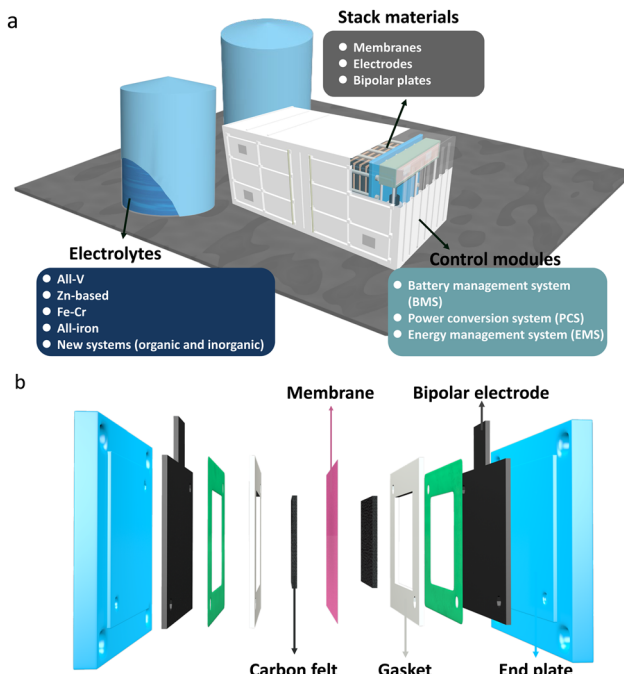


Fig. 1 (a) Schematic illustration of FB technology. (b) Single cell structure.

provide prospects for their future development.^{5–11} A triangular approach consisting of economic, social, and environmental parameters is used to assess the sustainability of energy projects after the 2002 Johannesburg conference.¹² Based on this, Kolagar *et al.* considered a five-dimensional approach (technic, economy, environment, society and politics) for assessing the sustainability of renewable energy sources as a strong and reliable way of managing the energy sector.¹³ In this review, we mainly focus on the sustainability of FB key materials when considering the current stage of FB development. We will provide a comprehensive analysis of state-of-the-art progress in FBs from the viewpoints of technological and environmental sustainability, in terms of the design, production, application,



Guilhua Yu

Guilhua Yu is the Temple Foundation Endowed Professor of Materials Science and Mechanical Engineering at the University of Texas at Austin. He received his BS degree with the highest honor from USTC, PhD from Harvard University, followed by postdoc research at Stanford University. His research has been focused on the rational design and synthesis of nanoarchitected polymeric materials and hybrid organic-inorganic nanomaterials, the fundamental understanding of their chemical and physical properties, and an exploration of their technologically important applications in the fields of environment, energy, and sustainability.

fundamental understanding of their chemical and physical properties, and an exploration of their technologically important applications in the fields of environment, energy, and sustainability.

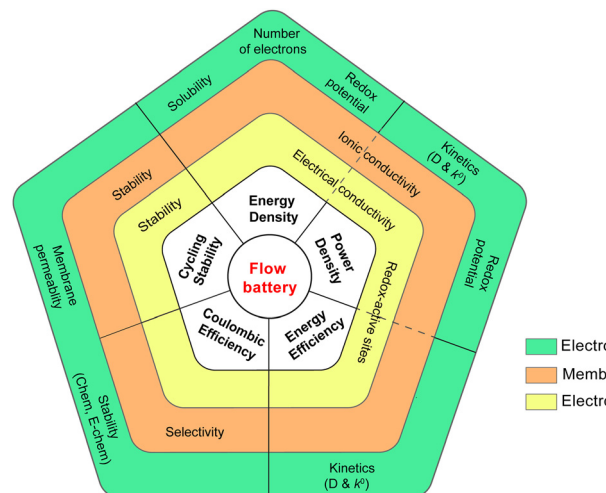


Fig. 2 The evaluation criteria, components, and performance parameters for the development of FB.

and recycling of the key components. The technological sustainability is assessed by the aspects of performance, preparation/process and recovery/regeneration, while the environmental sustainability is assessed by the aspect of emission/waste disposal (Fig. 3). The performance of key materials is a prerequisite for practical application and details of the performance evaluation parameters involved are shown in Fig. 2.

The evaluation of sustainable preparation and processes focuses on the low carbon and economy of key materials which mainly refer to the upstream and downstream production activities of materials production, reliable supply, and affordability of materials. This involves whether the extraction and processing (mineral resource development, natural product extraction *etc.*) is green, environmentally-friendly, economical, and safe. Environmental sustainability in Fig. 3 mainly includes the issues of waste treatment in production. For example, liquid wastes such as acids and alkalis in the mining and processing of inorganic redox species, large solvent volumes in the preparation of organic electrolytes and membrane materials as well as emissions of greenhouse gases (SO_2 , NO_x , and CO_2) during the high-temperature treatment of electrode materials.

The recycling or regeneration of materials emphasizes the recovery capability after simple processing when critical materials lose all or part of their performances, alternatively, they can be recycled, processed, and retreated to gain other values. For example, some of the decayed redox species can regain redox activity through chemical or electrochemical methods, or the electrolyte/membrane can be recovered, and the useful elements can be extracted for other uses.

Finally, waste released during operation and at the end of life of FBs should ensure that disposal or emissions with cumulative potential are not allowed to accumulate at a rate that exceeds the natural removal or absorptive capacity of ecosystems, which will bring high load to the environment.¹²

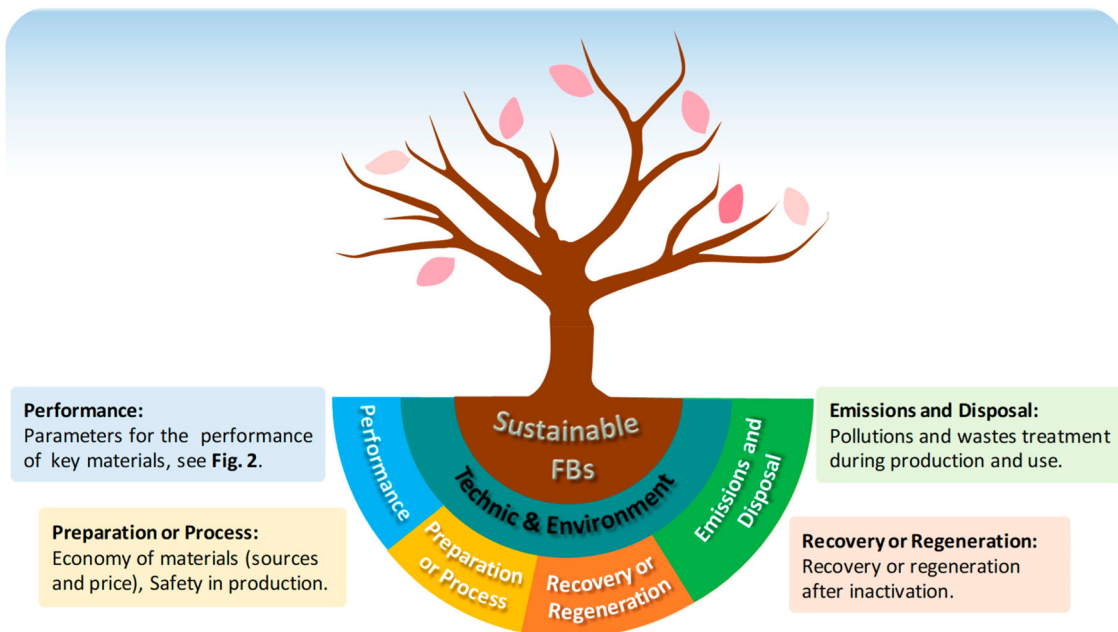


Fig. 3 Sustainability of FBs and evaluation parameter details.

Based on the above discussions, we provide 9 principles, as summarized in Table 1, to evaluate the sustainability of FB technology.^{14–16}

In this review, we will analyse the specific evaluation criteria for the inorganic and organic redox species, advanced membranes, and electrode materials. We mainly focus on the progress in the aqueous system, although organic solvents expand the voltage window and promote the theoretical energy

density of FB, all-organic systems still confront some critical issues including low solution ionic conductivity, lack of high-performance and stable membranes, and stable redox-active molecules (RAMs), and the progress lags behind the aqueous system. Some novel FB systems have also been discussed as a possible outlet for a sustainable battery future. Finally, the perspective on FBs towards the goals of low-carbon and sustainable energy storage systems (ESS) is provided as well.

Table 1 Principles of sustainable chemistry for FB technology

| No. Principles | Description |
|---------------------------------|--|
| P1 Stability and lifetime | Stability, the most essential parameter of FB materials, directly determines the battery lifetime. The performance decay in any part of FBs will shorten the FB lifetime. Some possible factors such as pH, temperature, oxygen contamination, etc. may negatively affect the stability of FB materials thus shortening battery lifetime. |
| P2 High atom economy | The synthesis route for organic redox-active molecules should be designed to maximize the incorporation of all reagents involved in the reaction into the target product, together with a high yield and only one or a few reaction steps. |
| P3 Renewable sources | Natural and innocuous organic materials would be the priority as FB feedstocks, which do not require complex modification. |
| P4 Simple preparation/synthesis | From lab-scale preparation to industrial production, the synthesis methodology should be simplified as much as possible, especially, the separation and purification should be slimmed down based on reaching the target purity. Some unnecessary or complicated steps should be skipped or replaced. |
| P5 Safer chemicals | Low/non-toxic raw materials, solvents, intermediates, catalysts, and products are preferred. In contrast to volatile, harmful organic solvents, high boiling point solvents or water are the priority especially for large-scale production. |
| P6 Safer production | The preparation process should meet the safety requirements. If possible, the synthetic process should be carried out under mild conditions and avoid high-risk operations, such as high temperature, high pressure, explosive, concentrated acid/alkali, and other corrosive reagents. |
| P7 Waste disposal | Innocuous emission and waste disposal are critical to human health and the environment. Sewage, toxic vapors and solid waste will cause serious damage to the atmosphere and hydrology. On-demand deconstruction, detoxification and harmlessization are important for industrial production, and further recycling, and regeneration will be the ultimate goals of sustainable development. |
| P8 Low carbon | FB technology can greatly improve the utilization rate of renewable energy to realize carbon emission reduction, but the processing and production of battery materials may face high energy consumption. Low carbon footprint (such as the utilization of renewable energy and low energy consumption) is of great significance to construct a green economy and carbon-neutral society. |
| P9 Low cost | The cost issue is a comprehensive analysis of each procedure of key components. Cost-effectiveness involves low-cost raw materials and reagents, high yields, simple reactions, easy purification, and feasible waste disposal. |

2. Redox species

2.1 Sustainable design in traditional inorganic redox species

Generally, inorganic ions with multiple valence changes can serve as redox active materials. In this section, the widely studied traditional inorganic FB, such as VFB, zinc-based FB, all-iron FB, and some new systems are evaluated from the viewpoint of technological and environmental sustainability.

2.1.1 Performance

VFB. VFBs employ $\text{V}^{2+}/\text{V}^{3+}$ and $\text{VO}^{2+}/\text{VO}_2^+$ redox species as the anolyte and catholyte, respectively, with an open circuit voltage (OCV) of 1.26 V. The $\text{V}^{2+}/\text{V}^{3+}$ reaction is a simple one-electron transfer reaction. The $\text{VO}^{2+}/\text{VO}_2^+$ reaction is a multi-step reaction involving an oxygen transfer reaction before or after an electron-transfer step, hence the kinetics of $\text{VO}^{2+}/\text{VO}_2^+$ is slower than that of $\text{V}^{2+}/\text{V}^{3+}$.^{17–19} The surface area and functional group of electrode materials significantly influence the kinetics of vanadium redox species, which we will discuss in the following section. The solubility of V(II), V(III) and V(IV) ions increases along with the decreasing acid concentration and increasing temperature, while V(V) ions exhibit opposite trends.²⁰ The most commonly used concentration is around 1.7 M in H_2SO_4 solution and the energy density of VFB is $\sim 25 \text{ W h L}^{-1}$.²¹ The V(II), V(III) and V(IV) ions tend to precipitate when the temperature is below 10 °C, while V(V) ions are stable at low temperature, but prone to precipitate in the form of V_2O_5 above 40 °C, which limits the operating temperature in the range of 10–40 °C. To improve the temperature stability of V(V), mixed acids (H_2SO_4 and HCl) were employed, changing the solvation structure of vanadium ions.²² The solubility of vanadium reached 2.5 M and the operating temperature was extended to –5 to 50 °C.²³ The mixed-acid strategy has been adopted by several companies.

In the past few decades, great progress has been made in VFBs. In the lab scale, the VFB stably cycled for over 20 000 cycles at 600 mA cm^{-2} with an EE of 80.43% by optimizing the membrane, electrode and flow field, which simultaneously reduced the ohmic resistance and boosted the transport of electrolytes.²⁴ In actual application, the current density of the VFB system has been significantly improved from $60\text{--}80 \text{ mA cm}^{-2}$ to $200\text{--}300 \text{ mA cm}^{-2}$ when EE is not less than 80%.²⁵

Thanks to the long lifespan (up to 20–30 years), no cross-contamination and recyclability, VFBs have been extensively demonstrated all over the world. Many companies are engaged in the commercialization of VFBs, including Sumitomo Electric Industries (SEI), Dalian Rongke Power Corp., Prudent Energy, Australian Vanadium Ltd, CellCube, VRB Energy, Invinity Energy Systems, Singapore's VFlowTech, and Largo Clean Energy. SEI installed a 4 MW/6 MW h VFB in Hokkaido to smooth the output power of 30 MW wind farm in 2005 and a 15 MW/60 MW h VFB energy storage power station in 2016, which has stably run for 6 years.²⁶ Dalian Institute of Chemical Physics, Chinese Academy of Sciences (DICP, China) has been committed to the research on VFB materials and stack designs. A 5 MW/10 MW h VFB station on a 50 MW wind farm in Liaoning Province was built by DICP-Rongke Power in 2012 and

the station has now been operating for more than 10 years.²⁵ A 200 MW/800 MW h national VFB demonstration project is being built in Dalian, and the first phase, a 100 MW/400 MW h system, was successfully connected to the Dalian grid in 2022.

Iron–chromium FB (ICFB). In ICFBs, $\text{Fe}^{2+}/\text{Fe}^{3+}$ and $\text{Cr}^{2+}/\text{Cr}^{3+}$ redox species are dissolved in HCl as the catholyte and anolyte, respectively. The redox kinetics of $\text{Cr}^{2+}/\text{Cr}^{3+}$ is more sluggish than that of $\text{Fe}^{2+}/\text{Fe}^{3+}$. Catalysts, such as Tl, Bi, Au/Pb and high temperature (above 50 °C) are required to accelerate the $\text{Cr}^{2+}/\text{Cr}^{3+}$ reaction in ICFBs.^{27–30} However, high temperature reduces the selectivity of the membrane, resulting in the severe redox species crossover. Mixed electrolytes compromising the solubility are employed in both catholyte and anolyte to alleviate the crossover. The optimized concentration of the mixed electrolytes is 1.0 M CrCl_3 , 1.0 M FeCl_2 , and 3.0 M HCl with an energy density of 15.8 W h L^{-1} when considering the influence of viscosity, conductivity and electrochemical activity.^{6,31} On the other hand, the severe hydrogen evolution reaction (HER) due to the low redox potential of $\text{Cr}^{2+}/\text{Cr}^{3+}$ (–0.41 V vs. SHE) also causes an imbalance of the state of charge between the catholyte and anolyte, thus increasing the maintenance frequency.

The ICFB, first proposed in the 1970s at NASA, has been well-studied benefiting from the low cost and low toxicity of redox species. In recent years, progress has been made in the lab and scale-up of ICFBs. Zhao *et al.* adopted an interdigitated flow field to facilitate the even distribution of catalyst and mass transport of redox species. The ICFB demonstrated a capacity decay rate of 0.5% per cycle over 90 cycles with an EE of 80.7% at 320 mA cm^{-2} and 65 °C.³² Additionally, the operating current density can reach up to 480 mA cm^{-2} with an EE of 80.5% at 65 °C by optimizing the membrane thickness, electrode compression ratio, electrode pre-treatment and catalyst loading.³³ In practical application, NASA first developed 1 kW/13 kW h ICFB stacks between 1973 and 1982.³⁴ Then Japan successfully developed 10 kW and 66 kW ICFB systems in 1984 and 1986, respectively. In 2014, EnerVault company finished the world's first 250 kW/1 MW h ICFB energy storage power station in California.⁵

Zinc–bromine FB (ZBFB). ZBFB is a promising technology for distributed electrochemical energy storage due to the advantages of high theoretical energy density and low cost. Benefiting from the high solubility of ZnBr_2 (>15 M) and a high OCV of 1.84 V, the theoretical energy density of ZBFB reaches up to 440 W h kg^{-1} .³⁵ The practical energy density is $\sim 65 \text{ W h L}^{-1}$ as allowable areal capacity is not high enough to ensure cycling stability and high CE.³⁶ To address this issue, considerable studies focus on the electrolyte optimization (bromine complexing agents) and electrode materials design to induce uniform zinc deposition morphology.^{37–40} The concentration of ZnBr_2 significantly influenced the nucleation modes (Fig. 4a). Dense blocky Zn was formed *via* instantaneous nucleation in concentrated electrolyte ($\geq 0.4 \text{ M}$), while Zn is mossy due to progressive nucleation in dilute electrolyte ($\leq 0.3 \text{ M}$).⁴¹ In addition, the self-discharge resulting from the

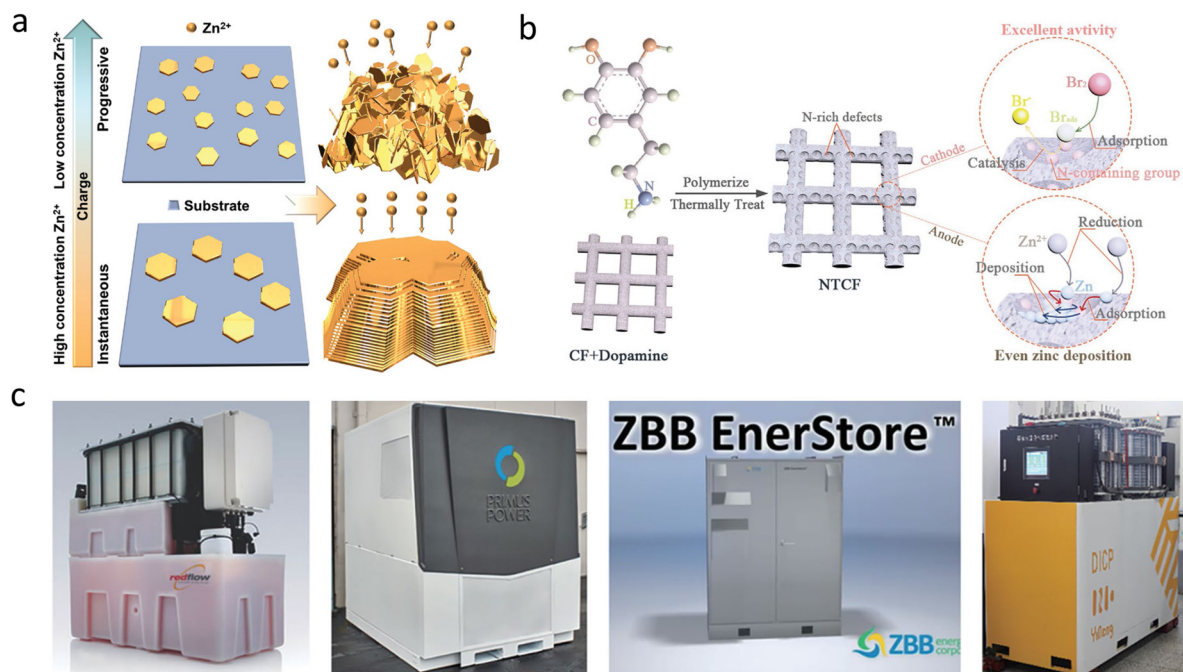


Fig. 4 (a) Schematic diagram of Zn deposition at decreasing concentrations. (b) NTCF electrode with abundant N-rich defects for high-power density and long-cycle life ZBFBs. (c) The ZBFB system developed by different institutions. Adapted with permission from ref. 41. Copyright 2022 The Royal Society of Chemistry. Ref. 47. Copyright 2021 Wiley-VCH GmbH. ref. 48. Copyright Energy Storage Science and Technology.

high diffusivity and sluggish kinetics of bromine tends to decrease the CE, EE and operating current density of ZBFBs. Therefore, various bromine complexing agents are introduced to inhibit the diffusion of bromine and electrode materials with high electrocatalytic activity and Br₂-complex-entrapping capability are extensively studied.^{42–46} Lu *et al.* designed a multi-functional N-rich defect carbon felt-based electrode (NTCF), which not only facilitated the kinetics of Br₂/Br⁻, but also induced uniform zinc deposition (Fig. 4b).⁴⁷ The N-rich defects provided more active reaction sites and enhanced the absorption ability of bromine and zinc atoms. The current density of ZBFB can reach up to 180 mA cm⁻² with a high EE of ~63%. Additionally, a high areal capacity of 66.6 mA h cm⁻² with a high EE of 75.91% at 80 mA cm⁻² can be achieved, which are the highest values reported for ZBFBs. Regarding industrial application, Redflow Ltd (Australia), ZBB (USA), Primus Power (USA), Zbest Power Co. Ltd (China), etc. have made important progress. As shown in Fig. 4c, Redflow, Primus Power and ZBB have achieved the industrialization of ZBFBs. The operating current density is low (10–20 mA cm⁻²), limiting the power density. In 2017, DICP developed a 5 kW Zn-Br single FB system with a high areal capacity of 140 mA h cm⁻². Recently, a 30 kW h ZBFB system was also developed, which can be applied to distributed energy and household energy storage.⁴⁸

Zinc-iron FB (ZIFB). ZIFBs can be classified into alkaline ZIFBs (AZIFBs) and neutral ZIFBs. AZIFBs use Zn(OH)₄²⁻/Zn and Fe(CN)₆⁴⁻/Fe(CN)₆³⁻ as redox species with an OCV of 1.58 V. Both Zn(OH)₄²⁻/Zn and Fe(CN)₆⁴⁻/Fe(CN)₆³⁻ exhibit fast redox kinetics, enabling a high operation current density.

The solubility of K₄Fe(CN)₆ or Na₄Fe(CN)₆ (only 0.4 M) in alkaline solution is a limitation for AZIFBs. Recent research found that the solubility of K₄Fe(CN)₆ reached 1.46 M in 0.5 M NaOH by the “diverse ion effect”.⁴⁹ Replacing the cation ion with NH₄⁺ is also an effective strategy (1.91 M for (NH₄)₃[Fe(CN)₆], 1.60 M for (NH₄)₄[Fe(CN)₆]) due to the hydrophilicity of NH₄⁺.⁵⁰ Additionally, a symmetry-breaking strategy was proposed by replacing parts of cyanide ligands with water-soluble bipyridine ligands 2,2'-bipyridine-4,4'-dicarboxylic acid (H₂Dcbpy) to improve the solubility, which can be attributed to the enhanced polarizability and stronger intermolecular interaction with water.⁵¹ Recent years have witnessed conflicting perspectives on the stability of Fe(CN)₆⁴⁻/Fe(CN)₆³⁻. Some studies revealed that the fast capacity decay of the Fe(CN)₆⁴⁻/Fe(CN)₆³⁻ symmetric battery in alkaline solution (pH = 14) mainly resulted from the chemical decomposition *via* cyanide ligand dissociation and subsequent irreversible hydroxylation.^{52,53} While other studies attributed the capacity decay to the electrochemical oxygen evolution reaction (OER)⁵⁴ and electroless oxygen evolution reaction of ferricyanide to ferrocyanide⁵⁵ rather than chemical decomposition.

In the past decade, attention has been focused on designing membranes with high ion conductivity, stability, and selectivity for AZIFBs. Li *et al.* demonstrated the *in situ* vertical growth of a layered double hydroxide membrane (LDH-G) with high hydroxide ion conductivity and precise control of direction ion transport, endowing AZIFB with an EE of 80% at a high operating current density of 260 mA cm⁻² for 800 cycles (Fig. 5a and b).⁵⁶ Moreover, the positive charge on the surface

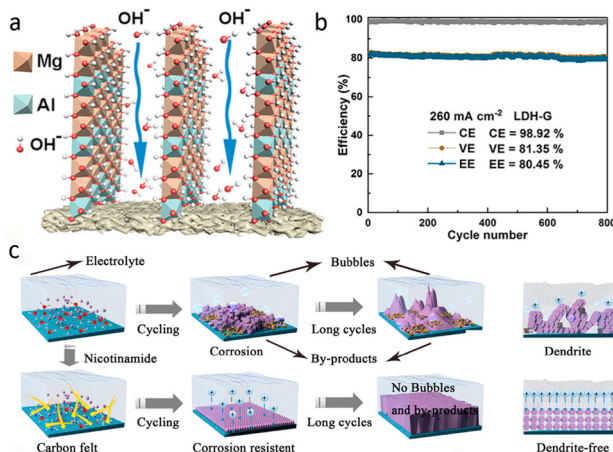


Fig. 5 (a) The directional hydroxide ion transport in the interlayer channels of LDHs on the surface of LDH-G. (b) The cycling performance of AZIFBs assembled with LDH-G at 260 mA cm^{-2} . (c) Illustration of the NAM impact on Zn deposition. Adapted with permission from ref. 56. Copyright 2021 Wiley-VCH GmbH. Copyright ref. 60. 2022 American Chemical Society.

of LDH-G enabled uniform ion distribution and induced a uniform Zn deposition, resulting in a high areal capacity to 240 mA h cm^{-2} at 80 mA cm^{-2} . The same group also demonstrated a pilot-scale roll-to-roll synthesis of SPEEK membrane and scaled up the AZIFB from a single cell to 4 kW stack.⁵⁷ In 2019, a 200 kW/600 kW h AZIFB demonstration project was implemented by Power China based on the technology of the ViZn company, and successfully connected to the grid.

Neutral ZIFBs utilize Zn/Zn^{2+} and $\text{Fe}^{2+}/\text{Fe}^{3+}$ as the anolyte and catholyte, respectively. The concentration of positive electrolyte can reach 2 M, which means a higher energy density than AZIFB. While the irreversible hydrolysis of Fe^{n+} at neutral pH, cross-contamination and zinc dendrites are the main challenges. A neutral ZIFB adopted ZnBr_2 and FeCl_2 as redox species with glycine as an iron complexing agent to suppress hydrolysis and contamination.⁵⁸ The high solubility of electrolyte resulted in a high energy density of 56.3 W h L^{-1} and the strong bonding interaction of iron-glycine and large radius effectively enhanced the cycling performance with an EE of 86.66% at 40 mA cm^{-2} for over 100 cycles. Recently, bromine ions were used to improve the reversibility of zinc plating/stripping by the formation of the lower energy barriers $\text{Zn}[\text{Br}_n(\text{H}_2\text{O})_{6-n}]^{2-n}$ ($1 \leq n \leq 4$, n is integer). The neutral ZIFB with $\text{ZnBr}_2 + \text{KBr}$ as the anolyte and $\text{K}_3\text{Fe}(\text{CN})_6 + \text{KBr}$ as the catholyte delivered an energy density of 26.9 W h L^{-1} and displayed excellent cycling performance over 2000 cycles with an EE of 86.7% at 30 mA cm^{-2} .⁵⁹ Additionally, the synergistic modulation of a nicotinamide molecule on the solvation structure of the Zn^{2+} and electrode interface could induce smooth zinc deposition (Fig. 5c).⁶⁰

All-iron FB (IFB). The first all-iron hybrid FB was pioneered by Hruska and Savinell in 1981, employing the low cost and environmentally friendly $\text{Fe}^{2+}/\text{Fe}^0$ (-0.44 V vs. SHE) and $\text{Fe}^{3+}/\text{Fe}^{2+}$ (0.77 V vs. SHE) redox species as the anolyte and catholyte,

respectively.⁶¹ ESS Corp. has achieved important progress on IFBs recently. In 2021, ESS signed a deal with SDenergy to supply a 2 GW h IFB system by 2026. The poor Fe plating/stripping reversibility in IFB brings about a concern regarding dendrite formation (Fig. 6a).⁶² Additionally, severe HER rises the electrolyte pH due to the more negative potential of $\text{Fe}^{2+}/\text{Fe}^0$ than HER at pH = 0, causing the precipitation of Fe^{3+} in the form of ferric hydroxide at pH > 2. Subsequently, all-liquid IFBs with iron complexes as redox species are widely studied.^{63–65} The stable hexa-coordinate structure of the iron-gluconate complex enabled a battery with a high CE of 99% and EE of 83% at 80 mA cm^{-2} over 950 cycles and long duration energy storage (12, 16 and 20 h per cycle) (Fig. 6c).⁶⁶ While the low solubility of redox active iron complexes limited the energy density of IFBs ($\sim 4 \text{ W h L}^{-1}$).⁶⁷

Overall, among these inorganic-based FBs, VFB is the most widely commercialized type due to its long lifetime and excellent battery performance, while the high original cost and relative low energy density are the main challenges. ICFB faces the same low energy density problem due to the utilization of mixed electrolyte. Moreover, ICFB typically operates at a temperature of 65°C . A thermal management system is necessary. ZBFB has the advantages of high cell voltage and high energy density, while the zinc dendrite and Br_2 corrosion significantly limit the cycling lifespan, areal capacity and operating current density. ZIFB and IFB are also confronted with the low energy density, limited by the low solubility of positive electrolyte and iron complexes, respectively. A detailed comparison of cell voltage, energy density, and cycling life is displayed in Fig. 7. Considering the principles of sustainable chemistry of FB relative to performance of FBs above, VFBs definitely score highest at P1 (stability and lifetime), followed by ICFB, ZBFB, ZIFB and IFB.

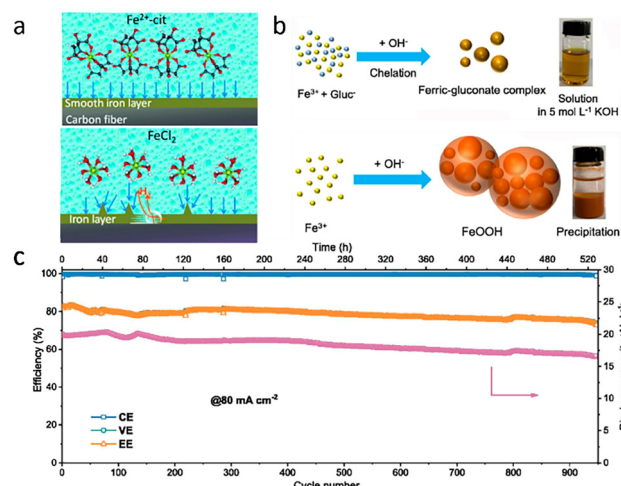


Fig. 6 (a) Redox species of iron complexes that have been tested for FB applications. (b) Schematic diagram of the molecular mechanism for iron-gluconate complexes (in 5 M KOH solution) and FeOOH . (c) Cycling performance of IFB at 80 mA cm^{-2} . Adapted with permission from ref. 62. Copyright 2021 The Royal Society of Chemistry. ref. 66. Copyright 2022 Elsevier B.V.

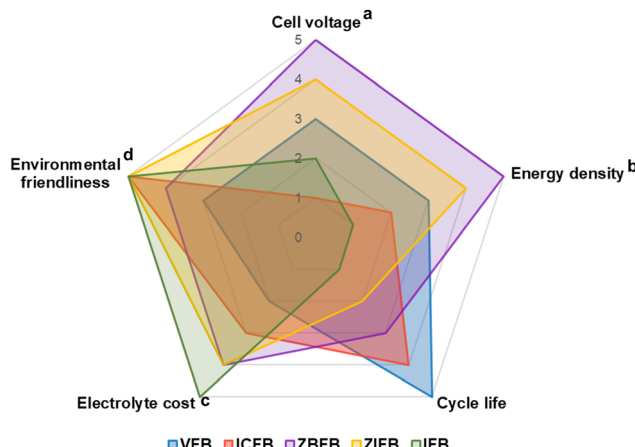


Fig. 7 Itemized comparison of VFB, ICFB, ZBFB, ZIFB and IFB. (a) The cell voltages of VFB, ICFB, ZBFB, ZIFB, and IFB are 1.26 V, 1.18 V, 1.83 V, 1.58 V and 1.2–1.4 V. (b) The energy densities are ~25, ~15.8, ~65, 20–55, and ~4 W h⁻¹. (c) The electrolyte costs are \$122, \$17, \$5, \$5, and \$3.37 per kW h. (d) The environmental friendliness was estimated from the reference.

2.1.2 Preparation

Vanadium electrolytes. High-purity vanadium pentoxide (V_2O_5) is the raw material for preparing VFB electrolyte. Primary vanadium sources are stone coal, vanadium titanomagnetite, oil ash and spent catalyst. More than 40% of V_2O_5 production is produced from vanadium slag, a by-production of vanadium titanomagnetite (Fig. 8). The most commonly used method to produce V_2O_5 from vanadium slag is sodium salt roasting followed by water leaching, ammonium precipitation and calcination.⁶⁸ However, the roasting process inevitably generates toxic waste gas (Cl_2 , HCl , SO_2 and SO_3) and heavy metal tailings of CrO_4^{2-} . 30–50 ton high salinity and ammonia-containing wastewater will be generated for one ton V_2O_5 product, leading to fresh water eutrophication and marine ecosystem damage.⁶⁹ Calcium roasting-acid leaching is then applied to produce V_2O_5 , which can eliminate the emission of waste gas and water.⁷⁰ However, the impurities of heavy metals can also dissolve during the acid leaching process, reducing the product quality. Some novel methods have been developed for the efficient and clean production of V_2O_5 , such as non-salt

roasting,⁶⁹ sub molten salt extraction,⁷¹ directing acid leaching,⁷² and microwave roasting.⁷³ In addition, bioleaching was proposed to extract vanadium by microorganisms through biological oxidation, which features low cost and environmental friendliness.⁷⁴ These novel methods need more research for the future industrial application.

As for the electrolyte preparation, there are mainly two categories: chemical reduction and direct electrolysis.²⁰ The chemical reduction includes the reduction of V_2O_5 to $\text{V}(\text{IV})$ or $\text{V}(\text{III})$ and $\text{V}(\text{II})$ with organic reducing agents such as citric acid, SO_2 , and sodium oxalate. The excess organic molecule contamination during chemical reduction should be considered. The direct electrolysis method involves the electrolysis of vanadium pentoxide powder suspension in acid to produce $\text{V}(\text{III})$ and $\text{V}(\text{IV})$ mixed electrolytes, which avoids the use of reducing agents and poison gas.⁷⁵ In future, it would be highly desirable if the electrolyte can be directly obtained from raw materials while inhibiting the impurity effects on VFB performance (Fig. 8).

Iron and chromium electrolytes. Iron and chromium are earth-abundant elements and mainly exist in chromite. The ICFBs employ mixed electrolytes in both positive and negative electrodes. The electrolytes can be directly produced from the chrome ore containing iron and chromium. The production costs are much lower than the manufacture of pure chemicals as the separation process is unnecessary. The Fe/Cr smelting process mainly proceeds in the smelter, in which reductants (carbon) are used to reduce the chromo ore at a high temperature. Furnace gases comprised of CO gas, volatiles, and water vapour are generated subsequently. The gas purification system is inevitable to minimize the environmental impact.

Zn-Based electrolytes. The zinc smelting process can be divided into pyrometallurgy and hydrometallurgy. The pyrometallurgy method is constrained by a large amount of electrical energy consumption and emission of waste gas containing CO. Above 80% of zinc is produced via hydrometallurgy, involving roasting, calcine leaching, leaching solution purification, net electrodeposition and ingot casting. Zinc leaching residues are classified as hazardous waste, which should be further processed into non-hazardous materials.

Bromine, known as a “marine element”, can be extracted from seawater. The production process of bromine mainly includes water steam distillation and an air blowing method, during which hazardous chemicals, chlorine and sulfuric acid are involved.

Iron-based electrolytes. As for iron smelting, more than 65% of the world's total steel production in 2006 adopted the route of blast furnace/basic oxygen converter, 32% by an electric arc furnace, and less than 3% by open hearth processes.⁷⁶ The blast furnace, as the predominant iron production process, is restricted by some inherent disadvantages, such as dependence on high-quality coke and iron oxide feed stocks, and environmental restriction (CO_2 and SO_2 emission). Some new iron manufacturing processes, such as direct reduction and

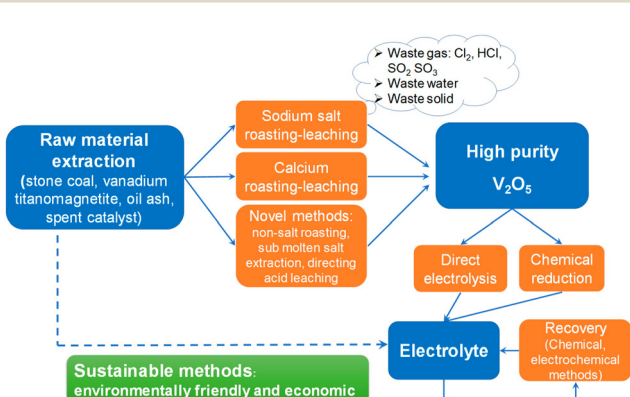


Fig. 8 The diagram of vanadium electrolyte preparation from raw materials.

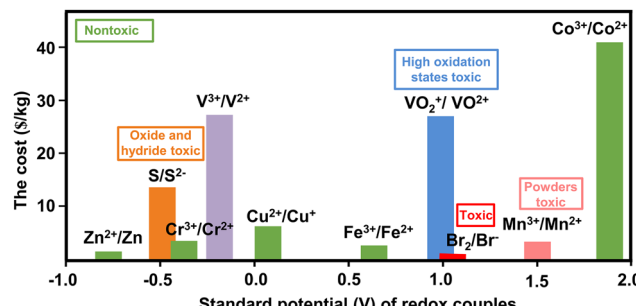


Fig. 9 The standard redox potential, cost, and toxicity of redox species. Adapted with permission from ref. 8.

smelting reduction processes are also developed to reduce CO₂ emission.

Fig. 9 displays the redox potential, cost and toxicity of the most commonly used traditional inorganic redox species.⁸ Among them, vanadium is relatively expensive and potentially toxic in the oxidized form which are the main obstacles for the wide application of VFB. The electrolyte cost is \$122 per kW h, accounting for 53% of the system capital cost.⁷⁷ While zinc, iron, and manganese redox species are highly desirable for their low cost and environmental friendliness. As the price of ferrochromium has been lower than one dollar per pound of chromium content, the cost of active materials of ICFB can be as low as \$17 kW h⁻¹.^{77,78} It should be noted that the high operation temperature increases the ICFB burden in stack cost. The cost of the whole ICFB system is higher than VFB now. Both ZBFB and ZIFB feature a low electrolyte cost of \$5 per kW h.³⁶ All-iron hybrid FB has the lowest electrolyte cost of \$3.37 per kW h due to the utilization of cheap ferrous salt and iron complexing agents.⁶⁶ The scores for electrolyte cost in Fig. 7 are derived from these data.

The preparation of these inorganic electrolytes involves the extraction and processing of mineral resources and fossil resources mainly accompanied by high energy consumption, high carbon emission, and high pollution. In addition, the metal smelting process requires high temperature, concentrated acid, alkali, and other high-risk operation. Toxic gas, wastewater and slag are subsequently generated and cause damage to the atmosphere, hydrology, and soil. Therefore, these FBs definitely score very low at P3 (renewable resource), P4 (simple preparation), P6 (safer production), P7 (waste disposal), and P8 (low carbon).

In future, advanced preparations are required for the sustainability of inorganic electrolytes: (1) improve the production process and technical equipment to increase the utilization rate of mineral resources and replace toxic and harmful auxiliary materials. (2) Strengthen the control of pollution emission. More strict pollutant emission standards should be established to optimize waste management processes. (3) Develop a circular economy and improve the utilization of waste resources. The waste gas, water and slag can be further utilized to improve the comprehensive utilization of waste resources. For example, the

harmless slag can be applied to produce building materials, roadbed materials, etc.

2.1.3 Recovery/regeneration

VFB. During the charging and discharging process, the vanadium ion crossover, water transfer, and hydrogen evolution side reaction lead to the imbalance of electrolyte volume, vanadium concentration and valence. As VFBs use the same element at the positive and negative electrodes, the volume and concentration can be balanced by a periodic full or partial remixing of the positive and negative electrolytes. Full remixing is usually carried out in the fully discharged state to avoid heat generation. Partial remixing can be conducted at any SOC through the overflow tube or connected tube with a valve at the base of two electrolyte tanks, which can be periodically opened to equalize the electrolyte levels.⁷⁹ The valence imbalance can be resolved through chemical or electrochemical methods.^{80–82} Chemical methods involve the addition of reducing agents, such as oxalic acid, ethanol, and H₂ to charged positive electrolyte.⁸⁰ These reductants reduce V(v) to V(iv) with CO₂ and H₂O as products. Electrochemical rebalancing can be achieved through an electrolysis cell, where the reduction of V(v) is coupled with an oxygen evolution reaction.⁸²

The online and offline recovery methods can significantly reduce the environmental impact of vanadium electrolyte preparation and prolong battery lifetime. The recovery process is also eco-friendly, as both chemical and electrochemical methods are simple and can eliminate the emission of harmful gases.

ICFB. The undesired HER causes the loss of protons, increasing the electrolyte pH, and the Fe³⁺ accumulation in the positive electrolyte. NASA proposed an electrochemical rebalance hydrogen–ferric ion cell to electrochemically reduce overconcentrated Fe³⁺, in which the hydrogen was supplied from an external tank (known as “external rebalancing”) or from the parasitic reaction at the negative electrode (internal rebalancing) (Fig. 10a).^{83,84} In the chemical rebalancing method, the Fe³⁺ ions directly react with H₂ on the reactor coated with catalyst. The liquid solution tends to cover the surface of the catalyst and block hydrogen from the catalyst, thus reducing the recovery efficiency (Fig. 10b).⁸⁵

The recovery/regeneration of ZBFB, ZIFB and IFB is rarely reported. The capacity decay of ZBFB caused by crossover of

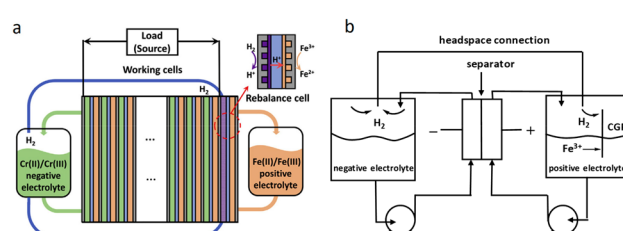


Fig. 10 (a) A schematic diagram of the hydrogen–ferric ion rebalance cell. (b) A schematic diagram of the chemical rebalancing reactor to rebalance the electrolyte. Adapted with permission from ref. 84. Copyright 2017 Elsevier B.V. ref. 85. Copyright 2016 Elsevier B.V.

active species and bromine accumulation can be recovered by remixing the electrolytes and adding reducing agents, such as formic acid. The accumulation of ferric ions of ZIFB and IFB can be recovered through the addition of reducing agents to catholyte.

The recovery of electrolyte plays an important role in reducing the environmental impacts induced by the electrolyte. Especially for VFB, the vanadium electrolyte accounts for the majority of the impacts on global warming (58.7%) and terrestrial acidification (57.6%). It is estimated that when 50% of the electrolyte is recycled, the environmental impacts are reduced significantly with 11.1% reduced global warming and 45.2% reduced terrestrial acidification, because the impacts of reprocessing and purification of electrolyte are negligible compared to the impacts of manufacturing electrolyte.⁸⁶ Moreover, the recovery can extend the lifespan of FBs, thus reducing the carbon emission related to the processing of battery components. Therefore, recovery/regeneration can improve the scores of VFB at P1 (stability and lifetime) and P8 (low carbon).

2.1.4 Environmental sustainability. Life cycle assessment was employed to evaluate the environment impact of VFB production. Without considering the actual operating mode (lifetime, recovering cost *et al.*), Schoenung *et al.* evaluated the environmental impact of three types of FB (VFB, ZBFB, and IFB), based on the data collected from manufacture and the Ecoinvent database on the production phase including raw materials extraction, materials processing, component manufacturing, and product assembly.¹¹ Considering the materials production, energy consumption, resource use, waste treatment, and others of each component of the battery, VFB has a high impact score for global warming potential (184 kg CO₂ eq per kWh), ozone depletion potential, fine particulate matter, acidification potential, fresh water eutrophication and cumulative energy demand (1090 MJ kW⁻¹ h⁻¹) (Fig. 11a). The global warming potential is primarily triggered by the production of electrolyte, which accounts for 72%. However, the proportion would be much lower when taking into account the full life cycle of VFB for its long lifetime and high residual value. Similarly, Martins *et al.* revealed that the vanadium electrolytes made a significant contribution to most of the analyzed environmental categories, such as photochemical ozone formation, acidification potential and mineral, fossil and renewable resource depletion, due to the high potential impacts of extraction and processing of raw materials and extensive distance and duration of transportation from the extraction activities.⁸⁷ In addition, Minke *et al.* displayed the detailed CO₂ emission of electrolyte preparation from ore mining (Fig. 11b).⁸⁸ The provision of electricity for furnace and pre-kiln treatment account for a significant share of CO₂ emission, which can be reduced through the use of renewable energies and of green hydrogen as the reduction agent in the future. Therefore, more studies should be concentrated on the exploration of sustainable methods and the optimization of traditional methods to reduce the environmental impact. While the vanadium electrolyte can be reused, the impacts on acidification, fossil and renewable resource depletion can be significantly reduced by avoiding the

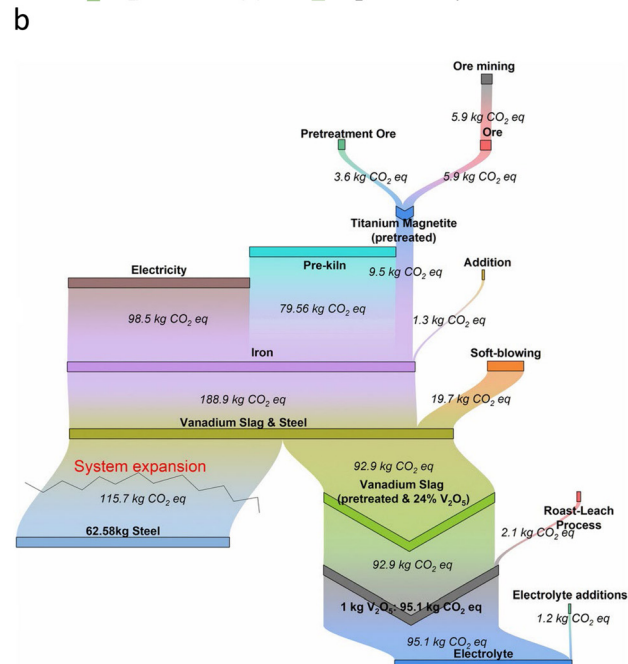
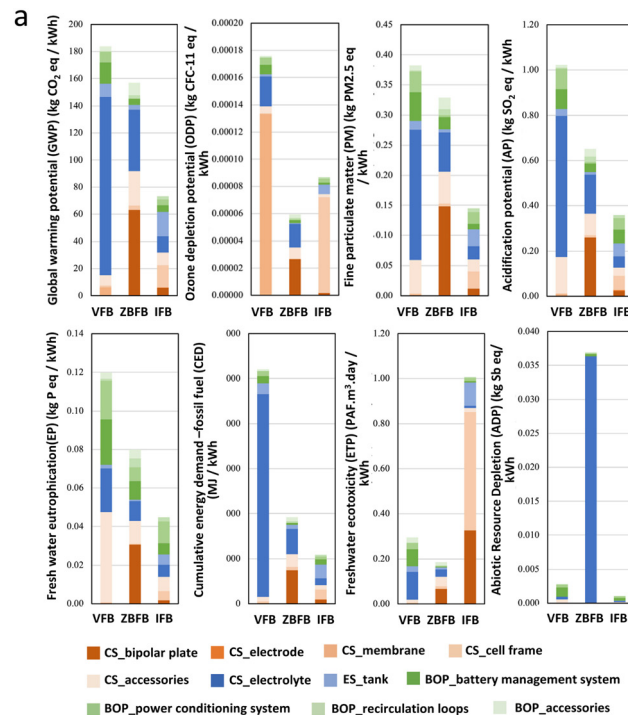


Fig. 11 (a) The potential environmental impact of FB production is shown, as distributed by the battery component. FB types include: VFB, ZBFB, and IFB. FB components include the cell stack (CS), electrolyte storage (ES) and balance of plant (BOP). (b) The CO₂ eq resulted in the production of steel and vanadium pentoxide (V₂O₅) from raw material extraction to the finished 1 kg of V₂O₅ with a purity of 97.5 wt%. Adapted with permission from ref. 87. Copyright 2020 Elsevier Ltd. ref. 88. Copyright 2022 Wiley Periodicals LLC.

extraction and consumption of raw materials.⁸⁶ Additionally, the long lifespan of VFBs can also reduce the emission of a large amount of CO₂ from the burning of fossil resources.

ZBFBs have relatively low global warming potential (~ 156 kg CO₂ eq per kW h), the lowest impact on ozone depletion potential and freshwater ecotoxicity, but the highest for abiotic resource depletion potential (Fig. 6a). The production of titanium for bipolar plates accounts for the highest proportion (40%) of the total global warming potential, followed by the production of electrolyte (29%). Additionally, the production of bromine dominates the high abiotic resource depletion potential. Bromine is highly volatile and corrosive, which poses a threat to the environment and human health. While the bromine can be complexed by complexing agents to alleviate bromine diffusion.^{89,90}

IFBs have the lowest global warming potential (73 kg CO₂ eq per kW h) and cumulative energy demand (1090 MJ kW⁻¹ h⁻¹) compared to VFBs and ZBFBs (Fig. 6a). The storage tank (39%) and cell frame (22%) are the main contributors. IFBs exhibit a low environmental impact mainly due to the use of low impact iron-based electrolyte.

In ICFB, the involved iron (Fe²⁺/Fe³⁺) and chromium ions (Cr²⁺/Cr³⁺) have low toxicity toward the environment and human body. It's estimated that the potential environmental impacts of ICFBs and ZIFBs are comparable with that of IFBs because of the similar preparation process and environmental friendliness of electrolytes. ICFBs, ZIFBs and IFBs receive the highest score of 5 for environmental friendliness, followed by ZBFBs and then VFBs (Fig. 7).

2.1.5 Novel inorganic FBs. In addition to the widely studied redox species mentioned above, some novel redox species have also been investigated to achieve low-cost, high-energy density and environmentally friendly FBs. Mn-Based materials have high solubility (> 4 M), high redox potential (1.56 V for Mn²⁺/Mn³⁺, 1.23 V for Mn²⁺/MnO₂), low cost and earth abundance. However, Mn³⁺ suffers from a disproportion side reaction from Mn²⁺ and dead MnO₂, leading to capacity decay and pump line blockage. Some complexing agents, such as TiO²⁺ or P₂O₇⁴⁻ were added to avoid the disproportion reaction and inhibit MnO₂ growth through coordination between Mn³⁺ and oxo-ligands.^{91,92}

In addition, Xie *et al.* achieved a two-electron transfer reaction between Mn²⁺ and MnO₂, through the coordination effect of acetate on Mn²⁺ to avoid the formation of Mn³⁺ (Fig. 12a).⁹³ The prepared Zn-Mn FB achieved a high areal capacity of 20 mA h cm⁻² and demonstrated the stable cycling performance for 400 cycles with a CE and EE of 99% and 78%, respectively at 40 mA cm⁻² (Fig. 12b). Several studies have introduced mediators, such as I₂/I⁻ and Br₂/Br⁻ to reduce dead MnO₂ *via* a chemical-electrochemical process, recovering the lost capacity from exfoliated MnO₂.^{94,95} The assembled Cd/Br-Mn FB exhibited an EE of 76% at 80 mA cm⁻² with a high energy density of 360 W h L⁻¹.⁹⁵

Meanwhile, Sn-based FBs also have the advantages of low cost, low toxicity and multiple electron transfer reactions. Sn/Sn²⁺ features fast kinetics, high solubility and high hydrogen overpotential.^{96,97} The Sn(OH)₆²⁻/Sn redox species undergo a four-electron transfer reaction at a low redox potential of -0.921 V *vs.* SHE and avoids the problem of dendrites due to

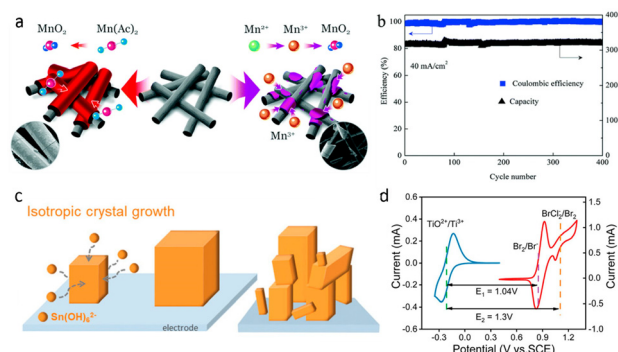


Fig. 12 (a) The electrochemical mechanism of Mn(Ac)₂ and MnSO₄. (b) The performance of the battery assembled with 1.5 M electrolyte (1.5 M Mn(Ac)₂ + 1.5 M ZnCl₂ + 3 M KCl) at 40 mA cm⁻². (c) The schematic representation of the growth mechanism of Sn cubes. (d) Cyclic voltammetry of Ti(SO₄)₂ and HBr + HCl in 1.0 M H₂SO₄ solution on a carbon felt electrode. Adapted with permission from ref. 93. Copyright 2020 The Royal Society of Chemistry. Ref. 95 and 98. 2022 Copyright Wiley-VCHGmbH. ref. 99 Copyright American Chemical Society.

its intrinsic low-surface energy anisotropy (Fig. 12c). The high solubility of K₂Sn(OH)₆ (2.25 M in 1 M KOH) provides the battery with a high theoretical capacity of 241.2 A h L⁻¹.⁹⁸

Halogen-based FBs have been widely studied due to their high solubility, redox potential and low cost. However, the reaction only involves a single-electron transfer. Several studies have achieved a two-electron transfer reaction based on Br⁻/Br⁺, which prominently improved the energy density. The Br⁺ can be stabilized by Cl⁻ to form halogen interactional BrCl₂⁻ (Fig. 12d) or by graphite to form Br-GIC.^{99,100} The energy density can be further increased if Br⁻ can be oxidized to the higher-valence products, such as BrO₃⁻.

2.2 From inorganic to organic redox species

Reducing the carbon footprint and constructing a novel energy system are the main trends of the current energy development. Inorganic metal-based batteries have surged all over the world. As requirements for the inorganic metal-based batteries have exploded, prices for the raw materials have undulated fiercely. Moreover, the present excessive exploitation of metal resources has been faced with an inevitable negative environmental impact. Organic redox-active molecules (ORAMs) are generally prepared under mild conditions and have been regarded as eco-friendly materials. In recent years, organic molecules have emerged in FBs possessing potential resource sustainability, synthesis tunability, structural diversity and feasible cost which render ORAMs as alternatives compared to the inorganic redox species (Fig. 13). These features potentially enable ORAMs to be competitive candidates which probably help them sprout and flourish in sustainable energy development as ESS and gradually keep the pace with inorganic species during the period of energy reconstruction. Regular criteria of ORAMs in FBs involve solubility, stability, redox potential, and kinetics, while for constructing a green economy and meeting the goal of decarbonization, material cost, synthesis appropriateness, safety and environmental impact definitely should also be taken into

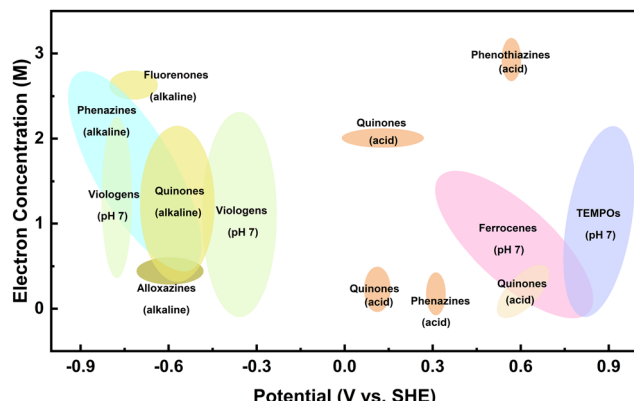


Fig. 13 The redox potentials and electron concentrations of the different reported RAMs.

consideration. Herein, the feasibility, cost-effectiveness and greenness are proposed as three key sustainability aspects to evaluate the practicality of ORAMs and the corresponding competitiveness in future FB technology. The feasibility (feasible or not) involves the stability and lifetime (P1), high atom economy (P2), simple preparation/synthesis (P4), safer chemicals (P5), safer production (P6), waste disposal (P7) and low cost (P9) of the ORAMs. As for cost-effectiveness (cost-effective or not), it is related to the simple preparation/synthesis (P4) and low cost (P9). And the green aspect (green or not) includes the high atom economy (P2), renewable sources (P3), safer chemicals (P5), waste disposal (P7) and low carbon (P8).

2.2.1 Technical sustainability

Structure, characteristics & performance. In order to achieve high energy density and battery lifetime, molecular engineering and electrolyte optimization (pH, supporting salts, additives, concentrations, and the counter RAMs) have been carried out to improve the water solubility and stability issue during redox process. Hitherto the ORAMs can be classified as follows quinone-based molecules, viologens, TEMPOs, phenazines, alloxazines, phenothiazines, fluorenones, polymer-based molecules, azobenzene-based molecules, and organometallic complexes.

Quinone-based RAMs. The quinone molecule is a kind of biologically active molecule and the electron transfer dominated by active oxygen atoms is based on enolization stabilizing electron-poor or electron-rich structures by the delocalization effect over the conjugated form.^{101–104} Both the reversibility and reaction rate of quinone-based molecules are impressive, and the electron transfer reaction is highly pH-dependent (Fig. 13).¹⁰⁵ Quinone compounds are generally divided into benzoquinone (BQ), naphthoquinone (NQ), and anthraquinone (AQ), etc.¹⁰⁴

BQ. The *ortho*-oxygenic BQ derivative, 4,5-dihydroxy-1,3-benzenedisulfonate (BQDS, 0.89 V vs. SHE) first trialed in FBs as the catholyte which pioneered the application of organic species in 2008.¹⁰⁶ BQDS possessed an improved water solubility of 1.0 M in 1 M H₂SO₄, but easily underwent a typical

Michael reaction with water resulting in an irreversible structure transition. More works turned to *para*-oxygenic derivatives.¹⁰⁷ 3,6-Dihydroxy-2,4-dimethylbenzenesulfonic acid (DHDMBS, 0.82 V vs. SHE) had two additional methyl groups besides the benzoquinone frame and hydrophilic sulfonic acid group.¹⁰⁸ The solubility of DHDMBS under acidic conditions increased to 2 M. The “substituent-occupied” strategy did help to enhance the stability of ORAMs, however, they are also prone to react with water and lose/gain functional groups. The earliest phenolic compounds with specific solubility in water and the electrochemical reversibility were sulfonic acid-modified phenol derivatives with a pair of hydroxyl groups.¹⁰⁶ Besides the sulfonic acid modified phenol derivatives, polyhydroxyl BQs are also used as RAMs.¹⁰⁹ A fully-substituted quinone with four sulfonated thioether substituents, 3,3',3'',3'''-((3,6-dihydroxybenzene-1,2,4,5-tetrayl)tetrakis(sulfanediyl))tetrakis(propane-1-sulfonate) (DHTTSTPS) (0.60 vs. SHE) was synthesized by an electrochemical process and the water solubility was around 1 M in 1 M H₂SO₄ after ion-exchanging.¹⁰⁹ There was no obvious capacity decay over 150 cycles in a full quinone-based cell with 0.2 M tetrasubstituted BQ catholyte and AQ anolyte.

NQ. NQ derivatives render an expanded conjugated region compared with BQ. NQ molecules are always in alkaline solution as hydroxyl or carboxyl groups on the NQ ring could effectively deprotonate under alkaline conditions to improve water solubility. 2-Hydroxy-1,4-naphthoquinone (NQ(1,4)H, −0.50 V vs. SHE) possesses seemingly reversible CV in 1 M KOH while there was a dramatic capacity loss during the cycling test which might be caused by irreversible side reactions such as epoxidation and specific crossover as its small size.¹¹⁰ 2-Hydroxy-3-carboxy-1,4-naphthoquinone (2,3-HCNQ, −0.51 V vs. SHE) has an improved solubility of 1.2 M in alkaline solution.¹¹¹ A cell voltage of 1.02 V was achieved by a FB of 2,3-HCNQ anolyte matched with K₄Fe(CN)₆ catholyte. And the 2,3-HCNQ/K₄Fe(CN)₆ FB could be stable over 100 cycles with a capacity retention of 94.7% at 100 mA cm^{−2}. Besides, a NQ dimer, bislawsone (−0.55 V vs. SHE, 0.56 M (2.24 M electrons)), was introduced as the anolyte into FBs.¹¹² The dimer form has a larger molecular size and twice the electron transfer number than the monomer. A single cell pairing bislawsone anolyte with a K₄Fe(CN)₆ catholyte rendered a cell voltage of 1.05 V at an anolyte concentration of 0.5 M.

AQ. AQ is the most widely studied quinone derivative and delivers a large aromatic region delocalizing negative charge thus resulting in a more stable backbone than BQ and NQ. However, this bulky structure has poor water solubility. 9,10-Anthraquinone-2,7-disulphonic acid (AQDS, 0.21 V vs. SHE), modified by hydrophilic sulfonic acid groups, was used as an anolyte in AOFBs which afforded an improved water solubility greater than 1 M in 1 M H₂SO₄ solution.¹⁰³ A metal-free cell was successfully fabricated with bromine-based catholyte and 1 M AQDS anolyte. The additional electron-donating hydroxyl and methyl groups were introduced to lower the redox potential of AQ anolyte such as 1,8-dihydroxyanthraquinone-2,7-disulfonic

acid (DHAQDS, 0.12 V vs. SHE), alizarin red S (ARS, 0.08 V vs. SHE), and 1,4-dihydroxyanthraquinone-2,3-dimethylsulfonic acid (DHAQDMS, 0.02 V vs. SHE) in which methylene spacers can weaken the electronic effect of sulfonic acid groups.

Under alkaline conditions, the hydroxy-substituted anthraquinone derivative, 2,6-dihydroxyanthraquinone (DHAQ), delivered a low redox potential of -0.70 V vs. SHE and a water solubility of >0.6 M at pH > 12 .¹¹³ The DHAQ-based AOFB demonstrated a 1.20 V cell voltage and a capacity retention of 99.9% per cycle over 100 cycles with CE > 99% and EE > 84% at 100 mA cm $^{-2}$. Diverse structures have been designed to improve the stability of AQ derivatives.¹¹⁴ The nucleophilic hydroxyl ions in a strong alkaline environment (pH 14) will bring about undesired side reactions which may inactivate the RAMs and result in a capacity decay. To realize long-term energy storage with reliable capacity retention, one strategy is making the redox process carry out in a (near) neutral environment to alleviate side reactions. The hydroxyl groups of DHAQ are used as the specific sites to be functionalized with tethered highly alkali-soluble phosphoric groups. (((9,10-Dioxo-9,10-dihydroanthracene-2,6-diyl)bis(oxy))bis(propane-3,1-diyl)) bis(phosphonic acid) (2,6-DPPEAQ, -0.47 V vs. SHE in pH 9 and -0.49 V vs. SHE in pH 12) demonstrate a solubility of 0.75 M, *i.e.*, 1.5 M electrons at pH 9. And the near-neutral AOFB with 0.5 M 2,6-DPPEAQ exhibited an OCV of 1.0 V and a capacity fade rate of 0.00036% per cycle (0.014% per day) over 480 cycles at 100 mA cm $^{-2}$. Similarly, carboxylic-tethered AQ derivatives, 4,4'-(9,10-anthraquinone-2,6-diyl)dioxy) dibutyrate (2,6-DBEAQ, -0.5 V vs. SHE) afforded water solubility exceeding 1 M in pH 14 and 0.5 M in pH 12. By pairing 0.5 M 2,6-DBEAQ with 0.3 M K₄Fe(CN)₆ catholyte, the near-neutral AOFB yielded an OCV above 1 V and capacity fade of 0.04% per day over 400 cycles (6 days). In conclusion, adjusting the solution pH to near-neutral and tailoring the molecular structure to alleviate side reactions will contribute to the improvement of stability.¹¹⁵ Furthermore, AQs have been honed to pursue optimal structures with the desired performance in alkaline AOFBs under inert atmosphere protection. More molecular engineering was performed to modify anthraquinone to be more hydrophilic for higher solubility.^{116,117}

Viologens. Viologen is a typically heteroaromatic molecule with an N-substituted 4,4'-bipyridinium frame. Viologen derivatives are often used as anode materials in a redox process involving two independent steps of single electron transfer under pH neutral conditions. Methyl viologen, 4,4-dimethyl bipyridinium dichloride, (MV $^{2+}$, -0.45 and -0.76 V vs. SHE) affords the most simple form of viologen derivatives displaying a water solubility over 3 M at neutral pH.¹¹⁸ A stepwise 2e $^{-}$ transfer is enabled in viologen derivatives whereas the charge-neutral MV 0 state is insoluble in aqueous solution which limits the energy density of AOFBs.^{119,120} Hydrophilic modification of viologen derivatives especially on the nitrogen of pyridinium rings has been carried out to improve the solubility of charge-neutral MV 0 state.^{119,121} The pendant quaternary ammonium or sulfuric acid alkyl group on one or both viologen sides was

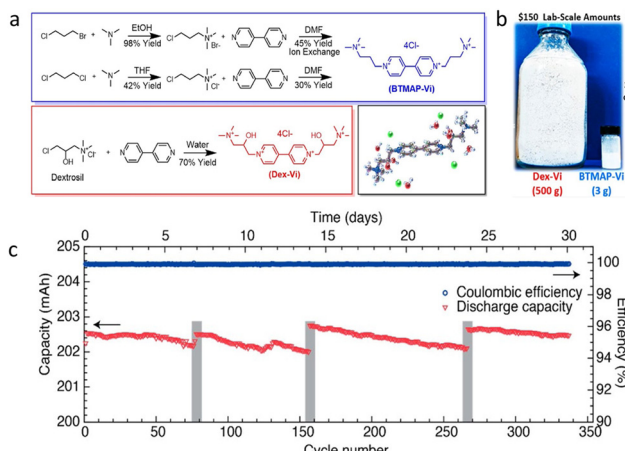


Fig. 14 (a) Comparison of the synthetic procedures and properties of BTMAP-VI and Dex-VI RAMs. (b) The photos of synthesized Dex-VI and BTMAP-VI RAMs. (c) Full cell cycling performance of 1.5 M Dex-VI with a volumetric excess of 0.75 M BTMAP-Fc catholyte and DSVN membrane. Adapted with permission from ref. 129. Copyright American Chemical Society.

achieved. 1-Methyl-1'-(3-(trimethylammonio)propyl)-4,4'-bipyridinium trichloride ($[(Me)(NPr)V]Cl_3$, -0.39 and -0.78 V vs. SHE), 1,1'-bis[3-(trimethylammonio)propyl]-4,4'-bipyridinium tetrabromide ($[(NPr)_2V]Br_4$, -0.35 and -0.72 V vs. SHE) and 1-[3-(trimethylammonio)propyl]-1'-(3-sulfonatopropyl)-4,4'-bipyridinium dibromide ($[(NPr)(SPr)V]Br_2$, -0.37 and -0.74 V vs. SHE) present the improved solubility of 1.4 M, 1.3 M and 1.3 M in 2.0 M NaCl respectively (Fig. 14a). Neutral AOFBs with 0.25 M viologen derivatives anolyte and 0.5 M (ferrocenylmethyl)trimethylammonium chloride (FcNCl) catholyte delivered cell voltages all above 1 V and showed the capacity retention of 99.82% to 99.99% in 50 to 100 cycles. A sulfonated viologen, 1,1'-bis(3-sulfonatopropyl)-4,4'-bipyridinium ($(SPr)_2V$, -0.43 V vs. SHE), with two pendant sulfuric acid alkyl groups was obtained by sulfonate alkylation of propane sultone. The $(SPr)_2V/KI$ AOFB delivered an OCV of 1.0 V and a capacity retention of 99.99% over 300 cycles (94.1% total capacity retention) at 60 mA cm $^{-2}$ with an average EE of 58% and CE of nearly 100%.¹²¹

An obvious capacity decay was thought to be mainly caused by crossover during the long duration time. A rod-shaped sulfonated viologen, 2,2',6,6'-tetramethyl-4,4'-bipyridine (R-Vi, -0.55 V vs. SHE), with a bulky structure was enabled by the steric hindrance effect of methyls. The weak charge attraction and large molecular size gave R-Vi a much lower permeability of 1.25×10^{-10} cm 2 s $^{-1}$ which is 14.7% of $(SPr)_2V$.¹⁴⁶ A phenylene-bridged bispyridinium, 1,1'-bis[3-(1,4-trimethylammonium)propyl]-4,4'-(1,4-phenylene)bispyridinium tetrachloride ($(APB-Py)Cl_4$, -0.76 V vs. SHE), was developed as a two-electron storage mediator.¹²⁷ By using 2,2,6,6-tetramethylpiperidin-1-yl oxyl derivative ($(TBABPy)Cl_3$) as the catholyte, a pH neutral AOFB with 0.5 M $(APBPy)Cl_4$ delivered a cell voltage of 1.73 V and a capacity of 20 A h L $^{-1}$. A 96% capacity retention was achieved in 100 cycles (2.88% per day and 0.04% per cycle of capacity decay). Researchers have recently reported a dextrosil-viologen (Dex-Vi) using a hydrothermal synthetic approach with

high yield (500 grams) and low-cost precursor (Fig. 14a).¹²⁹ Dex-Vi possessed an impressive solubility of 2 M in pure water. Paring with bis(3-trimethylammonio)propyl ferrocene dichloride (BTMAP-Fc) catholyte, a cell with 1.5 M Dex-Vi catholyte (40.2 A h L⁻¹ theoretical capacity) showed a stable cycling performance with no obvious capacity decay over one month at 50 mA cm⁻² (Fig. 14c).

TEMPOs. 2,2,6,6-Tetramethylpiperidine-1-oxyl (TEMPO) derivatives undergo a typical single-electron transfer. TEMPO derivatives are one of the most typical catholytes in pH-neutral AOFBs and the molecular stability was ascribed to the delocalization of electron on the nitrogen and oxygen redox center surrounded by four methyl groups, which also impedes undesired side reactions such as dimerization from bimolecular interaction. 4-Hydroxy-tetramethylpiperidin-1-oxyl (4-HO-TEMPO, 0.80 V vs. SHE), exhibited a water solubility of 0.5 M in 1.5 M NaCl.¹¹⁸ An AOFB employing 0.5 M 4-HO-TEMPO catholyte and 0.5 M MV anolyte presented a cell voltage of 1.25 V and a capacity retention over 99% per cycle after 100 cycles at 60 mA cm⁻². As the catholyte, TEMPO derivatives are faced with a common problem of irreversible capacity decay caused by crossover. Positively/negatively charged functional groups are introduced into the molecule to inhibit crossover by charge repulsion. A negatively charged TEMPO compound (TEMPO-4-sulfate potassium salt, 0.83 V vs. SHE) and a positively charged TEMPO compound, *N,N,N-2,2,6,6-heptamethylpiperidinyl oxy-4-ammonium chloride* (TEMPTMA, 1.01 V vs. SHE) were developed to match with the cation exchange membrane (CEM) and anion exchange membrane (AEM) respectively and obtained the improved capacity retention.^{130,131} On the other hand, TEMPO molecule size can be further enlarged so that the steric effect can be used to suppress the crossover as well. A pendant quaternary ammonium alkyl group modified 4-[3-(trimethylammonio)propoxy]-2,2,6,6-tetramethylpiperidine-1-oxyl chloride (TMAP-TEMPO, 0.81 V vs. SHE) was designed to realize an ultra-stable radical-based catholyte.¹⁴⁷ TMAP-TEMPO possesses an alkyl chain between oxygen and quaternary ammonium in which the steric hindrance resulting from peripheral methyl groups and the alkyl chain and the coulombic repulsion from the positively charged quaternary ammonium reduce bimolecular interaction and crossover, thereby effectively prolonging the TMAP-TEMPO lifetime. A concentrated pH-neutral AOFB assembled with 1.5 M TMAP-TEMPO as the catholyte and 1.5 M bis(trimethylammonio) propyl viologen (BTMAP-Vi) as the anolyte provided a cell voltage of 1.1 V and a capacity retention of 99.985% per cycle over 200 cycles at 100 mA cm⁻² (Table 2).

The bubbles which are numbered 1–5 indicate whether corresponding options are feasible, cost-effective or green. The higher the number, the more sustainable and low-carbon it is.

Score 5 indicates the corresponding system is extremely reliable (P1) and the ORAM preparation is quite easy to scale up (maybe 1 or 2 general steps without complicated purification, P4) which involves high yield (>90%, P2), low cost (P9),

renewable feedstocks (P3), safe reagents (P5) and process (P6) under mild conditions (P8).

Score 4 indicates the corresponding system is stable enough (P1) and the ORAM preparation is easy to scale up (maybe 1 or 2 general steps without complicated purification, P4) which involves a relatively high yield (>80%, P2), relatively low cost (P9), common feedstocks (P3), safe reagents (P5) and process, under mild conditions (P8).

Score 3 indicates the corresponding system is relatively stable (P1) and the ORAM preparation is not hard to scale up (2 or more general steps, maybe with a purification step, P4) which involves an acceptable yield (>70%, P2) and cost (P9), common reagents and feedstocks (P3 & P5). The process may be risky (P6, P7 & P8), such as the use of acids and bases or operating under specific conditions (high temperature or pressure).

Score 2 indicates the corresponding system may not be feasible (P1) and the ORAM preparation is hard to scale up (3 or more steps with a time-consuming purification step, such as ion-exchange or column chromatography, P4) which involves relatively low yield (>60%, P2) and high cost (P9), poisonous reagents and feedstocks (P3 & P5). The process may be risky (P6, P7 & P8), such as the use of strong acids and bases and operating under high temperature and pressure with some harmful waste.

Score 1 indicates the corresponding system is not feasible (P1) and the ORAM preparation is hard to scale up (3 or more steps with a complicated purification step such as ion-exchange and column chromatography, P4) which involves very low yield (<60%, P2) and considerable cost (P9), hypertoxic reagents and feedstocks (P3 & P5). The process may be highly risky (P6, P7 & P8), such as the heavy use of strong acid and alkali, operating under high temperature and pressure and a lot of harmful waste which would cause serious air or hydrology pollution.

Phenazines. As broad-spectrum antibiotics, phenazine derivatives are aromatic heterocyclic compounds. The solubility of phenazine is poor in whatever acidic, alkaline solutions and neutral aqueous solution which cannot meet the requirement of energy density. Different hydrophilic groups are introduced to the phenazine rings by condensation of the precursors or grafting.

A modified phenazine derivative, 7,8-dihydroxyphenazine-2-sulfonic acid (DHPS, -0.84 V vs. SHE), displayed an improved solubility from near-zero (pristine phenazine) to 1.8 M in 1 M NaOH.¹³⁴ Coupled with the K₄Fe(CN)₆ catholyte, 1.4 M DHPS based AOFB provided an OCV of 1.4 V and a capacity retention of 99.98% per cycle after 500 cycles with 82% VE at 100 mA cm⁻². By cyclization reaction between quinone and diphenylamine precursors, the 2-hydroxyphenazine (HP, -0.45 V vs. SHE), 2-amino-3-hydroxyphenazine (AHP, -0.56 V vs. SHE) and benzo[a]hydroxyphenazine-7/8-carboxylic acid (BHPC, -0.56 V vs. SHE) were synthesized and had the solubilities of 1.70 M, 0.43 M, and 1.55 M respectively.¹⁴⁸ When coupled with K₄Fe(CN)₆ catholyte, the phenazine based AOFBs delivered a tunable OCV of 1.16–1.27 V. Furthermore, the AOFB based on

Table 2 ORAMs with corresponding characters and evaluation for further production from a sustainable aspect

| No. Structure & name | Potential (vs. SHE) | Solubility/theoretical electron concentration/tested concentration (M) | Condition of solubility | Another side cm^{-2} | Current density (mA cm^{-2}) | Cycle number/cycle time | Capacity retention (%)/fade rate (%) | Feasible or not | Cost-effective or not | Green or not | Ref. |
|---------------------------|---------------------|--|------------------------------------|--|---|-------------------------|--------------------------------------|-----------------|-----------------------|--------------|------|
| 1 HO ₃ S-BQDS | 0.89 | 1.0/2.0/0.050 | 1 M H ₂ SO ₄ | PbSO ₄ /Pb | 10 | 100/N/A | N/A | 5 | 5 | 3 | 106 |
| 2 HO-S-BQS | 0.71 | 0.80/1.6/N/A | 1 M H ₂ SO ₄ | N/A | N/A | N/A | N/A | 5 | 5 | 3 | 106 |
| 3 HO ₃ S-DHDMB | 0.82 | 2.0/4.0/1.0 | 1 M H ₂ SO ₄ | AQDS | 100 | 25/N/A | 90.0 total/1.00 per cycle | 5 | 2 | 3 | 108 |
| 4 DHBQ | -0.72 | 4.0/8.0/0.50 | 1 M KOH | Potassium ferrocyanide | 10 A | Over 400/N/A per cycle | 99.0 total/0.0380 per cycle | 4 | 4 | 4 | 122 |
| 5 DHTTSTPS | 0.60 | 1.0/2.0/0.20 | 1 M H ₂ SO ₄ | AQDS | 50 | 150/N/A | 100/0.00 | 1 | 3 | 3 | 109 |
| 6 NQ(1,4)H | -0.50 | 0.48/0.96/0.20 | 1 M KOH | Ferrocyanide | 200 | Over 10/4 h | 50.0 per cycle/50.0 per cycle | 3 | 4 | 3 | 110 |
| 7 2,3-HCNQ | -0.51 | 1.2/2.4/0.50 | 2.0 M KOH | K ₄ Fe(CN) ₆ | 100 | 100/over 1.5 days | 94.7 total/0.0530 per cycle | 2 | 4 | 3 | 111 |
| 8 bislawsone | -0.55 | 0.56/2.24/0.50 | 1 M KOH | K ₄ Fe(CN) ₆ /K ₃ Fe(CN) ₆ | 300 | Over 250/over 20 days | 85.2 total/0.00800 per cycle | 5 | 4 | 3 | 112 |

Table 2 (continued)

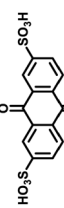
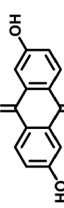
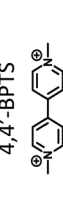
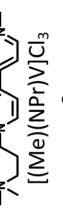
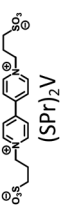
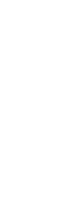
| No. Structure & name | Potential (vs. SHE) | Solubility/theoretical electron concentration/tested concentration (M) | Condition of solubility | Another side cm^{-2} | Current density (mA/cm ²) | Cycle number (cycles)/cycle time | Capacity retention (%)/fade rate (%) | Feasible or not | Cost-effective or not | Green or not | Ref. |
|----------------------|---|--|-------------------------|-----------------------------------|---|----------------------------------|--------------------------------------|--|-----------------------|--------------|-------|
| 9 AQDS |  | 0.21 | >1.0/>2.0/0.10 | 1 M H_2SO_4 | Br_2/HBr | 200 | 10/100 h | 99.2 per cycle/ 0.800 per cycle | 5 | 5 | 3 103 |
| 10 |  | -0.70 | >0.60/>1.2/0.50 | 1 M KOH. | $\text{K}_4\text{Fe}(\text{CN})_6$ | 100 | 100/N/A | 99.9 per cycle/ 0.100 per cycle | 5 | 5 | 4 123 |
| 11 |  | -0.47 in pH 9 | 0.75/1.5/0.50 | <10 ⁻⁵ M KOH (pH 9) | $\text{K}_4\text{Fe}(\text{CN})_6/\text{K}_3\text{Fe}(\text{CN})_6$ | 100 | Over 480/7 days | 99.9 total/ 0.000360 per cycle | 3 | 3 | 3 115 |
| 12 |  | -0.50 | 1.0/2.0/0.5 | 1.2 M/10 mM KOH (pH 14/ 12) | $\text{K}_4\text{Fe}(\text{CN})_6/\text{K}_3\text{Fe}(\text{CN})_6$ | 100 | Over 400/ over 6 days | 99.6 total/ 0.00100 per cycle | 3 | 3 | 3 123 |
| 13 |  | 0.91 | 1.5/3.0/0.10 | 2 M HCl | SWO | 60 | >900/N/A | 100/0.00 | 5 | 5 | 4 124 |
| 14 |  | 0.90 | 1.0/2.0/0.1 | 1 M H_2SO_4 | 1,8-DHAQDS 1000 | 100/N/A | N/A | 5 | 5 | 3 125 | |
| 15 |  | -0.45 and -0.76 | >3.0/>6.0/0.50 | Water | 4-HO- TEMPO | 60 | 100/N/A | 89.0 total/0.110 per cycle | 5 | 5 | 2 118 |
| 16 |  | -0.39 and -0.78 | 1.4/2.8/0.25 | 2.0 M NaCl | FcNCl | 60 | 50/N/A | 99.8 per cycle/ 0.00360 per cycle | 3 | 3 | 2 119 |
| 17 |  | -0.35 and -0.72 | 1.3/2.6/0.25 | 2.0 M NaCl | FcNCl | 60 | 50/N/A | 99.9 per cycle/ <0.0100 per cycle | 4 | 3 | 2 119 |
| 18 |  | -0.43 | 2.0/4.0/0.50 | Water | KI | 60 | 300/N/A | 94.1 total or 99.9 per cycle/0.0190 per cycle | 4 | 3 | 2 121 |
| 19 | | -0.55 | 1.1/2.2/0.10 | 1 M KCl | $\text{K}_4\text{Fe}(\text{CN})_6$ | 50 | 3200/17 days | 99.9 per cycle/ 0.00700 per cycle | 2 | 2 | 2 126 |

Table 2 (continued)

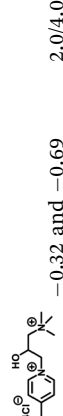
| No. Structure & name | Potential (vs. SHE) | Solubility/theoretical electron concentration/tested concentration (M) | Condition of solubility | Another side cm ⁻²) | Current density (mA cm ⁻²) | Cycle number (cycles)/cycle time | Capacity retention (%)/fade rate (%) | Feasible or not | Cost-effective or not | Green or not | Ref. |
|---|------------------------|--|--|--|--|----------------------------------|--|-----------------|-----------------------|--------------|------|
| 20  (APBPY)Cl ₄ | -0.76 | 1.3/2.6/0.50 | N/A | TEMPO derivative | 80 | 100/N/A | 96.0 total/2.88 per day, 0.0400 per cycle | 3 | 2 | 2 | 127 |
| 21  | -0.25, -0.44 and -0.63 | 1.1/3.5/0.30 | N/A | FcNCl | 80 | 50/N/A | N/A | 2 | 2 | 2 | 128 |
| 22  | -0.32 and -0.69 | 2.0/4.0/1.5 | Water | BTMAP-Fc | 50 | >300/>30 days | N/A | 5 | 4 | 2 | 129 |
| 23 Dex-Vi  | 0.80 | 0.50/0.50/0.50 | 1.5 M NaCl | Viologen derivative | 60 | 100/N/A | 89.0 total/0.110 per cycle | 4 | 3 | 3 | 118 |
| 24 4-HO-TEMPO  | 0.83 | 1.0/1.0/0.035 | 2 M ZnCl ₂ and 1 M NH ₄ Cl | Zn/Zn ²⁺ | 3 | 1100/9 days | 93.6 total/0.00580 per cycle | 4 | 3 | 3 | 130 |
| 25 TEMPO-4-sulfate  | 1.01 | 3.2/3.2/2.0 | 1.5 M NaCl | Viologen derivative | 80 | 100/N/A | 100/0.00 | 4 | 2 | 3 | 131 |
| 26 TMPTMA  | 0.81 | 4.6/4.6/1.5 | Water | BTMAP-Vi | 100 | 250/171.7 h | 99.9 per h/0.00420 per h | 4 | 3 | 3 | 132 |
| 27 g ⁺ -TEMPO  | 0.82 | 1.2/1.2/0.20 | 1 M NaCl | Zn/Zn ²⁺ | 20 | 140/N/A | 93.6 total/0.0460 per cycle | 5 | 4 | 3 | 133 |
| 28 DHPS  | -0.84 | 1.8/3.6/1.4 | 1 M NaOH | K ₄ Fe(CN) ₆ /K ₃ Fe(CN) ₆ | 100 | 500/14.3 days | 99.9 per cycle/0.0190 per cycle, 0.680 per day | 3 | 3 | 3 | 134 |

Table 2 (continued)

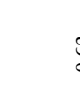
| No. Structure & name | Potential (vs. SHE) | Solubility/theoretical electron concentration/tested concentration (M) | Condition of solubility | Another side cm ⁻²) | Current density (mA cm ⁻²) | Cycle number/cycle time | Capacity retention (%)/fade rate (%) | Feasible or not | Cost-effective or not | Green or not | Ref. |
|--|---------------------|--|--|--|--|-------------------------|--|-----------------|-----------------------|--------------|-------|
| 29 HP | -0.45 | 1.7/3.4/0.50 | 1 M KOH | K ₄ Fe(CN) ₆ | 100 | 100/N/A | N/A | | | | 3 135 |
| 30 ③ | -0.56 | 0.40/0.80/0.50 | 1 M KOH | K ₄ Fe(CN) ₆ | 100 | 100/N/A | >99.0 total/ <0.0100 per cycle | ③ | ② | ③ | 135 |
| 31 HOOC-  -NH ₂ BHPC | -0.56 | 1.5/3.0/0.50 | 1 M KOH | K ₄ Fe(CN) ₆ | 100 | 13.00/23 days | 98.0 total/ <0.0800 per day | ③ | ③ | ③ | 135 |
| 32 HOOC-  -NH ₂ 1,6-DPAP | -0.56 | 1.0/2.0/0.50 | Trace KOH (pH 8) | K ₄ Fe(CN) ₆ / K ₃ Fe(CN) ₆ | 20 | >90/5.3 days | 99.9/0.00 000 200 per cycle, 0.00150 per day | ② | ③ | ③ | 136 |
| 33 HOOC-  -NH ₂ 1,8-PFP | -0.58 | 1.5/2.9/0.50 | 1 M KOH | K ₄ Fe(CN) ₆ | 40 | >300/53 days | 100/0.00 | ② | ② | ③ | 137 |
| 34 HOOC-  -NH ₂ FMN-Na | -0.51 | 1.5/3.0/0.24 | 3 M Na ⁺ | K ₄ Fe(CN) ₆ | 80 | 100/N/A | 99.0 total/0.0100 per cycle per cycle | N/A | ⑤ | ⑤ | 138 |
| 35 HOOC-  -NH ₂ ACA | -0.62 | 2.0/4.0/0.50 | pH 14 KOH | K ₄ Fe(CN) ₆ | 100 | 400/N/A | 95.0 total/0.0120 | ③ | ② | ⑤ | 139 |
| 36 HOOC-  -NH ₂ MB | 0.57 | 1.8/3.6/1.0 | H ₂ O + acetic acid (AA) + V(n) H ₂ SO ₄ mixture | V(n) | 100 | 520/24 days | 99.6 total/ 0.000760 per cycle | ⑤ | ④ | ⑤ | 140 |
| 37 HOOC-  -NH ₂ P1 | 0.92 | N/A | 1.5 M NaCl | P2 | 20 | 10000/N/A | 80.0 total/ 0.00200 per cycle | ② | ② | ③ | 141 |

Table 2 (continued)

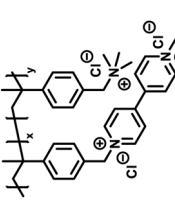
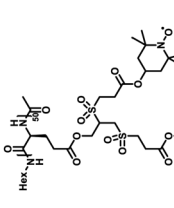
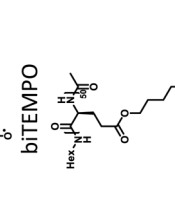
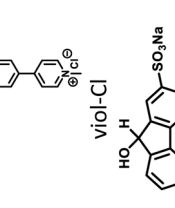
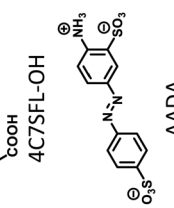
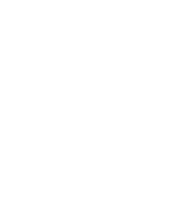
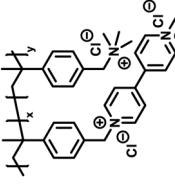
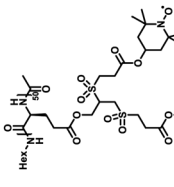
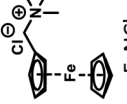
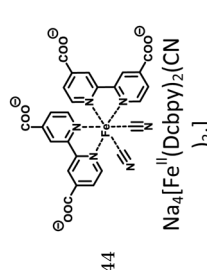
| No. Structure & name | Potential (vs. SHE) | Solubility/theoretical electron concentration/tested concentration (M) | Condition of solubility | Another side cm^{-2} | Current density (mA) | Cycle number (cycles)/cycle time | Capacity retention (%)/fade rate (%) | Feasible or not | Cost-effective or not | Green or not | Ref. |
|----------------------|---|---|-------------------------|-------------------------------|---|--|--------------------------------------|------------------|-----------------------------|--------------|------|
| 38 | -0.18 and -0.58 | N/A | 1.5 M NaCl | P1 | 20 | 10000/N/A | 80.0 total/ 0.00200 per cycle | ② | ② ③ | 141 | |
| P2 |  |  | 0.63 | N/A | 0.5 M TBACF ₃ SO ₃ | Viol-Cl | N/A | 30/N/A | 70.0 total/1.00 per cycle | ① | ② ⑤ |
| 39 | | | | | | | | | | | 142 |
| biTEMPO |  |  | -0.48 | N/A | 0.5 M TBACF ₃ SO ₃ | Bi-TEMPO | N/A | 30/N/A | 91.0 total/0.300 per cycle | ① | ② ⑤ |
| 40 | | | | | | | | | | | 143 |
| viol-Cl |  |  | -0.63 | 1.5/1.5/1.0 | 2 M NaOH | K ₄ Fe(CN) ₆ / K ₃ Fe(CN) ₆ | 100 days | 780/over 16 days | 87.8 total/0.020 per cycle | ② | ② ③ |
| 4C7SFL-OH |  |  | -0.50 and -0.07 | 2.0/4.0/0.50 | 2 M NaOH | K ₄ Fe(CN) ₆ / K ₃ Fe(CN) ₆ | 20 | 500/N/A | 76.0 total/0.0480 per cycle | ③ | ② ③ |
| 42 | | | | | | | | | | | 144 |
| AADA |  |  | | | | | | | | | |

Table 2 (continued)

| No. Structure & name | Potential (vs. SHE) | Solubility/theoretical electron concentration/tested concentration (M) | Condition of solubility | Another side cm ⁻² | Current density (mA cm ⁻²) | Cycle number (cycles)/cycle time | Capacity retention (%)/fade rate (%) | Feasible or not | Cost-effective or not | Green or not | Ref. | |
|----------------------|---|--|-------------------------|-------------------------------------|--|----------------------------------|--------------------------------------|---------------------------------|---|---|---|-----|
| 43 |  | 0.61 | 4.0/4.0/0.50 | Water | Viologen derivative | 60 | 700/N/A | 99.9 per cycle/0.0100 per cycle |  |  |  | 51 |
| 44 |  | 0.87 | 1.2/1.2/1.0 | 1.2 M NaCl and 0.4 M sodium acetate | Viologen derivative | 24 | 250/over 10 days | 99.9 per cycle/2.30 per day |  |  |  | 145 |

0.5 M BHPC catholyte exhibited an improved capacity retention of 99.986% per cycle (99.92% per day) with 80% EE over 1300 cycles. Amino acid and propionic-acid units were introduced into different positions of phenazine. 1,6-Amino acid substituted phenazine, 3,3'-(phenazine-1,6-diylbis(azanediyl))dipropionic acid (1,6-DPAP, -0.56 V vs. SHE) was much more stable than other derivatives.¹³⁶ The 0.5 M 1,6-DPAP based AOFB with 0.3 M K₄Fe(CN)₆ catholyte at pH = 8 exhibited an OCV of 1.15 V and a capacity fade rate of 0.5% per year (calculated) at 20 mA cm⁻². The propionic-acid-functionalized phenazine (PFP), 3,3'-(phenazine-1,8-diyl)dipropionic acid (1,8-PFP, -0.58 V vs. SHE) had the stable molecular structure even under strong alkaline solutions and elevated temperature with 1.46 M (1.0 M KOH at 25 °C) and 2.05 M (1.0 M KOH at 45 °C).¹³⁷

Alloxazines. Inspired by the natural flavin cofactors, alloxazine, consisting of pyrazine rings and fused benzene, was prepared for AOFBs. Alloxazine is a tautomer derived from vitamin B2 with a planar alloxazine ring structure. An alloxazine derivative, riboflavin-5'-phosphate sodium salt (FMN-Na, -0.51 V vs. SHE at pH 13), hydrophilized with a pendant phosphate alkyl group and hydroxyl groups shows a saturation solubility of nearly 1.5 M.¹³⁸ A concentrated biomimetic FMN-Na/K₄[Fe(CN)₆] AOFB based on 0.4 M K₄[Fe(CN)₆] catholyte and 0.24 M FMN-Na anolyte in 1 M nicotinamide (NA, used as hydrotropic agent) in 1 M KOH delivered a stable cycling performance with a capacity retention of 99% over 200 cycles (76 h) at 50 and 80 mA cm⁻². More alloxazine derivatives have been exploited with functionalized substituents of carboxylic acid (alloxazine7/8-carboxylic acid (ACA), -0.62 V vs. SHE), hydroxyl (7/8-hydroxyalloxazine, -0.73 V vs. SHE) and methoxy groups (7,8-dimethoxyalloxazine, -0.73 V vs. SHE) by rational design.¹³⁹ Using 0.5 M ACA anolyte and 0.4 M K₄[Fe(CN)₆] catholyte, a capacity retention of 91% over 400 cycles at 100 mA cm⁻² was achieved.

Phenothiazines. A natural dye, methylene blue (MB, 0.57 V vs. SHE) is a heteroaromatic phenothiazine with low toxicity and abundant resources and is regarded as a green candidate for AOFBs.¹⁴⁹ The improved solubility in acidic aqueous solution is obtained by the ammonium group on both sides of the aromatic ring. When coupled with vanadium anolyte, MB based AOFBs (1.0, 1.2, and 1.5 M MB) delivered impressive cycling performance with no obvious capacity loss over 500, 160, and 50 cycles at 80 mA cm⁻² (Fig. 15).¹⁴⁰ By virtue of electrolyte optimization and *in situ/ex situ* NMR and EPR techniques, it is found that both the oxygen resistant MB radicals generated by the comproportionation reaction and the reduced MB states in acidic electrolyte displayed much more stable structures, which played a vital role in the high reversibility of MB molecules under ambient air conditions. A kW-scale AOFB stack was assembled for the first time and exhibited stable capacity at 80 mA cm⁻² for over 500 cycles. Moreover, the stack still achieved a stable long-life cycle performance for ~32 days.¹⁵⁰

Polymer-based RAMs. Polymer-based organics species have emerged in ESS early in solid-state batteries and later come into

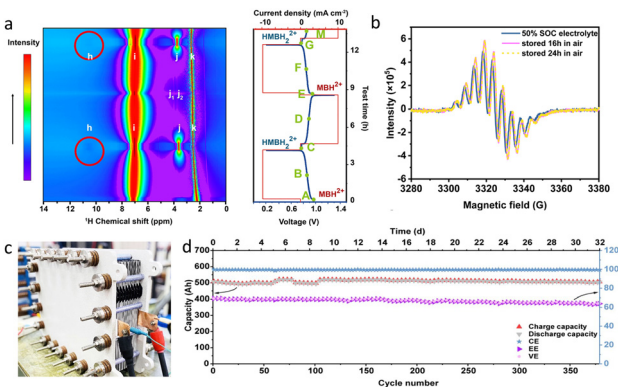


Fig. 15 (a) *In situ* pseudo-2D ¹H NMR spectra of the MB electrolyte. (b) EPR spectra of the MB electrolyte stored in air after 0 h, 16 h and 24 h, respectively. (c) and (d) The V-MB stack image and the life cycle of 0.5 M MB/V flow stack batteries at 50 mA cm⁻². Adapted with permission from ref. 140. Copyright 2023 The Royal Society of Chemistry.

FBS.^{151,152} The electrolytes are presented in oligomers to have a larger size with steric hindrance eliminating the capacity decay caused by crossover. Low-cost dialysis membranes can be used as the separator to block polymer RAMs with high molar mass while allowing smaller balance ions to pass through. The polymer design should be divided into two parts, the active center moiety to provide redox capacity and the hydrophilic unit to ensure the water solubility. A polymer based AOFB was composed of TEMPO-based catholyte, viologen-based anolyte and cellulose-based dialysis membrane.¹⁴¹ A 1.1 V OCV and the reversible redox process were achieved by the polymer-based cell with long-term cycling (10 000 cycles in a static) with 80% capacity retention at 20 mA cm⁻². L-Glutamic acid, a common amino acid, was used to construct the polypeptide-based batteries with sustainable materials, non-hazardous disposal and on-demand deconstruction and reconstruction.¹⁴²

Fluorenones. Recently, a reversible fluorenone hydrogenation and dehydrogenation without catalyst for AOFB was enabled by rational molecular design.¹⁴³ 4-Carboxylic-7-sulfonate fluorenol (4C7SFL-OH) with a rigid π-conjugated region delivered an available electron concentration of nearly 3 M in 1 M NaOH after introduction of sulfuric acid groups. When paired with K₄Fe(CN)₆ catholyte, the fluorenone based AOFB (1 M 4C7SFL) exhibited a capacity retention of 87.8% over 780 cycles at 100 mA cm⁻² and 50 °C outside of a glovebox with an average CE of 99.8% and EE of 70.6%. Continuous inert gas protection in practical application will bring about additional costs as most organic species are air sensitive. Additionally, once air permeates into the reservoirs, it will cause irreversible capacity loss for RAMs. The development of air-insensitive RAMs under the atmosphere is of great value for the practical application of AOFBs when looking towards large-scale deployment.

Azobenzenes. 4-Amino-1,1'-azobenzene-3,4'-disulfonic acid monosodium salt (AADA, -0.50 V and -0.07 V vs. SHE) with asymmetrical configuration has achieved improved solubility of 2 M in alkaline aqueous solution in the presence of urea as the

hydrotropic solubilizing additive.¹⁴⁴ Pairing with the ferro/ferrocyanide catholyte, AADA-based AOFB (0.5 M AADA) displayed an OCV above 1 V and a capacity retention of 76% after 500 cycles at 20 mA cm⁻². In this work, a new series of RAMs for AOFBs were proposed and the relationship between molecular symmetry and solubility was simulated and identified.

Metal complexes. Metal complexes consist of metal ions as redox centers and an additional array of bound ligands. Bulky organic ligands can mitigate the crossover issue of metal ions and be modified to tailor with distinctive properties.

The ferrocene-based species, ferrocenylmethyltrimethylammonium chloride (FcNCl, 0.61 V vs. NHE) and *N*¹-ferrocenylmethyl-*N*¹,*N*²,*N*²,*N*²-pentamethylpropane-1,2-diaminium dibromide (FcN₂Br₂, 0.61 V vs. SHE) were prepared to acquire high solubility of 4.0 M and 3.1 M in water.¹⁴⁵ When coupled with MV anolyte, the resulting AOFBs (0.5 M catholyte) yielded an OCV of 1.05 V and a capacity retention of 99% over 700 cycles.

A symmetry-breaking strategy has been used to enhance the solubility of iron complexes and the potential of iron complexes has been shifted positively by coordinated ligands.⁵¹ The water-soluble bipyridine ligand, 2,2'-bipyridine-4,4'-dicarboxylic acid (H₂Dcbpy) was chosen for complex design thus resulting in symmetric iron complexes [M₄[Fe^{II}(Dcbpy)₃], M = Na, K], and asymmetric iron complexes [M₄[Fe^{II}(Dcbpy)₂(CN)₂]] and M₄[Fe^{II}(Dcbpy)(CN)₄], M = Na, K]. The water solubilities of the symmetric complexes (0.26 and 0.60 M) are much lower than the asymmetric ones (1.09, 1.02, 1.22 and 1.12 M). AOFB with 0.1 M Na₄[Fe^{II}(Dcbpy)₂(CN)₂] catholyte demonstrated an outstanding stability with a low-capacity fade of 0.00158% per cycle over 6000 cycles.

2.2.2 Preparation. Many synthesis methods have been applied in AOFBs to develop highly desirable ORAMs. Zachary Deller *et al.* evaluated the greenness of the synthetic methodology used to prepare the ORAMs using the 12 principles of green chemistry.¹⁴ They discussed the most common synthetic strategies involving acid catalysis, catalyst free procedures, and oxidative polymerisation and also considered the 'greenness' of several key commercial materials. ORAMs in AOFBs should seek to adhere to green and sustainability principles in renewable energy sectors. However, frankly speaking, AOFBs are still at the basic research stage, and it is not practical to require the ORAMs to have strict sustainability before finding the right promising molecules. Therefore, we will discuss the applied methods for ORAMs design and compare the synthetic processes of several potential ORAMs in this section.

The synthesis methods for ORAMs generally involve the sulfonation, oxidization, alkylation grafting, coupling and condensation reactions.

Sulfonation. The sulfonation reaction is conducted under the condition of fuming or concentrated sulfuric acid to improve ORAM solubility. This reaction is straightforward without complicated steps (P4) and the target product can be obtained from the acidic solution by adjusting the pH thus leading to a

relatively high yield (P2) including the sulfonic BQ, AQDS, and TEMPO-4-sulfate. TEMPO-4-sulfate is prepared by sulfonation (93% yield) initiating from the cost-effective material 4-HO-TEMPO (US\$7 per kg). Both sulfuric acid and potassium bicarbonate in the reaction are commercially available and the target product is estimated to be US\$3.9 per kg which is affordable to large-scale application for ESSs (P9). While the sulfonation reaction has poor controllability, that is, it is difficult to control (P6 & P7) either the modification site or the number of sulfonic acid groups.

Oxidation. The oxidation reaction is a method commonly used in ORAM modification. The oxidized reagents can be Cr(IV), KMnO₄, K₂Cr₂O₇, H₂O₂, and O₂ etc. The oxidation of benzene, biphenyl, naphthalene, anthracene, and phenanthrene molecules can obtain different types of quinones. For instance, DHBQ is prepared by the oxidation of hydroquinone under alkaline conditions. The reaction is simple and does not require harsh conditions (P4, P5, P6, P7 & P8).¹²² The reaction yield is high (P2) without expensive catalysts (P9) which are available for large scale production. The HNQ was also synthesized from 2-naphthol US\$19.7 per kg (Aladdin) via a chemical oxidation of O₂ and NaOH for 2.5 h.¹⁵³

AQDS and DHAQ as typical AQ derivatives could be obtained from anthracene. They are estimated at about US\$0.92 to US\$3.92 per kg calculated from a techno-economic model and such a low cost meets the US\$4.02 per kg goal of the Department of Energy (DOE) at the industrial scale (P9).¹⁵⁴ These AQ derivatives are launched from anthracene which is obtained by crude tar distilling and refining.^{155,156} An active quinone center was introduced by oxidizing under an air atmosphere at elevated temperature, then following the functional modification process (Fig. 16). Another way is to alkylate grafting the specific groups on the anthracene molecule firstly, and then oxidizing them to obtain the AQ derivative product.¹⁵⁷ The Aziz group recently introduced the electrochemical oxidation of an anthracene derivative to a redox-active AQ at room temperature (P4 & P6) in a flow cell without the use of hazardous oxidants (P5) or noble metal catalysts (Fig. 17). The *in situ* generated AQ electrolyte was used without further modification or purification. This potentially green electro synthetic method can also be applied to another anthracene-based derivative and may be extended to other redox-active aromatics.¹⁵⁸

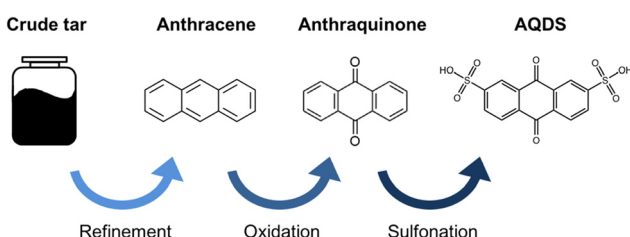


Fig. 16 Schematic overview of the production process to generate AQDS from coal tar. Adapted with permission from ref. 157. Copyright 2018 IOP Publishing Ltd.

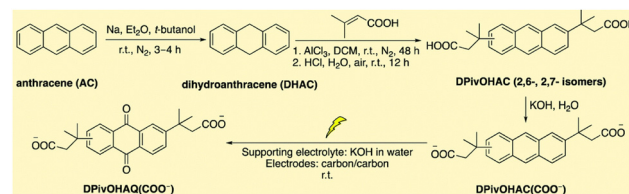


Fig. 17 The synthetic route and conditions of DPivOHAQ starting from anthracene. Adapted with permission from ref. 158. Copyright 2020 The Royal Society of Chemistry.

Alkylation grafting. Alkylation grafting reactions have been widely used to decorate the hydrophilic groups ($-\text{PO}_3^{2-}$, $-\text{CO}_2^-$, $-\text{SO}_3^-$, $-\text{NR}_4^+$, $-\text{O}^-$) on aromatic rings of ORAMs. For bipyridine derivatives, it is a highly targeted reaction using halogenated alkyl reagents or nucleophiles to quaternize the nitrogen embedded in the pyridine ring to produce highly soluble species.^{119,121,127,129} A current synthesized strategy of hydrophilic alkylation grafting is that nitrogen alkylating reagents are limited including high cost (P9), less efficient and low yield (less than 60%, P2). More troubling is that the ion-exchange steps of counteranions are always inevitable (P4), e.g., from bromide to chloride. A high-yield (70%) hydrothermal synthetic approach tailored for a viologen derivative (chloride form) with a cost-effective reagent (3-chloro-2-hydroxypropyl trimethylammonium chloride, commonly known as dextrosil) has been designed and yields a large quantity on a lab scale (609 g product).¹²⁹ The cost of target product, Dex-Vi, was calculated to be US\$6.8 per A h (US\$0.30 per g) on a lab scale and it was further estimated to be US\$8.7 per kA h on an industrial scale (P9). It is worth noting that the ion-exchange step is not required in this way which effectively slims the synthesis route and reduces the cost in large-scale preparation (P4). The TMAP-TEMPO was synthesized by a two-step reaction of alkylation on the oxygen (33.4% yield) of hydroxyl and quaternization (63.3% yield). The reaction is relatively simple and doesn't require sensitive catalysts, a long time or high temperature (P6 & P8), but the overall yield is too low (21%, P2) and the crude products obtained by alkylation need to be purified by column chromatography which is not attractive in industrial production (P4). The cationic grafting of 4-hydroxy-TEMPO was prepared by a one-step reaction between the hydroxyl group of 4-hydroxy-TEMPO and the epoxy group of the glycidyltrimethylammonium cation (GTMA^+) and this approach was a typically feasible and affordable example (P4).¹³³ The grafting method is more general for phenazine and AQ molecules. Grafting reactions specifically include bromination/iodination and then substitution, and some products also involve the reduction and hydrolysis processes. Such reactions could introduce hydrophilic substituents at different positions of phenazine and AQ thus yielding a series of derivatives.^{114,136} The target product can be obtained by simple filtration which is beneficial to reduce the purification cost (P4 & P9). As for grafting reactions, a series of phenazine derivatives start from the corresponding brominated phenazines with acrylates.^{136,137,159} A three-step approach involving alkylation, alkene reduction and hydrolysis has been

carried out to yield phenazine derivatives with pendant carboxyl alkyl groups and the overall yield is nearly 65%. Fc molecules including C_x -FcNCl ($x = 1, 2$, and 3), $Fc_2N_2Br_2$,¹⁶⁰ $Fc-SO_3Na$ are synthesized through direct alkylation. For the FcNCl molecule, it is easy to scale up by using low-cost commercial materials and the process is simple at a high yield of 90–95% (P2). The material price of FcNCl has been estimated around US\$3 per kg (P9).

Coupling. The coupling and cyclization reactions are also used to construct diverse viologen derivatives.^{146,161} However, it is worth noting that the reaction conditions of both coupling and cyclization reactions are relatively strict involving multi-step reactions and complex processes which are not conducive to the cost reduction or scalable preparation (P2, P4 & P9). The conditions of coupling and cyclization are always rigorous involving elevating temperature, long time, extra catalysts, column chromatography, etc (P2 & P8). Hence, the reported coupling methods in FB have a lack of cost advantages (reagent cost, time cost, and additional disposal, P9), especially in large-scale production compared with simple hydrophilic alkylation grafting.

Condensation reaction. DHPS, HP, AHP and BHPC phenazines were synthesized by condensation reaction. The corresponding *ortho*-phenylenediamines and BQs which possessed hydrophilic groups were used as precursors to fabricate the phenazine derivatives. *ortho*-Phenylenediamines accounted for the main cost of the products. For instance, 3,4-diaminobenzoic acid is US\$243.8 per kg (Local) and 3,4-diaminobenzenesulfonic acid is US\$1598.2 per kg (Adamas). Most of these phenazine derivatives are of relatively good yield except for AHP (35%) and the estimated prices of these products on a lab-scale are acceptable at US\$0.22 per g (HP), US\$0.47 per g (AHP) and US\$1.86 per g (BHPC) respectively which are economically promising and competitive (P2 & P9). The synthesis of phenothiazine derivatives also involves condensation processes, although they are commercially available.

Additionally, the Mannich reaction on a biphenol substance can be a low-cost and feasible process with a yield of 94% (P2 & P4), in which all the solvents and reagents are commercially available which are conducive to scale up (P9).¹⁶² In addition to the general synthesis method, manipulating the intermolecular interactions between different components (ORAMs, solvents, supporting salts, additives, the counter RAMs, and other surroundings) is a trouble-free strategy to tune the ORAM solubility directly such as eutectic electrolytes,^{150,163–167} hydrophilic additives¹³⁹ and electrochemical reversibility by incorporating ionic liquid-like ions in the supporting electrolytes to interfere with the solvation structure of ORAMs.¹⁶⁸

Inspired by naturally occurring bio ORAMs, some trials have been applied using natural dye (indigo carmine which can be extracted from plants of the genus *Indigofera*),¹⁶⁹ lignin¹⁷⁰ from plants and phoenicin by biosynthetic approaches involving scalable amounts by *Penicillium astrosanguineum* (P3) (Fig. 18).¹⁷¹ However, these ORAMs delivered limited solubility

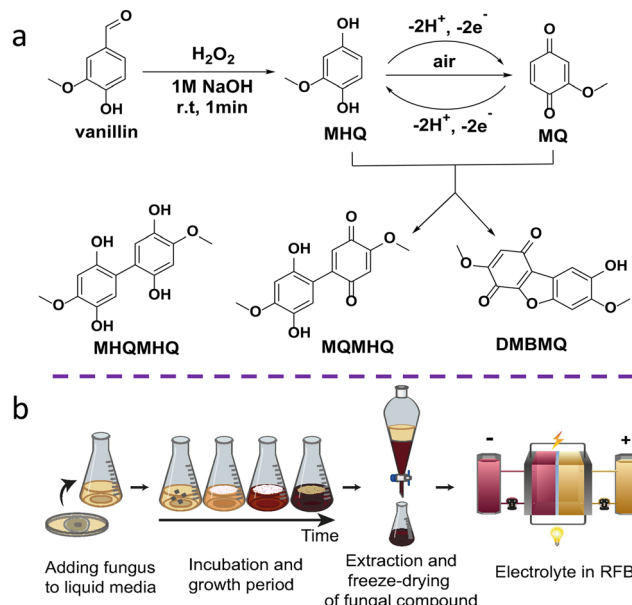


Fig. 18 (a) Oxidation of vanillin to MHQ, redox reaction to MQ and potential insoluble dimeric side-products MHQMHQ, MQMHQ, and DMBMQ. (b) Schematic representation of the workflow to produce the redox-active fungal compound phoenicin, which can then be directly used to prepare the FB electrolyte. Adapted with permission from ref. 171. Copyright 2023 Wiley-VCHGmbH.

and poor reversibility, and the method needs to be optimized for high-performance ORAMs in the future.

One crucial thing to note is that most organic ORAMs are sensitive to air, and more precisely, organic ORAMs are prone to react with oxygen, resulting in an irreversible capacity decay (P1).¹⁷² The oxygen-sensitive possibility has been identified from previous works, such as viologen, ferrocene and quinone.^{110,173–175} Some oxidizing agents, e.g. extremely reactive superoxides and hydrogen peroxide, are prone to attack the sensitive intermediates thus leading to deactivation.¹⁷⁶ In order to keep the redox stable and maintain a long battery lifetime, most FBs assembled with organic ORAMs are running under inert-gas protection in a purge-box or a glove-box. Although some works have proposed air-stable organic ORAMs, more efforts in understanding the mechanism and exploring more promising air-insensitive structures for practical application are required.^{124,140,143,150,177}

2.2.3 Safety & environmental sustainability. As we discussed above, many organic synthetic processes require a large number of organic solvents and even some toxic reagents to obtain the target molecules which is a challenge for sustainability (P5 & P7). While the *in situ* synthesis and plant extraction methods look more desirable. Meanwhile, ORAM regeneration is also a possible approach to extend the battery lifetime and meet the goal of low-cost and sustainability. The degradation product of AQ molecules revealed that it could be regenerated by chemical or electrochemical means and the renewed capacity is close to the initial capacity. Surprisingly, the capacity loss in some AQ-based AOFBs could also be recovered by air

exposure.^{178–181} ORAM regeneration is of significance for the construction of low-cost, high economic benefit and environment-friendly long-term ESS.

On the other hand, we know that some quinones, alloxazines, can be obtained from living beings, but some are toxic. For instance, MV, also known as paraquat, is a commercial herbicide which has been banned in the U.S., China and European Union as it has alleged neurotoxicity (P5).¹⁸² Although the toxicity changes after modification, the better hydrophilicity makes viologen derivatives easier to mix into the water cycle and spread through the ecosystem posing serious challenges to the environment and safety for human beings and other creatures. Similar trends would occur on other ORAMs, however, there is a lack of sufficient data on the biological hazards of the newly-synthesized ORAMs.

The technical, environmental, and economic sustainability of ORAMs is based on the available synthetic routes and affordable precursors (P3 & P9). One of the most critical considerations for pilot application is cost including materials cost, service life and maintenance costs. The feedstocks should be accessible *via* facile and scalable routes from low-cost chemicals and the electrolyte should be robust, specifically air-stable, temperature-insensitive, and light-insensitive, etc. (P1, P4 & P9).

Hitherto, most of the design, synthesis, analysis, characterization, and performance evaluation of AOFBs are still at the lab-scale. There are not adequate reports on the preparation of industrial production and cost analysis, and most data are based on empirical analysis. This is because AOFBs are a relatively new field which is diverse and uncertain compared with traditional inorganic FBs. Recent studies have reduced the gap between AOFBs and inorganic FBs, but they still cannot meet the practical applications. The main concerns involve the ORAM stability under high concentration, economical and feasible synthetic routes, and accurate potential regulation.

3. Membranes

As the critical component of FBs, ion-conducting membranes (ICMs) act as the filter in FBs, permitting ion transport and restricting ORAMs.^{183–186} The selectivity, conductivity, and stability of ICMs are highly determined by the chemical and topological structure.¹⁸⁷ According to the membrane structure, ICMs in FBs are normally divided into dense ion exchange membranes (IEMs) with/without ion exchange groups and porous membranes with inherent or acquired pores, and composite membranes. In this section, the membranes with specific functions for different FBs will be reviewed and analysed (Table 3). The evaluation criteria for membranes are similar to those of ORAMs mentioned above, all of which comply with the sustainable principles (Table 1, P1–P9).

3.1 Technical sustainability

3.1.1 Morphology & performance

Dense IEMs. Dense membranes in FBs can be divided into charged membranes fixed with ion exchange groups and non-

charged membranes without charged groups but hydrophilic moieties. The IEMs contain cation exchange membranes (CEMs), anion exchange membranes (AEMs) and amphoteric ion exchange membranes (AIEMs). These charged IEMs contain ion exchange channels, benefiting from the hydrophilic clusters by positively or negatively charged ion exchange group aggregation.^{185,218} The microphase-separated structures are always spontaneously obtained as the polarity difference from the hydrophobic region and hydrophilic region.¹⁸⁷ Since the parameters such as lifetime and preparation are directly related to sustainability, the ideal membranes are required to have good dimensional and chemical stability, high conductivity and selectivity.

3.1.2 Perfluorinated based IEM. Perfluorinated sulfonic acid (PFSA) is known for its excellent mechanical properties and corrosion resistance. Nafion fluorinated ionomers were initially developed by the E. I. DuPont Company and successfully used in the field of ESS.^{219–221} Nafion series membranes have attracted considerable attention due to their high chemical stability, mechanical strength, dimensional stability, and ion conductivity.^{219,222,223} These advantages come from the hydrophobic polytetrafluoroethylene backbone and hydrophilic pendant sulfonic acid groups. The abundance of adjacent C–F bonds from the hydrophobic fluoropolymer mainchain gives Nafion ultra-high stability and hydrophobicity which makes it have strong resistance toward strong acidic and oxidizing species attack. While the hydrophilic side chains can spontaneously gather into ion clusters when entrusting or dispersion-casting due to its high flexibility.²²⁴

Nafion 115 membrane has been widely used in VFBs not only for single cell evaluation but also MW scale demonstration. However, the Nafion membrane has relatively low ionic conductivity in neutral solution, resulting in large overpotential polarization.¹⁹⁰ For alkaline systems, Nafion 212 should firstly be treated with NaOH/KOH supporting electrolytes, and a CE of 99% and VE of 86% were achieved at 80 mA cm^{-2} over 100 cycles in the zinc–iron FB.¹⁹¹ The alkaline treated Nafion 212 was also applied in AOFB, the DHAQ/K₄Fe(CN)₆ FB with Nafion 212 displayed a CE of 99% and a VE of 84% at 100 mA cm^{-2} over 100 cycles.¹²³

Here comes the limitation of redox species crossover thus leading to a low CE and continuous capacity decay. The morphology of the clusters is crucial to the selectivity and conductivity of membranes. The precise microstructure and ion cluster dimension control of Nafion is essential to improve the membrane selectivity. The disordered ion channels from the commercial Nafion membranes lead to a relatively low selectivity of protons/vanadium ions, while the precise construction of ion channels has been enabled by the Langmuir–Blodgett (LB) technique (Fig. 19a).¹⁹² The ordered and narrow ion channels in the as-prepared ultrathin PFSA membrane not only displayed extremely high impressive selectivity (500 times higher compared to the pristine Nafion membrane) but also required a small amount of PSFA which improved the utilization and efficiency and reduced the cell cost. It is believed that the PSFA layer-by-layer deposition restricts the expansion of ion

Table 3 Membranes with different structures and morphologies and evaluation for further production from a sustainable aspect

| No. | Types | Name | CE/% | EE/% | Current density/ cm^{-2} /mA | Cycle number | Application | Feasible or not | Green or not | Cost-effective or not | Ref. |
|-----|------------|-----------------------|------|------|---------------------------------------|--------------|---------------------|-----------------|--------------|-----------------------|------|
| 1 | Dense IEM | Nafion 212 | 92 | 81 | 80 | 50 | VFB | 5 | 2 | 2 | 188 |
| 2 | Dense IEM | Nafion 115 | 99 | 82 | 5 | >30 | Zn/I | 5 | 2 | 2 | 189 |
| 3 | Dense IEM | Nafion 115 | 93 | 73 | 40 | 100 | NZIFB | 5 | 2 | 2 | 190 |
| 4 | Dense IEM | Nafion 212 | 99 | 86 | 80 | 100 | AIZFB | 5 | 2 | 2 | 191 |
| 5 | Dense IEM | Nafion 212 | 99 | 84 | 100 | 100 | AOFB | 5 | 2 | 2 | 123 |
| 6 | Dense IEM | PC50NB30 (PFSA) | 94 | 78 | 200 | 800 | VFB | 2 | 2 | 2 | 192 |
| 7 | Dense IEM | Nafion/PVDF | 97 | 83 | 100 | 200 | VFB | 5 | 2 | 3 | 193 |
| 8 | Dense IEM | GO/Nafion | 98 | 83 | 80 | 200 | VFB | 3 | 2 | 1 | 188 |
| 9 | Dense IEM | Crosslinked GO/Nafion | 97 | 86 | 80 | 180 | VFB | 2 | 2 | 1 | 194 |
| 10 | Dense IEM | Nafion/h-BN/SPEEK | 95 | 91 | 40 | none | VFB | 1 | 2 | 1 | 195 |
| 11 | Dense IEM | SPEEK | 96 | 84 | 80 | 100 | VFB | 5 | 3 | 5 | 196 |
| 12 | Dense IEM | SPEEK | 95 | 78 | 40 | 30 | NZIFB | 5 | 3 | 5 | 197 |
| 13 | Dense IEM | SPEEK | 99 | 80 | 80 | 400 | AIZFB (pilot stack) | 5 | 3 | 5 | 57 |
| 14 | Dense IEM | SPEEK | 99 | 66 | 250 | 100 | AOFB | 5 | 3 | 5 | 198 |
| 15 | Dense IEM | PBI | 99 | 83 | 160 | 150 | AIZFB | 4 | 3 | 4 | 199 |
| 16 | Dense IEM | PBI | 99 | 88 | 80 | >300 | AIZFB (pilot stack) | 4 | 3 | 4 | 200 |
| 17 | Dense IEM | PBI | 99 | 80 | 200 | 500 | VFB (pilot stack) | 4 | 3 | 4 | 201 |
| 18 | Dense IEM | QPPP-2 | 99 | 86 | 80 | 100 | VFB | 2 | 4 | 1 | 202 |
| 19 | Dense IEM | CSPI-DMDA | 99 | 78 | 160 | 1000 | VFB | 2 | 3 | 3 | 203 |
| 20 | Dense IEM | PBPip | 96 | 85 | 120 | 500 | VFB | 3 | 3 | 3 | 204 |
| 21 | Dense IEM | CQSPK | 98 | 81 | 60 | 100 | VFB | 2 | 2 | 2 | 205 |
| 22 | Porous ICM | M3 | 95 | 76 | 80 | >200 | VFB | 5 | 5 | 5 | 206 |
| 23 | Porous ICM | CPSF-Py | 97 | 83 | 100 | 130 | VFB | 5 | 5 | 5 | 207 |
| 24 | Porous ICM | CMPSF | 99 | 86 | 80 | 6000 | VFB | 5 | 2 | 4 | 208 |
| 25 | Porous ICM | M20-24 | 99 | 90 | 80 | 120 | VFB | 5 | 5 | 4 | 209 |
| 26 | Porous ICM | M(IPA)-24 | 99 | 90 | 80 | 450 | VFB | 5 | 5 | 4 | 210 |

Table 3 (continued)

| No. | Types | Name | CE/% | EE/% | Current density/ mA cm^{-2} | Cycle number | Application | Feasible or not | Green or not | Cost-effective or not | Ref. |
|-----|------------|----------------------|-------------|--------|--------------------------------------|--------------|-------------|-----------------|--------------|-----------------------|------|
| 27 | Porous ICM | PS-IPA | 98 | 90 80 | | 500 | VFB | 5 | 5 | 4 | 211 |
| 28 | Porous ICM | NaCl-5 M | 99 | 89 90 | | 10000 | VFB | 5 | 5 | 4 | 212 |
| 29 | Porous ICM | PFBA-QA-p | 98 | 91 80 | | 300 | VFB | 3 | 3 | 3 | 213 |
| 30 | Porous ICM | PIM-1/PAN | 97 | 90 20 | | 100 | VFB | 3 | 2 | 3 | 214 |
| 31 | Porous ICM | DMBP-TB ⁺ | 99 | 80 150 | | 100 | VFB | 3 | 2 | 3 | 215 |
| 32 | Porous ICM | AO-PIM-1 | >99.8% >60% | 80 | | >200 | AOFB | 3 | 2 | 3 | 216 |
| 33 | Porous ICM | PIM-EA-TB TFC | >99.8% >60% | 80 | | >200 | AOFB | 3 | 2 | 3 | 216 |
| 34 | Porous ICM | IP2-0.15 | 99 | 80 260 | | 1000 | VFB | 3 | 2 | 4 | 217 |

Score 5 indicates that the corresponding process is highly likely to be feasible, cost-effective and green enough. Score 4 indicates that the corresponding process is likely to be feasible, cost-effective and green enough. Score 3 indicates that the corresponding process may be feasible, cost-effective and green, but there is still some uncertainty. Score 2 indicates that the corresponding process may be less feasible, cost-effective and green. Score 1 indicates that the corresponding process is likely to be unfeasible, not cost-effective and green and even associated with some risk.

channels thus leading to confined ion channels and hindering vanadium crossover. The VFB cell with the remoulded Nafion membrane exhibited stable cycling (800 cycles) and higher EE of 75% than the Nafion 211 (73%) at 200 mA cm⁻². Nafion is one of the most reliable ICMs across all types of FBs, but the high price and the limitations on battery performance make it encounter a barrier in further application. Nafion composite membranes are prepared by combining the advantages of different functional polymers. To alleviate the unmanageable swelling issue of Nafion, polyvinylidene fluoride (PVDF) was introduced in the Nafion/PVDF blends.¹⁹³ The water uptake of polymer blends decreased upon PVDF addition while the mechanical strength increased which confirmed that PVDF can reinforce the mechanical properties and suppress the water adsorption of polymer blends. The vanadium ion permeability and capacity decay were alleviated by the miscible strategy. A Nafion/PVDF blend membrane with 60 wt% Nafion exhibited an improved 83% EE at 100 mA cm⁻² and a stable cycling performance with no obvious efficiency decay after 200 cycles.

In order to elevate the membrane selectivity, graphene oxide (GO)/Nafion composite membranes were prepared by spin coating orientated GO nanosheets on the Nafion substrate.¹⁸⁸ Vanadium ions could be blocked by the barrier effect of orientated GO. The vanadium cross-contaminant was mitigated while the proton conduction was retained. The GO/Nafion composite membranes rendered improved CE of 92.9–98.8% and EE of 81.5–88.4% at 20–100 mA cm⁻². Besides, further cross-linking was achieved on the basis of the orientated GO layer and the improved cell performance was achieved.¹⁹⁴ Similarly, a composite membrane of sandwich structure, Nafion/hexagonal boron nitride (h-BN)/sulfonated poly(ether

ether ketone (SPEEK), was designed by space-confined chemical vapor deposition (CVD).¹⁹⁵ This sandwiched membrane showed a distinguished improvement in proton/vanadium ion selectivity. The thought of nanoparticle (WO₃, TiO₂, ZrO₂, SiO₂), nanotube (CNT) and nanosheet (GO, MoS₂, g-C₃N₄) doping into Nafion membranes was put forward to introduce versatile functional sites.^{208,212,213,225–227}

3.1.3 Other dense IEMs. Although PSFA membranes have been commercialized and widely used in many fields, the cost is very high (*e.g.*, DuPont's Nafion, US\$500–800 per square meter).²²² Some alternative IEMs with diverse structures and more attractive cost advantage have been considered, especially for non-fluorinated IEMs. The non-fluorinated polymers can be divided into polyolefin and aromatic polymers according to the backbone. The aromatic polymers are widely regarded as the more stable structure with π - π dissociation energy compared with polyolefin.²²⁸

The sulfonated poly(ether ether ketone) (SPEEK) membrane with good mechanical properties and high conductivity has been used in various FBs. The *in situ* and *ex situ* oxidative experiments showed that the sulfonic acid functional group, as a strong electron-withdrawing group (EWG) fixed on the aromatic backbone made the main chain charge distribution uneven which is vulnerable to attack by oxidative species and finally accelerated the degradation of the SPEEK membrane (Fig. 19b).¹⁹⁶ More specifically, the protonated ether structure in strong acid solution together with the adjacent strong EWG induced a strong electrophilic site on the backbone, which can be heavily affected by oxidative vanadium oxygen species. Therefore, the future work on highly-stable VFBs membranes should be focused on hetero-atom free main chains meanwhile

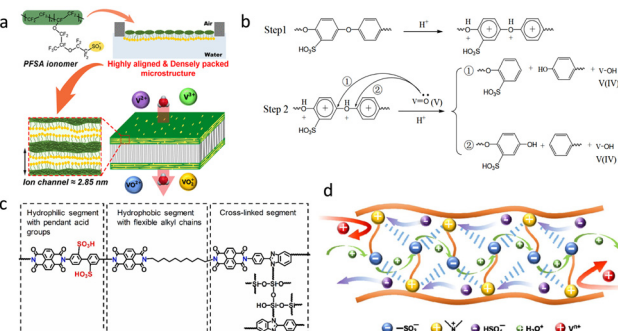


Fig. 19 (a) Ultra-thin and highly ordered PSFA membrane prepared using the LB technique. (b) The degradation mechanism of SPEEK in VFBs. (c) The covalent-crosslinking structure of CSPI-DMDA. (d) The ionic-crosslinking PBPip membrane for VFBs. Adapted with permission from ref. 192. Copyright 2020 American Chemical Society. ref. 196. Copyright 2014 the Owner Societies. ref. 203. Copyright 2021 Elsevier B.V. ref. 204. Copyright 2019 American Chemical Society.

to escape from the negative effects of functionalized groups. In an alkaline zinc–iron FB, a K^+ -formed SPEEK was applied which resulted in a CE of 95% and an EE of 78% at 40 mA cm^{-2} in 30 cycles.¹⁹⁷ A 4 kW AZIFB stack with the SPEEK membrane showed a high EE of 85.5% operated at 80 mA cm^{-2} and long-term stable cycling over 400 cycles (800 h).⁵⁷ The SPEEK membrane featured both good mechanical properties and high chemical stability under strong alkaline conditions which was considered a promising alternative with low cost compared to Nafion. In AOFB, the DHAQ/ $\text{K}_4\text{Fe}(\text{CN})_6$ cell with the SPEEK membrane displayed a competitive cell performance of 99% in CE and 67% in VE at 250 mA cm^{-2} over 100 cycles.¹⁹⁸ A 40% decrease in capacity decay per day, a 10% power density increase and an 85-fold decrease in the permeation of ferricyanide was achieved by replacing Nafion with a SPEEK membrane. It is a better choice for AOFB than the commercially available Nafion.

It is noted that the ion exchange groups, *e.g.*, sulfonated or quaternary ammonium groups may bring about the challenge of instability under the strong oxidative or alkaline conditions, especially when the EWGs directly click on the main chain or there is a weak covalent bond (ether or amide) nearby.^{196,229,230} Accordingly, an alternative strategy is to design charge-free IEMs, such as polybenzimidazole (PBI) membranes.²⁰⁰ Different from charged IEMs, the dense PBI membrane does not have a distinct microphase-separation structure and it conducts ions by the electrolyte soaking in the membrane. Abundant hydrogen bonding networks (structure diffusion) are formed when absorbing adequate electrolyte especially in acidic or alkaline solution.²³¹ This large number of hydrophilic sites can be efficiently protonated in strong acid solution or deprotonated in alkaline solution to achieve hydrophilicity and the construction of ion transport channels enabling protons or hydroxyls to hop in the hydrogen bonding of the PBI membrane.^{231–233} Many efforts have been devoted to PBI modification to pursuing better battery performance.^{234–237} Introducing uncharged functionalized flexible chains into the backbone can increase

hydrophilic sites strengthening the hydrogen bonding network and regulating the morphology of the PBI membrane.^{238,239} A self-made PBI membrane with a dramatic elasticity modulus of 2.9 GPa was first applied for AZIFB which could easily avoid the membrane damage caused by zinc dendrites.¹⁹⁹ Additionally, the PBI membrane showed good endurance in alkaline solution (3 M NaOH) at 30 °C for a month and such a treated PBI membrane still provided a long-term cycling performance of AZIFB (500 cycles). A 1 kW alkaline Zn–Fe flow stack was executed based on the H_3PO_4 –PBI membrane and the CE of 99% and an EE of 88% over 300 cycles were successfully achieved at 80 mA cm^{-2} .²⁰⁰ The H_3PO_4 –PBI membrane was also available in VFBs.²⁰¹ The membrane conductivity was improved by the weak Donnan effect in the acidic solution. A 3 kW VFB stack equipped with H_3PO_4 –PBI membrane demonstrated a CE of 99% and an EE of 80% over 500 cycles at 200 mA cm^{-2} without performance decay.

In light of the above design, an ether-free structure, poly(*p*-phenylene)-based AEM was fabricated through a Ni-catalyzed cross-coupling reaction.²⁰² The strong aryl–aryl linkage in the backbone is a strong support to construct a robust aromatic membrane for VFBs. The as-prepared ether-free membrane, quaternized poly(*p*-phenylene)-based copolymer (QPPP-2) showed low vanadium ion permeation ($2.12 \times 10^{-9} \text{ cm}^2 \text{ min}^{-1}$), high anion (Cl^- , SO_4^{2-} , and OH^-) conductivity (6, 2.5, 17 mS cm^{-1} at 25 °C and 17, 8, 28 mS cm^{-1} at 60 °C respectively) and an outstanding efficiency of 99% CE, 87% VE and 86% EE over 100 cycles at 80 mA cm^{-2} .

In addition to the backbone selection, the stability and structure of the side chains also play a vital role in membrane morphology and stability.^{192,202–204,219,224,228} An ideal side chain should be stable under strong acidic and oxidizing conditions and it can effectively form a distinct microphase-separated structure to suppress excessive swelling of IEMs. The resulting precise ion transport channels can substantially enhance the proton conductivity and effectively block vanadium ions.

The covalent-crosslinking and/or ionic-crosslinking (*i.e.* AIEM) structures are obtained when the side chain is anchored on another adjacent main chain or side chain. The limited segment movement of polymer chains and interlocking network in these types give the membranes lower water uptake, a lower swelling ratio, higher dimensional stability and mechanical properties.¹⁸⁷

A crosslinked sulfonated polyimide (CSPI-DMDA) membrane was prepared for VFBs by one-step polycondensation and following a solution cast method (Fig. 19c).²⁰³ There was a distinct microphase-separation structure observed in the atomic force microscope (AFM) phase images which can be attributed to hydrophobicity with aliphatic groups and a hydrophilic moiety with aromatic groups of the backbone of the CSPI-DMDA membrane. The optimized CSPI-DMDA (1:1) membrane provided a much lower permeability of vanadium ions (nearly 1/20 of Nafion 115) and a better proton conductivity (nearly 9-fold higher). As expected, the single cell delivered an improved cell performance of 99.2% CE, 76.0% VE and

75.3% EE at 200 mA cm⁻² and there was no obvious efficiency decay over 1000 cycles at 160 mA cm⁻².

The ionic-crosslinking membranes (AIEM) have both negatively charged and positively charged groups and the electrostatic interactions between the polymer chains narrowed the ion transport channels thus possible improving proton/vanadium ion selectivity (Fig. 19d). The amphoteric side chain delivered a high ion-exchange capacity (IEC) of 4.19 mmol g⁻¹ accomplishing excellent conductivity and low area resistance.²⁰⁴ The ionic-crosslinking structures also resulted in a low swelling ratio of 13.9% and low VO₂⁺ permeability (1.31×10^{-8} cm² s⁻¹). There was no obvious efficiency decay in cycling testing indicating that despite having a large number of ion exchange groups, high stability can be obtained as long as the ion crosslinking had been attained.

Dual-crosslinking, that is both ionic crosslinking and covalent crosslinking, has also been used.²⁰⁵ Different from a regular polymer blend, the cross-linked AIEM with a six carbon chain (CQSPK) membrane exhibited good stability which maintained a stable cell performance during a cycling test over 100 cycles with a CE of 98.4% and EE of 81.4% at 60 mA cm⁻². Although this performance does not reach the researchers' expectations, this strategy can be used as a reference for the construction of highly stable IEMs.

Porous membranes. In a porous membrane, the transport of charge carriers is mainly tuned by the pore size, facilitating the conductivity of the membrane. The selectivity in a porous membrane is mainly achieved by the porous sieving mechanism. Hence, the pore size control and the pore architecture are key factors for the selectivity and conductivity of porous membranes.

3.1.4 Porous membranes with acquired pores. Polyacrylonitrile (PAN) nanofiltration membranes were employed *via* a typical nonsolvent induced phase separation (NIPS) method for VFBs.²⁰⁶ The birth of the nanofiltration membrane can be traced back to the 1950s when the Loeb-Sourirajan (L-S) cellulose acetate (CA) membrane was used for the desalination of seawater. Unlike ultrafiltration membranes or reverse osmosis (RO) membranes, the nanofiltration membrane's morphology and pore size are suitable for FBs and will neither cause a serious cross-contamination of the cathode and anode nor bring high membrane resistance. A CE of 95% and EE of 76% at 80 mA cm⁻² demonstrated the PAN nanofiltration membrane was available for VFBs which was a pioneering work (Fig. 20a). After the first successful trial, lots of porous membranes for VFBs have been reported such as the polysulfone/sulfonated poly(ether ether ketone) (PSF/SPEEK) blend.^{206,225,240}

Bulky sponge-like pores were prepared by a vapor induced phase inversion (VIPI) method and this novel porous chloromethylated poly-sulfone formed in a pyridine aqueous solution (PSF-Py) membrane accompanying positive charges on pore walls showing better cell performance than Nafion 115 in VFB (Fig. 20b).²⁰⁷ The high selectivity and proton conductivity are attributed to the Donnan repulsion from charged pore walls

and size exclusion of spongy pores. Furthermore, a crosslinked imidazole on the pore walls of the polysulfone (PSF) membranes can enhance the mechanical strength of the porous membrane.²⁰⁸ A single cell with the as-prepared pore-wall crosslinked membrane delivered a CE of 99%, an EE of 86% at 80 mA cm⁻² and a stable cycling performance of 6000 cycles indicating the strategy of pore-wall crosslinking was capable for VFBs.

The main challenge of the porous membrane is the precise control of pore structure, especially using the NIPS method. A solvent pre-treatment method was introduced when preparing a porous poly(ether sulfone) (PES) membrane.²⁰⁹ Immersing in IPA will bring about a game of pull-and-push between swelling force and cohesive force which allow the PES polymer chain to rearrange. Along with the IPA treatment time, these two forces oriented in the opposite direction were reached in equilibrium thus stabilizing the polymer morphology. The balance between swelling force and cohesive force would be tipped when the solvent evaporated from the pores. And the swelling force gradually decreased as less IPA remained and the pore started shrinking. The porous PES membrane with well-defined pores was finally obtained. Compared with the untreated porous PES membrane, both the average pore size and porosity markedly decreased (from 22.79 nm, 95.77% to 3.99 nm, 76.20%). In VFB, a CE of nearly 99% and an EE of over 90% at 80 mA cm⁻² was obtained by the uncharged porous PES membrane indicating the solvent treatment method could effectively narrow the pore. The solvent treatment method was further optimized by tuning the treating solvents, solvent composition, solvent evaporation temperature, treating time and initial morphology of the porous membrane.^{210,241} The interconnected pores can be employed in the PBI matrix by the solvent treatment to further improve the PBI conductivity.²⁴² The polymer–solvent interaction was engaged in constructing porous PBI membranes with tunable morphology. A CE of 99.29% and an EE of 81.93% at 200 mA cm⁻² have been realized by applying the porous PBI membrane in VFBs. The prepared porous PBI membrane combined the advantages of PBI polymer and porous membrane.

PES/SPEEK (PS) blend membranes with a slit-like selective layer were reported (Fig. 20c).²¹¹ Some PS membranes treated with different solvents, PS-water, PS-EtOH and PS-IPA possess different morphology due to the instantaneous demixing (PS-EtOH) and delayed demixing (PS-IPA). There are some oriented strips and slits on the top surface of all these PS membranes because of the polymer chain rearrangement. This phenomenon could be attributed to surface segregation of PES and SPEEK polymer chains.²⁴³ An uneven distribution of different polymer chains resulted in an asymmetric morphology during phase inversion in nonsolvent coagulation baths. The compact thick skin including narrow slits and sponge-like supporting substrate were in favor of proton conduction and it achieved a new balance between proton/vanadium ion selectivity and an improved ion conductivity.

The concept of salt-solution-induced phase separation has been proposed which is a good attempt to lower the

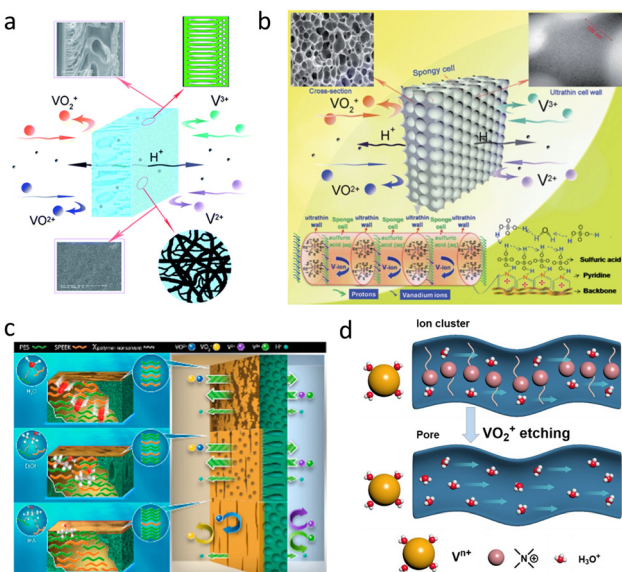


Fig. 20 (a) The ion transport mechanism in the PIM layer. (b) The Tröger's Base (TB) membranes for VFBs. (c) Chemical structures of the functionalized PIM. (d) The ultra-thin microporous membrane obtained by interfacial polymerization. Adapted with permission from ref. 206. Copyright 2013 American Chemical Society. ref. 207. Copyright The Royal Society of Chemistry. Ref. 211 and 213 Copyright 2012 The Royal Society of Chemistry.

environmental impact from the volatilization of organic solvents.²¹² The well-tuned pores from finger-like pores to sponge-like pores by adjusting the ion strength of the coagulation bath have been accomplished. The more compact membrane would lead to a positive effect on preventing vanadium crossover without sacrificing proton conductivity, improving the selectivity of the membrane for VFBs. The prepared sponge-like PBI membrane exhibited a long-term cycling test which remained stable over 10 000 cycles of charge and discharge processes at 160 mA cm^{-2} .

Oxidation, a recognized challenge to membrane stability, may not always be unfavourable. One strategy is to introduce macropores into the membrane by using the oxidation differences between the main chains and side chains which renders a new way for preparing highly stable porous membranes with a microstructure from aggregated ion clusters in dense membranes (Fig. 20d).²¹³ A partial etching process both *in situ* or *ex situ* was executed to make side chains detach from the main chain *via* high levels of oxidation thus leading to micropores. Some relatively unstable side chains anchored on the ether-free main chain with high stability under oxidizing conditions then detached from the main chain and left specific spaces, *i.e.*, pores in the polymer matrix.

3.1.5 Porous membranes with inherent pores. Polymers of intrinsic microporosity (PIM) have recently attracted considerable attention in ESS.²⁴⁴ Rigid aromatic units and contorted linking groups ensure space-inefficient packing which provides the polymer with large surface areas and void space, *i.e.*, free volume. Different from conventional microporous polymer

materials, most of these inherent micropores are always nano- or sub-nanoscale which are well suited for tuning the structure-activity relationships between ions and ion channels.

The sizes of hydrated protons and hydrated vanadium ions are around 0.24 nm and 0.6 nm respectively, so a membrane with a pore size within this range can effectively conduct protons and block vanadium ions theoretically. The mechanical stability of the PIM has been a concern, especially in the case of the long-term compression and continuous erosion in VFBs. PIM-based composite membranes with robust substrates are proposed. The PIM-1/PAN composite membrane was prepared by coating PIM-1 on the PAN ultrafiltration membrane with $\sim 750 \text{ nm}$ PIM-1 selective layer which was expected to effectively transfer hydrated protons while blocking the hydrated vanadium ions with the intrinsic subnano-pores of less than 2 nm (Fig. 21a).²¹⁴ Although PIM-1 is a hydrophobic material and has a limited swelling in aqueous solution, the interconnected pores were found to be capable of water permeation. A single cell fabricated with this nanocomposite membrane delivered a CE of 97% and an EE of around 90% at 20 mA cm^{-2} over 100 cycles.

Another example of microporous polymers for VFBs was Tröger's Base (TB) membranes. Aromatic units and ladder-shaped linking groups with high rigidity and contortion enable the polymer with high microporosity. Some TB membranes, 4,4'-diamino-3,3'-dimethyl-biphenyl (DMBP-TB⁺) and 4,4''-diamino-3,3'-dimethylphenylmethane (DMDPM-TB⁺) have inherent subnano-pores in TB membranes which allow fast proton transfer *via* the Grotthuss mechanism while the hydrate vanadium ions ($\sim 0.8 \text{ nm}$) are impeded by steric hindrance ($\sim 0.67 \text{ nm}$) and coulombic repulsion (protonated amine) (Fig. 21b). Meanwhile, the N-rich polymer skeleton further facilitates proton transport. An attractive proton permeability ($8.19 \times 10^{-5} \text{ cm s}^{-1}$), a low resistance ($0.57 \Omega \text{ cm}^2$), and the proton/vanadium ion selectivity of a high level of 6374 were achieved in the DMBP-TB⁺ membrane.²¹⁵

Combining the advantages of intrinsic microporosity contributed by rigid units or Tröger's base, hydrophilic microporous membranes with precise ion channels (subnanometer) were designed to achieve rapid conduction of charge carriers and efficient blocking of organic species by size-exclusion effect (Fig. 21c).²¹⁶ As specific hydrophilic sites, the amidoxime groups and Tröger's base have fast ion conduction. Both AO-PIM-1 and PIM-EA-TB possess high porosity and a narrow pore size distribution of 2–8 Å which is lower than the $\text{Fe}(\text{CN})_6^{3-}$ anions ($\sim 9.5 \text{ Å}$). The AO-PIM-1 and PIM-EA-TB demonstrated the desirable selectivity of K^+ over Mg^{2+} is up to 30–40. The FMN-Na| $\text{K}_4\text{Fe}(\text{CN})_6$ batteries assembled with AO-PIM-1 and PIM-EA-TB membranes showed impressive long-term cycling stability. The capacity retention of 84.5% and 86.5% over 200 cycles at 80 mA cm^{-2} were achieved by AO-PIM-1 and PIM-EA-TB respectively. Moreover, more hydrophilic ionizable amidoxime and sulfonic acid groups are introduced to improve the hydrophilicity of PIM membranes.^{245–247} The functional PIM membrane is expected to be more outstanding in the field of AOFB membrane design.

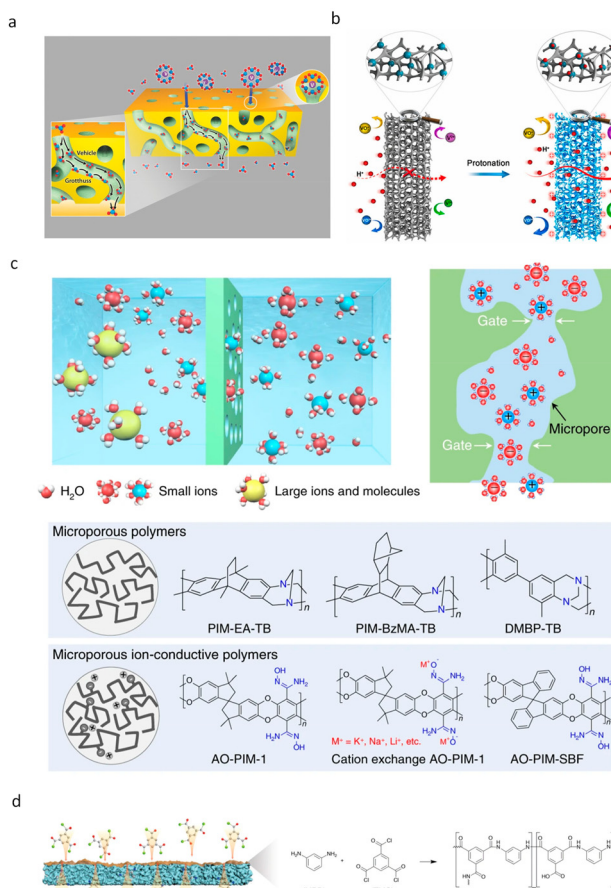


Fig. 21 (a) The preparation process of carbon felt: from materials to product. (b) The IFF and SFF from a Bi-catalyzed ICFB. (c) The CNF/CNT composite catalysts loaded on CF VFB electrode. (d) A sandwich-like electrode (SPHC) for ZBFBs. Adapted with permission from ref. 214. Copyright 2016 WILEY-VCH Verlag GmbH & Co. KGaA, Weinheim. Ref. 215. Copyright 2021 Elsevier B.V. Ref. 216 and 217. Copyright 2020 Nature.

The microporous structure can not only be obtained by a rigid bridging moiety, but can also be constructed by an ultra-thin selective layer. A thin-film composite membrane (TFCM) with uncovered microporosity (sub-1 nm) was found to make a breakthrough in ion selectivity and conductivity for VFB membranes (Fig. 21d).²¹⁷ The highly cross-linked ultrathin PA selective layer (~ 180 nm) delivered the “ridge-and-valley-like” structure and some voids positioned at the junction of the PES SPEEK porous substrate.

3.2 Membrane preparation

The preparation of membranes generally involves two processes: monomer polymerization and manufacturing technology.

3.2.1 Polymerization. The main polymerization method in FB membranes is random copolymerization. Some polymerization reactions require high temperature (P6 & P8). For instance, perfluorosulfonic acid polymers are prepared by copolymerization of a series of perfluorinated comonomers under high temperature (always over 200 °C) induced by peroxide

initiators.^{220,248} The commonly-used fluorinated monomers including ethanesulfonyl fluoride and tetrafluoroethylene are prepared with 2-chloro-1,1,1-trifluoroethane at high temperatures (800 – 1000 °C) and hexafluoropropylene. Different monomers in copolymerization will lead to large differences in polymer structure, molecular weight, and distribution. Functional groups can be introduced into polymers through both the polymerization of functionalized monomers and the post-modification after polymerization. For instance, SPEEK is to sulphonate the poly(ether ether ketone) (PEEK) by heating it (40 °C) in highly concentrated sulfuric acid (98 wt%). Sulfonic acid groups are successfully introduced into PEEK and the polymer changes from hydrophobic to hydrophilic thus leading to a great decrease in membrane resistance. PBI membranes are generally prepared by a condensation reaction of various diamines and carboxylic acids monomers under heating within a common temperature range of 100 – 200 °C, PBIs use a variety of main chains with benzimidazole moieties which are expected to render a positive effect on the morphology build. For another example, a linear polymer was synthesized by a one-pot high-temperature reaction then crosslinked to yield the target sulfonate CSPI-DMDA membrane (P2, P4 & P8).²⁰³ The reaction temperature was near to 200 °C. Except for the conventional high-temperature reactions, the polymerization reaction can occur at mild temperature with highly-active catalysts (P8). The quaternized poly(*p*-phenylene)-based copolymer BrPPP-w (QPPP-w or IMPPP-w) can be obtained *via* Ni(0)-catalyzed polymerization accompanying subsequent bromination and Menshutkin reaction and all steps were at less than 100 °C which was considered safe (P6).²⁰² An ether-free polymer, poly[(fluorene alkylene)-co-(biphenyl alkylene)] was synthesized by a superacid-catalyzed polycondensation reaction.²¹³ The superacid-catalyzed reaction aimed to build a robust polymer with a high molecular weight and ether-free backbone which was firstly executed at 0 °C and gradually elevated to room temperature.

3.2.2 Manufacturing technology. The common membrane manufacturing techniques include solution casting, chemical vapor deposition, spray coatings, spin coatings, phase inversion, interfacial polymerization, etc.¹⁸⁷ For homogeneous membranes, the most common way is solution casting. Selecting the appropriate solvent, *i.e.*, DMAc, THF, DMSO *etc.* to dissolve the polymer, the membrane can be obtained after solvent evaporation. Another example is the LB technique. The highly ordered PSFA membrane with nm thickness was deposited on a porous polycarbonate substrate *via* a layer-by-layer method.¹⁸⁷ PFSA monolayer was spread on the air/water interface. The hydrophilic side of the PFSA monolayer attached to the “top surface” while the hydrophobic side interacted with the “bottom side” during the up stroke. Finally, the composite membrane was dried at 80 °C for at least 16 h. A spin coating method is always applied in composite membranes including the GO/Nafion composite membrane and PIM-1/PAN membranes.¹⁸⁸ GO/Nafion suspension was uniformly dropped on the Nafion membrane (700 rpm, 2 min) then dried (40 °C, 2 h) and thermally annealed (140 °C, 8 h), thereby obtaining well-

adhesive GO/Nafion composite membranes. PIM-1 was dissolved in chloroform then coated onto the commercial PAN ultrafiltration (UF) membrane supports (PA350) *via* spin coating.²⁴⁹ A spray coating method was applied to fabricate boron nitride nanosheet (BNNS) composite membranes which afforded a zig-zag pathway in the highly selective layer for AZIFB.²⁵⁰ The thicker the PEI layer, the less defects on the composite film, which effectively limits vanadium permeability. As for porous membranes, NIPS is definitely the star strategy to lead free volume into polymer. This method is suitable for most polymers except those with high IEC which is prone to gelation. Different solvents and concentrations of PAN casting solution were used to adjust the pore size distribution.²⁰⁶ The NIPS method was the key factor for PAN nanofiltration membrane formation from a polymer-rich phase to a polymer-lean phase. The corresponding symmetric membranes (PS-water) and asymmetric membranes (PS-EtOH and PS-IPA) were obtained after the PS membrane was treated with different solvents including water, ethanol (EtOH) and isopropanol (IPA).²¹¹ A salt-induced NIPS was also applied to the porous PBI membranes.²¹² Different concentrations of NaCl solutions (0–5 M) were used to tune the pore structure and it is considered as a pretty green method (P5, P6 & P8).

Interfacial polymerization is an exclusive technique for the large-scale preparation of ultrathin and defect-free layers especially for TFCM and free-standing composite membranes.^{250,251} A composite membrane based on the polyamide (PA) selective layer and porous PES/SPEEK support was prepared by the interfacial polymerization method. Water-phase solution comprising *m*-phenylenediamine (MPD) and oil-phase solution comprising trimesoyl chloride (TMC) were used for interfacial polymerization. Firstly, the PES/SPEEK substrate was immersed in the water-phase solution to absorb adequate MPD monomer and the excessive solution was wiped off. Then the MPD-doped substrate was transferred to the oil-phase solution to yield PA skin, and finally obtained the composite membrane.²¹⁷

3.3 Safety & environmental sustainability

Polymerization conditions are always harsh, including high temperature, high pressure, and hazardous reagents, *etc.* (P5, P6 & P8). For instance, commercial perfluorosulfonic acid polymers were prepared under the conditions of high temperature and high pressure.^{220,248} The energy consumption caused by high-temperature reaction during preparation is likely to be compensated by the carbon emission reduction brought by its high stability in future application which is anticipated. There lies considerable risk in the synthesis process (P5, P6 & P7). Furthermore, fluorinated compounds are always highly toxic and carcinogenic (P5). The synthesis process of fluorinated ionomers involves various fluorine compounds, other highly polluting reagents (P5), and high energy consumption (P8), thus the Nafion cost is pretty high (P9). Although the membrane has been commercialized, these are still some problems to solve that would pose a great threat to ecological sustainability. Moreover, a lot of unfriendly conditions are applied in other types of membrane preparation. For instance,

benzene, a precursor monomer for QPPP-2, is a kind of toxic organic compound which should be used under conditions of ventilation (P5).²⁰² And *m*-cresol is a biotoxic organic reagent which is water-soluble and may contaminate hydrology, so the waste solution must be appropriately disposed of (P5 & P8). Superacid-catalyzed polycondensation is a prevalent way to fabricate polymers with a heteroatom-free main chain but the extreme acidity of TFSA would bring about risk especially when used on a large scale.^{204,213} TFSA waste must be diluted and neutralized, otherwise it will pollute the water when discharged to sewerage (P8).

By contrast, some benign polymerization reactions with mild conditions have attracted attention. The LB method is safe and does not require high temperature, high pressure, and highly toxic reagents (P5, P6 & P8). The reagents and operations are eco-friendly, not a burden to the environment and therefore are highly consistent with the concept of green chemistry (P7 & P8). On the other hand, the preparation of regular PBI is relatively simple, and the polymer can be produced in pilot scale which has a wide range of applications (whether acidic or alkaline system) and reliable battery performance.

4. Electrodes

The electrode provides a specific site for the redox reaction for FBs.²⁵² The electrochemical polarization, ohmic polarization, and concentration polarization of cells are associated with the electrochemical reversibility of redox species at the electrode materials, the electrode conductivity, and the electrode morphology and hydrophilicity, respectively. Furthermore, the mechanical strength and chemical stability of the electrodes also have an influence on the lifetime of FBs. Therefore, the selection and modification of electrodes are crucial to design high-performance FBs. The carbon materials, graphite felt (GF), carbon felt (CF), carbon paper and carbon cloth are now widely used as electrodes for FBs (Fig. 22a), meanwhile, thermal/gas, acid treatments, carbon materials, and metal/metal oxide doping have been applied to promote the activity of felt.^{253–258}

4.1 Structure & performance

In 1992, oxygen functional groups (*i.e.* hydroxyl and carbonyl group) can improve the hydrophilicity and electrochemical reaction activity of the electrode surface through thermal or acid treatments.^{259,260} The single VFB cell based on the modified electrode showed an obviously improved EE of over 88% which is higher than the pristine GF (78%).²⁶⁰

This improvement was attributed to the acquired oxygen functional groups and the –C–O–V bond would facilitate the electrochemical activity resulting in a faster electron transfer process.²⁵⁹ Additionally, oxygen functional groups can also be introduced by the electrochemical oxidation,^{261,262} plasma treatment,^{263–265} wet-chemical treatment,^{266,267} microwave treatment,²⁶⁸ gamma irradiation,²⁶⁵ and modified Hummers' method,²⁶⁹ *etc.*

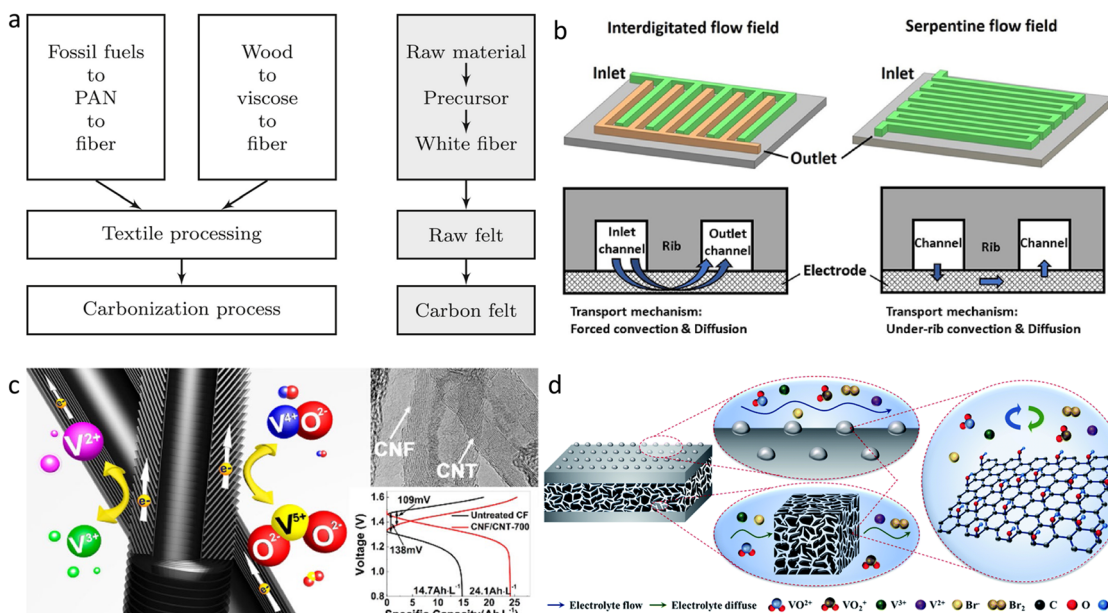


Fig. 22 (a) The preparation process of carbon felt: from materials to product. (b) The IFF and SFF from a Bi-catalyzed ICFB. (c) The CNF/CNT composite catalysts loaded on the CF VFB electrode. (d) A sandwich-like electrode (SPHC) for ZFBs. Adapted with permission from ref. 291 and 32. Copyright 2016 Elsevier B.V. Ref. 285. 2013 Copyright American Chemical Society. Ref. 290. 2020. Copyright The Royal Society of Chemistry.

Electrochemical activation is considered as an eco-friendly method with low energy consumption and no thermal treatment or concentrated acid.²⁶¹ By controlling the current density and treatment time, different amounts of oxygen functional groups could be introduced onto the electrode surface. The VE and EE of the OGF-based cell were increased 4% and 5% higher than the pristine GF.

With the continuous development and improvement of electrode preparation, more cost effective and eco-friendly preparation methods have been investigated, which are expected to be applied to industrial scale production. However, the introduction of oxygen functional groups should not be excessive, as it would lower the mechanical strength and chemical stability and even the electron conductivity.²⁷⁰ Research found that when the content of oxygen species is about 4–5%, the overall performance of the electrode is the best of all.²⁷¹ Nitrogen functional group modifications on carbon paper have also been made to improve the electrode performance *via* hydrothermal ammoniated treatment.²⁵⁵ The introduced nitrogenous groups elevate nitrogen content from 2.96 to 6.43% and enhance the hydrophilicity of carbon paper without changing the original morphology of the electrode after hydrothermal ammoniated treatment. Likewise, hydrothermal treatment has been used to introduce more nitrogenous groups on carbon cloth to improve the electrochemical performance for VFBs.²⁵⁸ N-Doped carbon cloth imposed the VFB cell with a 4.3% increased EE at 30 mA cm⁻² for 50 cycles. Apart from the afore-mentioned oxygen and nitrogen functional groups, some other functional groups containing N, P, S, and B elements have also been investigated to improve electrocatalytic activity.^{258,272–277}

On the other hand, the metal (Bi, Pt, Mn, Ir), metal oxides (RuO₂, MoO₃), and carbon catalysts (graphene, activated carbon, CNTs) have been implemented to improve the electrochemical kinetics and reversibility of redox reactions. Ir-Modified CF by pyrolysis delivered an enhanced conductivity and improved electrochemical catalytic activity.²⁷⁸ However, the noble metal Ir has a high cost limiting its practical application. The catalyst, Bi³⁺, is critically important to improve the ICFB performance (Fig. 22b).³² The Bi catalyst was loaded onto the negative electrode using an electrodeposition method. It was found that the more uniform catalyst distribution and enhanced mass transport limitation was achieved by the interdigitated flow field (IFF).

Common carbon-based catalysts are always carbon nanomaterials including graphite oxide,^{279,280} carbon nanoparticles,²⁸¹ carbon nanofiber (CNF),²⁸² CNT²⁸³ and thermal reduced graphite/graphene oxide.²⁸⁴ CNF/CNT composite catalysts were loaded on CF *via* a vapor deposition method at 700 °C with the presence of Ni-catalyst (CNF/CNT-700).²⁸⁵ The CNF/CNT-700 electrode in a VFB cell delivered an improved EE of ~64% and ~25% at 40 mA cm⁻² and 100 mA cm⁻² compared to the pristine CF electrode. The significant performance boost was attributed to the defect sites of the edge plane and the fast electron transfer of the CNT.

CNTs and graphene oxide carbon materials are still expensive. Biomass-based carbon materials have source diversity, various morphologies, and high specific surface area.^{286–290} A sandwich-like multi-scale pore-rich hydroxylated carbon (SPHC) prepared from withered platanus leaves *via* thermal treatment was used as an electrode material.²⁹⁰ The SPHC delivered a sandwich-like structure with protruding compact

outer skins and activated porous middle layer. The pore-opened integrated structure of the middle layer provides adequate active sites for redox reactions while the outer skins protected the porous layer against the electrolyte flow. Moreover, the even-distributed protuberances on the surface of the outer layer further afford active sites. The SPHC-based electrode yielded an EE of 76.1% at 80 mA cm⁻² in ZFBs and 77.8% at 200 mA cm⁻² in VFBs which were 8.2% and 28.3% higher than the pristine electrode, respectively.

4.2 Preparation

The most common CF and GF materials are usually based on rayon or PAN precursors (Fig. 22a). The precursors were put into a 3D structure then oxidized at nearly 200 °C in the air. A subsequent partial carbonization was executed at 320–800 °C and a carbonization step in a temperature range of 800–1800 °C under an inert atmosphere. The as-prepared felt may process a final graphitization step over 2000 °C to reach a higher carbon content of about 99%.²⁹¹ A further modification of carbon-based electrodes is decorating catalysts by thermal treatment. The active materials can be loaded on the carbon felt by repeated heat treatment heating.²⁷⁸ The vapor deposition method was another way to make the catalysed materials load on the electrodes (Fig. 22c).²⁸⁵ The CF samples soaked with the nickel nitrate solution were dried and calcined in a mixed atmosphere of H₂ and Ar gas for 7 h (600 °C). Then the CF samples with Ni were heated from 500 to 800 °C. Acids are also commonly used in electrode preparation. Oxygen species were introduced on the electrode surface to improve the hydrophilicity thus leading to a polarization reduction.²⁶⁰ The modified GF (3 mm) samples were obtained *via* a thermal treatment process (200–500 °C) of 10–50 h. And they could also be prepared by a refluxing process of H₂SO₄ (50% to 98%) and HNO₃ (70%) then washed with distilled water. The treatment process involves strong acid treatment and high temperature calcination. Some electrodes made from natural raw material also require acid treatment (Fig. 22d).²⁹⁰ The withered leaves were washed with EtOH and DI water then dried in a vacuum oven (60 °C 24 h). The resultant sample was heated at 1000 °C for 2 h with a stepped temperature program. Afterwards, the carbonized sample was milled into powders and immersed in 2 M HCl solution to remove impurities. Finally, after centrifugation, washing, filtration and drying were carried out to obtain the target product. Although the thermal treatment is general and effective for electrode preparation, the process is energy intense. Electrochemical activation, an eco-friendly method, is considered to be a more appropriate method for the future.²⁶¹ A PAN-based GF was washed with DI water and dried. Then the GF plate was placed in 1 M H₂SO₄ and electrochemically oxidized at 100 mA cm⁻². The resultant oxidized GF (OGF) was used for VFBs. Compared with high-temperature thermal treatment and concentrated acid treatment, the electrochemical oxidation method is definitely safer and deserves priority consideration (P5, P6 & P8).

4.3 Safety & environmental sustainability

Thermal treatment at high temperature for a long period, particularly aiming at large-scale preparation, would lead to a high carbon emission which is not conducive to the goal of decarbonization and building an energy-clean society. As to whether the additional CO₂ emissions from thermal treatment could be offset by the improved utilization of renewable energy, there is no sufficient analytical report to support this conjecture. Meanwhile, in addition to environmental issues, high temperature treatment would lead to an operational risk (P6). Another route that needs to be mentioned is the use of strong acids. The strong acids for surface modification need to be washed and diluted with a large amount of water and neutralization treatment is required if necessary (P7). Electrochemical processes do not require high-temperature treatment or large amounts of highly concentrated acid. It was safe and eco-friendly which is in accord with the goal for green and diverse reconstruction of an energy framework in the future.

5. Novel FB systems—is the development of new systems an outlet of a sustainable battery future?

In order to further improve the performance and reduce costs of FBs, several novel FB technologies have been proposed to design new cell structures. In this section, we highlight the recent progress in semi solid state FB (SSFB), solar FB (SFB), and membrane-free FB systems. The design concept of new cell structures can be divided into two types, which are integration or simplification. The integrated design focuses on combining the advantages of different systems to achieve a multifunctional system or performance improvement (SFB, SSFB). Simplified design focuses on reducing system components to achieve a lower system cost, for example, membrane-free FB.

5.1 SFBs

The direct conversion of sunlight energy into chemical energy would be the best way to effectively use solar energy. SFB combines the direct conversion of photochemical cells to solar energy and the storage advantages of FBs.^{292–295} According to different photocharging mechanisms, SFB can be divided into two architectures. One type of SFB has photo-assisted electrodes based on a photo-electrochemical cell (PEC) (Fig. 23a)^{296–300} or dye-sensitized solar cell (DSSC) (Fig. 23b).^{301–310} The PEC-based SFBs can use single photoelectrode (photoanode–catholyte or photocathode–anolyte) or dual photoelectrodes (photoanode–catholyte/photocathode–anolyte in series). Another type is a direct integration of photovoltaic (PV) cells with FB, in which the PV cell and FB operate autonomously (Fig. 23c).^{311–317} In the PECs or DSSC-based SFBs, the semiconductor–liquid junction cell is performed matching the energy-level of the semiconductor and redox species, defining the photovoltage of the cell. When the photoelectrode (semiconductor or dye materials) is irradiated by sunlight, electrons and holes generated by light

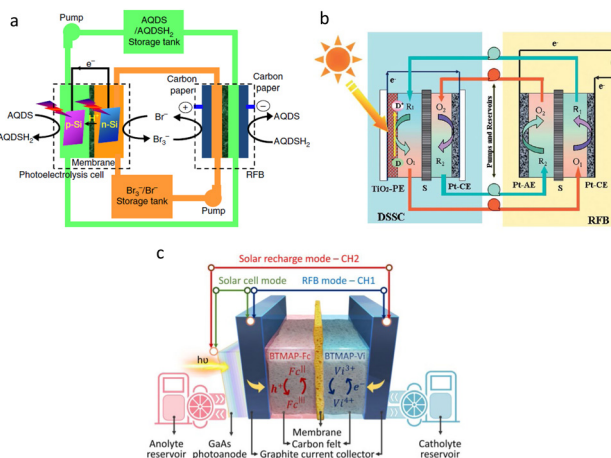


Fig. 23 Three configuration types of SFBs: (a) PEC-based SFB with dual-silicon photoelectrodes and (b) DSSC-based SFB, and (c) PV-based SFB. Adapted with permission from ref. 296. Copyright 2016 Springer Nature. ref. 302. Copyright 2013 Wiley-VCH Verlag GmbH & Co. KGaA, Weinheim. Ref. 317. Copyright 2021 Springer Nature.

excitation are absorbed by the photocathode and photoanode surfaces, respectively. Meanwhile, the electrolyte containing redox species pumped from the external tanks continuously consumes the electrons and holes at the surfaces of the photo-electrode. In this way, the sunlight energy is directly converted into chemical energy for charging. While in SFBs based on PV cells, the carriers (holes/electrons) are generated from the PV cells and transferred into the conductive cathode and anode of FB cells to trigger the oxidation and reduction reactions, respectively. The photovoltage is independent of the energy levels of the redox species and semiconductor. The redox species in SFBs can be metal (*i.e.*, all vanadium) or organic molecules or a combination of the two (*i.e.*, metal-organic molecules).

An aqueous PEC-based SFB with dual-silicon photoelectrodes was reported by Liao *et al.*²⁹⁶ $\text{Br}^{3-}/\text{Br}^-$ and AQDS/ AQDSH_2 were used as the redox species in the catholyte and anolyte, respectively. The conversion efficiency from solar energy to chemical energy to electrical energy is 3.2%. The relatively rapid redox charge transfer at the interface is attributed to the narrow band gap of silicon. In 2020, the same group reported an SFB with a Fe/AQDS redox species and an amorphous silicon (aSi) based photoanode. An overall solar-chemical-electricity conversion efficiency of 4.9% was achieved, which outperforms previous published SFB operating under an air atmosphere.³⁰⁰

Gao and co-workers³⁰¹ first built a DSSC-based SFB in organic solvent, but early DSSC-based SFBs had inferior performance because of the poor conductivity of organic solvents. Thus, an aqueous Li-I SFB was proposed by Wu and co-workers,³⁰⁴ and 19% energy can be saved to charge with the simulated Sun AM 1.5 illumination. However, it is worth mentioning that the I^-/I^{3-} redox species in DSSC-based SFBs is corrosive to many metals.

Furthermore, Li *et al.*³¹² realized a solar-to-electric energy conversion efficiency of 14% using a single photoelectrode ($\text{TiO}_2/\text{Ge}/\text{GaAs}/\text{InGaP}$) system. The photopotential of the SFB system is up to 2.4 V with the (0.1 M) 4-OH-TEMPO catholyte and (0.1 M) methylviolet anolyte. Under 1 sun illumination (100 mW cm⁻²), a 14 mA cm⁻² of photocurrent value was obtained. After that, they applied the back-illuminated single junction GaAs photoelectrode with an n-p-n sandwiched design to obtain an efficient and stable integrated PV-based SFB built with a high solar-to-electric energy conversion efficiency (15.4%). The SFB was continuously cycled for 408 h and showed a fairly stable performance with average CE and VE values of 98.6% and 96.2%, respectively, performed with 0.1 M BTMAP-Fc/NMe-TEMPO redox species in catholyte/anolyte under 1 sun solar illumination.³¹⁷

Although SFBs have made advanced progress, some performance issues need to be addressed.^{292,294,295} Firstly, most SFBs still have low energy density as the low concentration of redox species. Except for several static SFBs, the state of charge (SOC) of SFB is quite low, mainly because of the insufficient photovoltage for the increasing redox potential of the charged electrolyte. In addition, there is a significant energy loss during the solar to chemical and chemical to electrical energy conversion processes, let alone the low current density.

5.2. SSFBs

5.2.1 Traditional SSFBs. The traditional SSFB which combined both concepts of all liquid and hybrid FB was proposed by Chiang and co-workers.³¹⁸ In semi-solid FBs, insoluble redox species are mixed with conducting additives and electrolyte forming an electrically and ionically conducting slurry. Electron exchange is carried out on the surface of nanoscale conducting materials in the suspension during the charge and discharge process. The redox species of SSFBs can be inorganic^{319,320} or organic³²¹ and the system can be aqueous^{322–324} or non-aqueous.^{319,320,325} A representative configuration is shown in Fig. 24.³²⁰

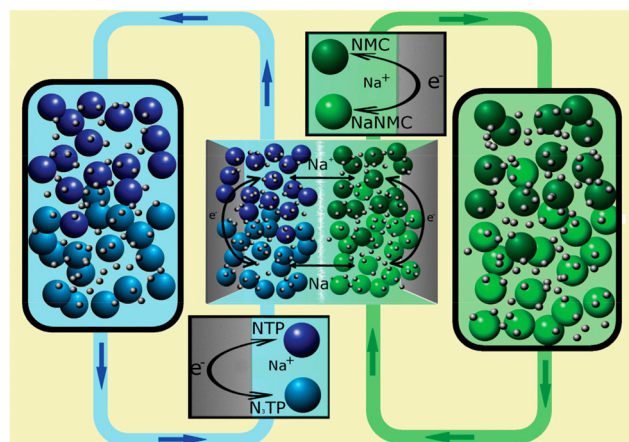


Fig. 24 Representation of a semi-solid FB. Adapted with permission from ref. 320. Copyright 2015 The Royal Society of Chemistry.

Since the concentration of redox species is not limited by their solubility, SSFBs can exhibit much higher energy density, which is the biggest advantage of SSBs. However, higher concentrations will increase the viscosity of the electrolyte and eventually increase the overpotential. Increasing the rheological properties of the slurry with dispersants^{326–328} or by using intermittent-flow operations to reduce pump consumption are possible solutions.^{204,319,322,329} In addition, the operating current density of SSFBs is much lower than that achieved in conventional FBs while the operating current density and specific power will determine whether the final power cost of SSFBs is competitive. Increasing the concentration of conductive additives (carbon particles) can improve the conductivity, but at the same time increase the viscosity of the suspension and reduce the ionic conductivity and energy density.^{322,330,331} Hence, the rheological properties of the slurry must be taken into account while exploring new electrically conductive networks. Finally, the problem of hydrolysis in aqueous systems and the enhancement of SEI in non-aqueous systems cannot be ignored.³³²

5.2.2 Redox-mediated FBs. In order to address the high pump consumption caused by the high viscosity of SSFBs electrolyte, Wang *et al.* proposed a redox-targeting-based FB^{333–337} where the solid redox species is confined to the external tank and a dissolved redox mediator in the electrolyte carry charges between the solid redox species and the electrode, that is, the redox mediator is pumped into the cell chamber and an electrochemical reaction occurs on the electrode surface, then returns to the tank to chemically react with the solid redox species. This type of battery is also called a redox mediated FB (RMFB) (Fig. 25).³³⁸ This strategy has been demonstrated in both non-aqueous^{336,339,340} and aqueous^{338,341–343} electrolyte systems. What's more, the RMFB not only reduces the voltage drop while maintaining a high energy density, but also enhances the power output by enhancing charge transfer with a redox mediator.³⁴⁴

The major challenges for RMFB are the choice of redox mediators because of the constrained utilization of solid materials, and reachable power, which is largely associated with the redox-targeting reaction kinetics. One approach is to use two dissolved redox mediators A and B with redox potentials above and below the solid redox species on one side of the reservoir, respectively. In this case, if mediator A carries charges back and forth between the electrode surface and the tank during charging, mediator B will work during discharging. Since two dynamic processes are involved, this strategy will lead to a decrease in VE.^{335,341,345} A solution demonstrated by Wang *et al.* is to use a single redox mediator where the charge transfer reaction between the dissolved redox mediator and the solid redox species is required to be reversible and spontaneous.³⁴⁶ Afterwards, a series of attractive works were reported. Nanda *et al.* reported a biphenyl and pyrene-mediated phosphorus anode for sodium-based FBs which can conceivably achieve energy densities exceeding 200 W h kg⁻¹. Soluble anion free radical species (biphenyl and pyrene) mediate reversible sodium storage in the red phosphorus (P) anode in the external

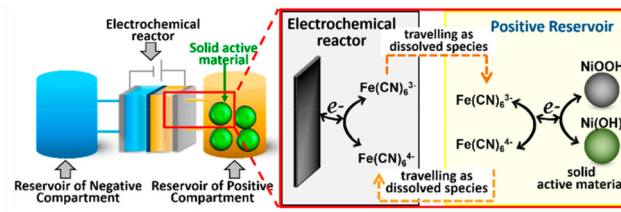


Fig. 25 Representation of a redox mediated FB. Adapted with permission from ref. 342. Copyright 2019 American Chemical Society.

packed bed reactor in the absence of adhesives or conductive additives.^{347,348} Lu *et al.* used self-mediation of inherently present redox shuttles (*e.g.*, polychalcogenides) to access charges stored in high-energy density solid materials (*e.g.*, S and Se). A high degree of material utilization ($\leq 99\%$) and high volumetric capacities (1096–1268 A h L⁻¹ of catholyte) were achieved.³⁴⁹ Small *et al.* demonstrated the marriage of the redox-mediated scheme to the engineered Li solid electrolyte interphase (SEI), enabling a scalable, high efficiency, membrane-less Li-S FB. Equivalent areal loadings of 50 mg cm⁻² (84 mA h cm⁻²) were demonstrated.³⁵⁰ However, screening the highly desirable matched mediator and solid redox species is undoubtedly difficult, but once realized, solid redox species would become the main contributor in terms of energy density and energy cost.²⁹⁵

5.3. Membrane-free FBs

An ambitious alternative to the high cost of ion exchange membranes in FBs is to design a configuration that does not rely on any membrane at all. Recently, membrane-free FB concepts based on biphasic systems have been proposed (Fig. 26a).³⁵¹ One aspect of membrane-free FBs is that redox species are confined to two immiscible solvents such as the ionic liquid/aqueous phase or organic solvent/aqueous phase, and the electrolytes separate spontaneously due to their partition coefficients.^{352–355} Another approach is an “all-aqueous” biphasic system (ABS) demonstrated by Marcilla and co-workers (Fig. 26b).^{356,357} In the ABS systems, two water soluble compounds (two polymers, one polymer-one salt, one ionic liquid-one salt) above certain concentrations lead to the spontaneous separation of the system into two liquid (water-rich)

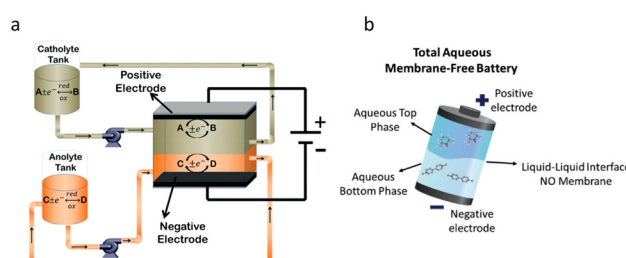


Fig. 26 Schematic diagram of the membrane-free FB's working principle: (a) immiscible membrane-free FB, and (b) ABS-based membrane-free FBs. Adapted with permission from ref. 351. Copyright 2017 Wiley-VCH Verlag GmbH & Co. KGaA, Weinheim. ref. 356. 2021 Elsevier B.V.

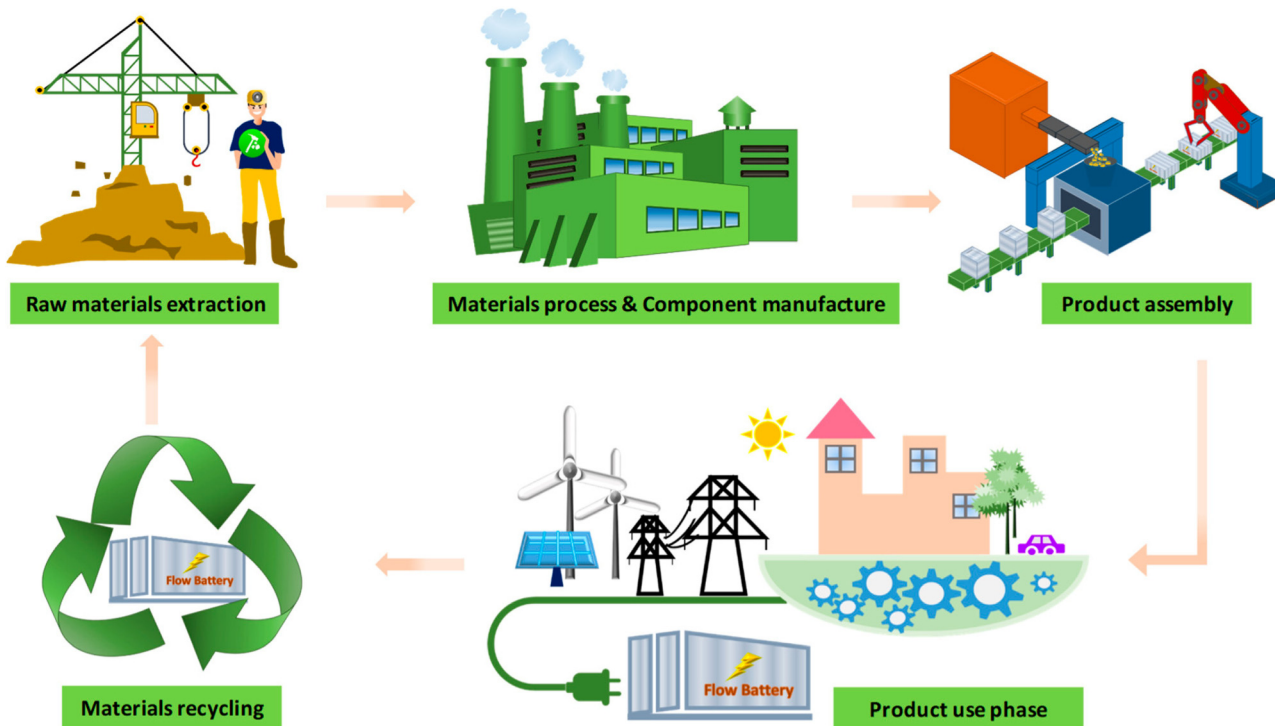


Fig. 27 The whole life of sustainable FBs.

phases. Except that the battery has no membrane, the composition is the same as in conventional FBs and the redox species can be organic or inorganic.

To date, the current density of membrane-free FBs is much lower than existing FB technologies, mainly due to the high resistance of the system. The highest operating current density reported so far is 10 mA cm^{-2} .³⁵⁵ The poor ionic conductivity in the non-aqueous phase or ionic liquid/polymer rich phase in ABS, leading to high ohmic losses. Using additives such as hydrophobic salts may improve the conductivity but may affect the phase composition and increase costs. Another limitation is the high self-discharge and lower CEs, which is due to the inevitable contact of the anode and cathode redox species at the interface and interfacial electron transfer.^{353,357,358} Aqueous biphasic systems (ABS) are an interesting research direction when they can be prepared with inexpensive components. Rebeca Marcilla *et al.* reported an ABS system based on PEG with TEMPO and MV as redox species. This membrane-free FB has an OCV of 1.23 V and a higher peak power density (23 mW cm^{-2}) than other membrane-free types and a stable long-cycling performance (99.99% capacity retention over 550 cycles). Moreover, essential aspects of this technology such as the crossover controlled by partition coefficients and the inherent self-discharge phenomena were addressed for the first time.³⁵⁸ The development of low-cost conductive additives and redox species with appropriate distribution coefficients in membrane-free FB can ensure the main advantages of this strategy.

Undoubtedly, the design concepts of these new systems are excellent, but there is still a long way to go before achieving low-

carbon sustainability in terms of system performance, cost, and resource utilization.

6. Conclusions

Large-scale FBs, as the key part for the exploitation of renewable energy sources, call for high-performance and sustainable key materials for FBs with the rapid development of carbon-neutral society. In this review, 9 principles are proposed to evaluate the low-carbon and sustainability of key materials. These principles are actually mutually dependent. We then summarize the progress of FB technologies from low-carbon and sustainable views and discuss the key materials design in terms of performance improving, preparation/process sustainability, recycling/regeneration, safety, and emission/waste disposal to reduce environmental impact.

Tremendous effort has been devoted to realizing the wide applications of FBs. Inorganic metal and halogen ions feature impressive solubility and simple chemistry with multiple valence changes. FBs based on vanadium, zinc, bromine, etc. inorganic redox species have been commercialized for large scale and distributed energy storage. In future, the availability and environmental sustainability of inorganic redox species will require the advancement of production and processing technology, especially advanced mining technology and low energy/environmental electrolyte preparation. For organic redox species, it is now difficult to compare them with inorganic systems as most reported molecules are still undergoing lab trials. The main challenge is the lack of suitable molecules especially under the harsh practical conditions. Therefore, the

priority for AOFB is to design high-performance molecules and it is encouraging that some synthetic processes have proven to use “greener” chemistry. It is foreseeable that more efforts must be devoted to reflecting the advantages of organic systems in the environment-friendly, green source aspects towards the truly low-carbon and sustainable technology.

So far, several companies such as DuPont, Dow Chemical, Fumatech, and AGC, etc. have launched various types of commercial FB membranes, however, the battery performance and membrane cost are still desirable. Visible progress has been made on both dense and porous IEMs. There is no doubt that the highly stable polymer with desirable ion conductivity and selectivity will be the first option that we pursue. Of course, at the same time, the raw material cost and preparation feasibility are indispensable considerations. From dense IEMs to porous ICMs there may be a new trend to achieve higher conductivity, selectivity and lower cost following the sustainable principles. Carbon-based electrode materials are the front-runner in the field of FBs and thermal treatment was the most frequent route to electrode preparation. As we know, high temperature and long-time processing is energy intensive, which is not friendly to decarbonization, so whether a greener way can be promoted to make the preparation carbon neutral is what we are looking forward to in the future (Fig. 27).

In addition to the sustainable design in key materials, new sustainable FB structures including SFB, SSFB, membrane-free FB and other types have also been explored. However, the fundamental studies in liquid/solid and liquid/liquid interfaces (junctions) and multicomponent coupling remain to be clarified, to facilitate high-efficiency and finally achieve “ $1 + 1 > 2$ ” energy storage not just the macroscopic combination of two devices. Overall, this review aims to provide a better perspective for the design of sustainable FB technologies, and although challenges remain to be overcome, the future offers enormous opportunities to explore new, risky but green directions which will also bring researchers from different fields together to engage in research for a bright future and low carbon society.

Conflicts of interest

The authors declare no conflicts of interest.

Acknowledgements

This work was supported by the China Natural Science Foundation (Grant No. U1808209) and the National Key R&D Program of China (2022YFB2405000). G. Y. acknowledges the support from the Welch Foundation Award F-1861.

Notes and references

1. S. Chu and A. Majumdar, *Nature*, 2012, **488**, 294–303.
2. H. Ritchie, M. Roser and P. Rosado, Available at: <https://ourworldindata.org/electricity-mix#citation> (accessed, 2021).

3. H. S. Chen, T. N. Cong, W. Yang, C. Q. Tan, Y. L. Li and Y. L. Ding, *Prog. Nat. Sci. Mater.*, 2009, **19**, 291–312.
4. M. Jafari, A. Botterud and A. Sakti, *Renewable Sustainable Energy Rev.*, 2022, **158**, 112077.
5. G. L. Soloveichik, *Chem. Rev.*, 2015, **115**, 11533–11558.
6. C. Zhang, L. Zhang, Y. Ding, S. Peng, X. Guo, Y. Zhao, G. He and G. Yu, *Energy Storage Mater.*, 2018, **15**, 324–350.
7. J. R. Minjoon Park, W. Wang and J. Cho, *Nat. Rev. Mater.*, 2016, **2**, 1–18.
8. B. Li and J. Liu, *Natl. Sci. Rev.*, 2017, **4**, 91–105.
9. J. Winsberg, T. Hagemann, T. Janoschka, M. D. Hager and U. S. Schubert, *Angew. Chem., Int. Ed.*, 2016, **56**, 686–711.
10. L. Zhang, R. Feng, W. Wang and G. Yu, *Nat. Rev. Chem.*, 2022, **6**, 524–543.
11. H. He, S. Tian, B. Tarroja, O. A. Ogunseitan, S. Samuelsen and J. M. Schoenung, *J. Cleaner Prod.*, 2020, **269**, 121740.
12. M. J. B. Kabeyi and O. A. Olanrewaju, *Front. Energy Res.*, 2022, **9**, 743114.
13. M. Kolagar, S. M. H. Hosseini, R. Felegari and P. Fattahi, *Environ. Syst. Decisions*, 2019, **40**, 485–509.
14. Z. Deller, L. A. Jones and S. Maniam, *Green Chem.*, 2021, **23**, 4955–4979.
15. P. Anastas and N. Eghbali, *Chem. Soc. Rev.*, 2010, **39**, 301–312.
16. G. Di Florio, I. Pucher, P. Todeschi, M. C. Baratto, R. Basosi and E. Busi, *J. Cleaner Prod.*, 2022, **343**, 130899.
17. M. Gattrell, J. Qian, C. Stewart, P. Graham and B. MacDougall, *Electrochim. Acta*, 2005, **51**, 395–407.
18. E. Ventosa, M. Skoumal, F. J. Vázquez, C. Flox and J. R. Morante, *J. Power Sources*, 2014, **271**, 556–560.
19. M. Gattrell, J. Park, B. MacDougall, J. Apte, S. McCarthy and C. W. Wu, *J. Electrochem. Soc.*, 2004, **151**, A123.
20. M. Skyllas-Kazacos, L. Cao, M. Kazacos, N. Kausar and A. Mousa, *ChemSusChem*, 2016, **9**, 1521–1543.
21. F. Rahman and M. Skyllas-Kazacos, *J. Power Sources*, 2009, **189**, 1212–1219.
22. M. Vijayakumar, W. Wang, Z. Nie, V. Sprengle and J. Hu, *J. Power Sources*, 2013, **241**, 173–177.
23. L. Li, S. Kim, W. Wang, M. Vijayakumar, Z. Nie, B. Chen, J. Zhang, G. Xia, J. Hu and G. Graff, *Adv. Energy Mater.*, 2011, **1**, 394–400.
24. H. R. Jiang, J. Sun, L. Wei, M. C. Wu, W. Shyy and T. S. Zhao, *Energy Storage Mater.*, 2020, **24**, 529–540.
25. H. Zhang, *Energy Storage Sci. Technol.*, 2022, **11**, 2772.
26. H. Wang, S. A. Pourmousavi, W. L. Soong, X. Zhang and N. Ertugrul, *J. Energy Storage*, 2023, **58**, 106384.
27. P. Leung, X. Li, C. P. De León, L. Berlouis, C. J. Low and F. C. Walsh, *RSC Adv.*, 2012, **2**, 10125–10156.
28. D. S. Cheng and E. Hollax, *J. Electrochem. Soc.*, 1985, **132**, 269.
29. C. Wu, D. Scherson, E. Calvo, E. Yeager and M. Reid, *J. Electrochem. Soc.*, 1986, **133**, 2109.
30. J. Giner and K. Cahill, *Adv. Screening Electrode Couples*, 1980, No. DOE/NASA/0794-80/1.
31. S. Wang, Z. Xu, X. Wu, H. Zhao, J. Zhao, J. Liu, C. Yan and X. Fan, *Appl. Energy*, 2020, **271**, 115252.

- 32 Y. K. Zeng, X. L. Zhou, L. Zeng, X. H. Yan and T. S. Zhao, *J. Power Sources*, 2016, **327**, 258–264.
- 33 Y. K. Zeng, T. S. Zhao, X. L. Zhou, L. Zeng and L. Wei, *Appl. Energy*, 2016, **182**, 204–209.
- 34 H. Zhang and C. Sun, *J. Power Sources*, 2021, **493**, 229445.
- 35 Y. Yin, Z. Yuan and X. Li, *Phys. Chem. Chem. Phys.*, 2021, **23**, 26070–26084.
- 36 A. Khor, P. Leung, M. R. Mohamed, C. Flox, Q. Xu, L. An, R. G. A. Wills, J. R. Morante and A. A. Shah, *Mater. Today Energy*, 2018, **8**, 80–108.
- 37 M. Kim, D. Yun and J. Jeon, *J. Power Sources*, 2019, **438**, 227020.
- 38 S. Bae, J. Lee and D. S. Kim, *J. Power Sources*, 2019, **413**, 167–173.
- 39 J.-H. Lee, R. Kim, S. Kim, J. Heo, H. Kwon, J. H. Yang and H.-T. Kim, *Energy Environ. Sci.*, 2020, **13**, 2839–2848.
- 40 Y. Yin, S. Wang, Q. Zhang, Y. Song, N. Chang, Y. Pan, H. Zhang and X. Li, *Adv. Mater.*, 2020, **32**, 1906803.
- 41 S. Wang, Z. Wang, Y. Yin, T. Li, N. Chang, F. Fan, H. Zhang and X. Li, *Energy Environ. Sci.*, 2021, **14**, 4077–4084.
- 42 C. Wang, W. Lu, Q. Lai, P. Xu, H. Zhang and X. Li, *Adv. Mater.*, 2019, **31**, 1904690.
- 43 L. Tang, T. Li, W. Lu and X. Li, *Sci. Bull.*, 2022, **67**, 1362–1371.
- 44 C. Wang, Q. Lai, P. Xu, D. Zheng, X. Li and H. Zhang, *Adv. Mater.*, 2017, **29**, 1605815.
- 45 X. Li, T. Li, P. Xu, C. Xie, Y. Zhang and X. Li, *Adv. Funct. Mater.*, 2021, **31**, 2100133.
- 46 X. Li, C. Xie, T. Li, Y. Zhang and X. Li, *Adv. Mater.*, 2020, **32**, 2005036.
- 47 W. Lu, P. Xu, S. Shao, T. Li, H. Zhang and X. Li, *Adv. Funct. Mater.*, 2021, **31**, 2102913.
- 48 Y. Zhizhang, L. Zonghao and L. Xianfeng, *Energy Storage Sci. Technol.*, 2022, **11**, 2944.
- 49 G. Wang, H. Zou, Z. Xu, A. Tang, F. Zhong, X. Zhu, C. Qin, M. Ding, W. You and C. Jia, *Mater. Today Energy*, 2022, **28**, 101061.
- 50 J. Luo, B. Hu, C. Debruler, Y. Bi, Y. Zhao, B. Yuan, M. Hu, W. Wu and T. L. Liu, *Joule*, 2019, **3**, 149–163.
- 51 X. Li, P. Gao, Y.-Y. Lai, J. D. Bazak, A. Hollas, H.-Y. Lin, V. Murugesan, S. Zhang, C.-F. Cheng and W.-Y. Tung, *Nat. Energy*, 2021, **6**, 873–881.
- 52 J. Luo, A. Sam, B. Hu, C. DeBruler, X. Wei, W. Wang and T. L. Liu, *Nano Energy*, 2017, **42**, 215–221.
- 53 M. Hu, A. Wang and T. Liu, *ChemRxiv*, Cambridge Open Engage, Cambridge, 2022.
- 54 T. Páez, A. Martínez-Cuevva, J. Palma and E. Ventosa, *J. Power Sources*, 2020, **471**, 228453.
- 55 E. Fell, D. De Porcellinis, Y. Jing, V. Gutierrez-Venegas, R. Gordon, S. Granados-Focil and M. Aziz, 2022, DOI: [10.26434/chemrxiv-2022-zl7l6](https://doi.org/10.26434/chemrxiv-2022-zl7l6).
- 56 J. Hu, C. Yuan, L. Zhi, H. Zhang, Z. Yuan and X. Li, *Adv. Funct. Mater.*, 2021, **31**, 2102167.
- 57 Z. Yuan, L. Liang, Q. Dai, T. Li, Q. Song, H. Zhang, G. Hou and X. Li, *Joule*, 2022, **6**, 884–905.
- 58 C. Xie, Y. Duan, W. Xu, H. Zhang and X. Li, *Angew. Chem., Int. Ed.*, 2017, **56**, 14953–14957.
- 59 M. Yang, Z. Xu, W. Xiang, H. Xu, M. Ding, L. Li, A. Tang, R. Gao, G. Zhou and C. Jia, *Energy Storage Mater.*, 2022, **44**, 433–440.
- 60 J. Yang, H. Yan, H. Hao, Y. Song, Y. Li, Q. Liu and A. Tang, *ACS Energy Lett.*, 2022, **7**, 2331–2339.
- 61 L. W. Hruska and R. F. Savinell, *J. Electrochem. Soc.*, 1981, **128**, 18.
- 62 Y. Song, K. Zhang, X. Li, C. Yan, Q. Liu and A. Tang, *J. Mater. Chem. A*, 2021, **9**, 26354–26361.
- 63 K. Gong, F. Xu, J. B. Grunewald, X. Ma, Y. Zhao, S. Gu and Y. Yan, *ACS Energy Lett.*, 2016, **1**, 89–93.
- 64 M. Shin, S. Oh, H. Jeong, C. Noh, Y. Chung, J. W. Han and Y. Kwon, *Int. J. Energy Res.*, 2022, **46**, 8175–8185.
- 65 A. Lê, D. Floner, T. Roisnel, O. Cador, L. Chancelier and F. Geneste, *Electrochim. Acta*, 2019, **301**, 472–477.
- 66 X. Liu, T. Li, Z. Yuan and X. Li, *J. Energy Chem.*, 2022, **73**, 445–451.
- 67 S. Sreenath, N. K. Sharma and R. K. Nagarale, *RSC Adv.*, 2020, **10**, 44824–44833.
- 68 B. Liu, H. Du, S.-N. Wang, Y. Zhang, S.-L. Zheng, L.-J. Li and D.-H. Chen, *AIChE J.*, 2013, **59**, 541–552.
- 69 M. Li, B. Liu, S. Zheng, S. Wang, H. Du, D. B. Dreisinger and Y. Zhang, *J. Cleaner Prod.*, 2017, **149**, 206–217.
- 70 J. Zhang, W. Zhang, L. Zhang and S. Gu, *Int. J. Mineral Process.*, 2015, **138**, 20–29.
- 71 Z.-H. Wang, S.-L. Zheng, S.-N. Wang, B. Liu, D.-W. Wang, H. Du and Y. Zhang, *Trans. Nonferrous Met. Soc. China*, 2014, **24**, 1273–1288.
- 72 S. M. J. Mirazimi, F. Rashchi and M. Saba, *Chem. Eng. Res. Des.*, 2015, **94**, 131–140.
- 73 G. Zhang, T.-A. Zhang, G. Lü, Y. Zhang, Y. Liu and W. Zhang, *JOM*, 2016, **68**, 577–584.
- 74 J. Li, B. Zhang, M. Yang and H. Lin, *J. Hazard. Mater.*, 2021, **416**, 125843.
- 75 S. Yu, X. Yue, J. Holoubek, X. Xing, E. Pan, T. Pascal and P. Liu, *J. Power Sources*, 2021, **513**, 230457.
- 76 C. B. Xu and D. C. Cang, *J. Iron Steel Res. Int.*, 2010, **17**, 1–7.
- 77 Y. Zeng, T. Zhao, L. An, X. Zhou and L. Wei, *J. Power Sources*, 2015, **300**, 438–443.
- 78 C. T.-C. Wan, K. E. Rodby, M. L. Perry, Y.-M. Chiang and F. R. Brushett, *J. Power Sources*, 2023, **554**, 232248.
- 79 N. Poli, A. Trovò, P. Fischer, J. Noack and M. Guarneri, *J. Energy Storage*, 2023, **58**, 106404.
- 80 A. H. Whitehead and M. Harrer, *J. Power Sources*, 2013, **230**, 271–276.
- 81 S. Rudolph, U. Schröder and I. M. Bayanov, *J. Electroanal. Chem.*, 2013, **703**, 29–37.
- 82 N. Poli, M. Schäffer, A. Trovò, J. Noack, M. Guarneri and P. Fischer, *Chem. Eng. J.*, 2021, **405**, 126583.
- 83 L. Thaller, *Redox flow cell energy storage systems*, Orlando, FL, USA, 1979.
- 84 Y. K. Zeng, T. S. Zhao, X. L. Zhou, J. Zou and Y. X. Ren, *J. Power Sources*, 2017, **352**, 77–82.

- 85 S. Selverston, R. F. Savinell and J. S. Wainright, *J. Power Sources*, 2016, **324**, 674–678.
- 86 L. da Silva Lima, M. Quartier, A. Buchmayr, D. Sanjuan-Delmás, H. Laget, D. Corbisier, J. Mertens and J. Dewulf, *Sustainable Energy Technol.*, 2021, **46**, 101286.
- 87 S. Weber, J. F. Peters, M. Baumann and M. Weil, *Environ. Sci. Technol.*, 2018, **52**, 10864–10873.
- 88 N. Blume, M. Becker, T. Turek and C. Minke, *J. Ind. Ecol.*, 2022, **26**, 1796–1808.
- 89 E. Lancry, B.-Z. Magnes, I. Ben-David and M. Freiberg, *ECS Trans.*, 2013, **53**, 107–115.
- 90 X. J. Li, T. Y. Li, P. C. Xu, C. X. Xie, Y. H. Zhang and X. F. Li, *Adv. Funct. Mater.*, 2021, **31**.
- 91 L. Qiao, C. Xie, M. Nan, H. Zhang, X. Ma and X. Li, *J. Mater. Chem. A*, 2021, **9**, 12606–12611.
- 92 J. Rubio-Garcia, A. Kucernak, D. Zhao, D. Li, K. Fahy, V. Yufit, N. Brandon and M. Gomez-Gonzalez, *JPhys Energy*, 2018, **1**, 015006.
- 93 C. Xie, T. Li, C. Deng, Y. Song, H. Zhang and X. Li, *Energy Environ. Sci.*, 2020, **13**, 135–143.
- 94 J. Lei, Y. Yao, Z. Wang and Y.-C. Lu, *Energy Environ. Sci.*, 2021, **14**, 4418–4426.
- 95 Y. Liu, C. Xie and X. Li, *Angew. Chem., Int. Ed. Engl.*, 2022, **61**, e202213751.
- 96 X. Zhou, L. Lin, Y. Lv, X. Zhang and Q. Wu, *J. Power Sources*, 2018, **404**, 89–95.
- 97 Y. Zeng, Z. Yang, F. Lu and Y. Xie, *Appl. Energy*, 2019, **255**, 113756.
- 98 Y. Yao, Z. Wang, Z. Li and Y. C. Lu, *Adv. Mater.*, 2021, **33**, e2008095.
- 99 Y. Xu, C. Xie, T. Li and X. Li, *ACS Energy Lett.*, 2022, **7**, 1034–1039.
- 100 Y. Xu, C. Xie and X. Li, *Trans. Tianjin Univ.*, 2022, **28**, 186–192.
- 101 H. Kurreck and M. Huber, *Angew. Chem., Int. Ed. Engl.*, 1995, **34**, 849–866.
- 102 D. T. Scott, D. M. McKnight, E. L. Blunt-Harris, S. E. Kolesar and D. R. Lovley, *Environ. Sci. Technol.*, 1998, **32**, 2984–2989.
- 103 B. Huskinson, M. P. Marshak, C. Suh, S. Er, M. R. Gerhardt, C. J. Galvin, X. Chen, A. Aspuru-Guzik, R. G. Gordon and M. J. Aziz, *Nature*, 2014, **505**, 195–198.
- 104 V. Singh, S. Kim, J. Kang and H. R. Byon, *Nano Res.*, 2019, **12**, 1988–2001.
- 105 M. Quan, D. Sanchez, M. F. Wasylkiw and D. K. Smith, *J. Am. Chem. Soc.*, 2007, **129**, 12847–12856.
- 106 Y. Xu, Y. Wen, J. Cheng, Y. Yanga, Z. Xie and G. Cao, 2009.
- 107 Y. Ding and G. Yu, *Angew. Chem., Int. Ed.*, 2016, **55**, 4772–4776.
- 108 L. Hoober-Burkhardt, S. Krishnamoorthy, B. Yang, A. Murali, A. Nirmalchandar, G. S. Prakash and S. Narayanan, *J. Electrochem. Soc.*, 2017, **164**, A600.
- 109 J. B. Gerken, C. W. Anson, Y. Preger, P. G. Symons, J. D. Genders, Y. Qiu, W. Li, T. W. Root and S. S. Stahl, *Adv. Energy Mater.*, 2020, **10**, 2000340.
- 110 K. Wedege, E. Dražević, D. Konya and A. Bentien, *Sci. Rep.*, 2016, **6**, 1–13.
- 111 C. Wang, Z. Yang, Y. Wang, P. Zhao, W. Yan, G. Zhu, L. Ma, B. Yu, L. Wang and G. Li, *ACS Energy Lett.*, 2018, **3**, 2404–2409.
- 112 L. C. Topg, M. A. Goulet, D. P. Tabor, E. F. Kerr, D. De Porcellinis, E. M. Fell, A. Aspuru-Guzik, R. G. Gordon and M. J. Aziz, *ACS Energy Lett.*, 2019, **4**, 1880–1887.
- 113 M. M. Barsan, M. E. Ghica and C. M. Brett, *Anal. Chim. Acta*, 2015, **881**, 1–23.
- 114 Y. Jing, E. M. Fell, M. Wu, S. Jin, Y. Ji, D. A. Pollack, Z. Tang, D. Ding, M. Bahari, M.-A. Goulet, T. Tsukamoto, R. G. Gordon and M. J. Aziz, *ACS Energy Lett.*, 2022, **7**, 226–235.
- 115 Y. Ji, M. A. Goulet, D. A. Pollack, D. G. Kwabi, S. Jin, D. De Porcellinis, E. F. Kerr, R. G. Gordon and M. J. Aziz, *Adv. Energy Mater.*, 2019, **9**, 1900039.
- 116 E. F. Kerr, Z. J. Tang, T. Y. George, S. J. Jin, E. M. Fell, K. Amini, Y. Jing, M. Wu, R. G. Gordon and M. J. Aziz, *ACS Energy Lett.*, 2022, 600–607, DOI: [10.1021/acsenergylett.2c01691](https://doi.org/10.1021/acsenergylett.2c01691).
- 117 S. J. Jin, Y. Jing, D. G. Kwabi, Y. L. Ji, L. C. Tong, D. De Porcellinis, M. A. Goulet, D. A. Pollack, R. G. Gordon and M. J. Aziz, *ACS Energy Lett.*, 2019, **4**, 1342–1348.
- 118 T. Liu, X. Wei, Z. Nie, V. Sprenkle and W. Wang, *Adv. Energy Mater.*, 2016, **6**, 1501449.
- 119 C. DeBruler, B. Hu, J. Moss, X. Liu, J. Luo, Y. Sun and T. L. Liu, *Chem*, 2017, **3**, 961–978.
- 120 C. L. Bird and A. T. Kuhn, *Chem. Soc. Rev.*, 1981, **10**, 49–82.
- 121 C. DeBruler, B. Hu, J. Moss, J. Luo and T. L. Liu, *ACS Energy Lett.*, 2018, **3**, 663–668.
- 122 R. G. Jones and H. Shonle, *J. Am. Chem. Soc.*, 1945, **67**, 1034–1035.
- 123 K. X. Lin, Q. Chen, M. R. Gerhardt, L. C. Tong, S. B. Kim, L. Eisenach, A. W. Valle, D. Hardee, R. G. Gordon, M. J. Aziz and M. P. Marshak, *Science*, 2015, **349**, 1529–1532.
- 124 W. Q. Liu, Z. M. Zhao, T. Y. Li, S. H. Li, H. M. Zhang and X. F. Li, *Sci. Bull.*, 2021, **66**, 457–463.
- 125 A. W. Lantz, S. A. Shavalier, W. Schroeder and P. G. Rasmussen, *ACS Appl. Energy Mater.*, 2019, **2**, 7893–7902.
- 126 H. B. Li, H. Fan, B. Hu, L. L. Hu, G. Chang and J. X. Song, *Angew. Chem., Int. Ed.*, 2021, **60**, 26971–26977.
- 127 S. Hu, T. Li, M. Huang, J. Huang, W. Li, L. Wang, Z. Chen, Z. Fu, X. Li and Z. Liang, *Adv. Mater.*, 2021, **33**, 2005839.
- 128 J. H. Huang, S. Z. Hu, X. Z. Yuan, Z. P. Xiang, M. B. Huang, K. Wan, J. H. Piao, Z. Y. Fu and Z. X. Liang, *Angew. Chem., Int. Ed.*, 2021, **60**, 20921–20925.
- 129 X.-L. Lv, P. Sullivan, H.-C. Fu, X. Hu, H. Liu, S. Jin, W. Li and D. Feng, *ACS Energy Lett.*, 2022, **7**, 2428–2434.
- 130 J. Winsberg, C. Stolze, A. Schwenke, S. Muench, M. D. Hager and U. S. Schubert, *ACS Energy Lett.*, 2017, **2**, 411–416.
- 131 T. Janoschka, N. Martin, M. D. Hager and U. S. Schubert, *Angew. Chem., Int. Ed.*, 2016, **55**, 14425–14428.
- 132 Y. H. Liu, M. A. Goulet, L. C. Tong, Y. Z. Liu, Y. L. Ji, L. Wu, R. G. Gordon, M. J. Aziz, Z. J. Yang and T. W. Xu, *Chem*, 2019, **5**, 1861–1870.

- 133 Z. Chang, D. Henkensmeier and R. Chen, *ChemSusChem*, 2017, **10**, 3193–3197.
- 134 A. Hollas, X. L. Wei, V. Murugesan, Z. M. Nie, B. Li, D. Reed, J. Liu, V. Sprenkle and W. Wang, *Nat. Energy*, 2018, **3**, 508–514.
- 135 C. X. Wang, X. Li, B. Yu, Y. R. Wang, Z. Yang, H. Z. Wang, H. N. Lin, J. Ma, G. G. Li and Z. Jin, *ACS Energy Lett.*, 2020, **5**, 411–417.
- 136 S. A. Pang, X. Y. Wang, P. Wang and Y. L. Ji, *Angew. Chem., Int. Ed.*, 2021, **60**, 5289–5298.
- 137 J. Xu, S. Pang, X. Wang, P. Wang and Y. Ji, *Joule*, 2021, **5**, 2437–2449.
- 138 A. Orita, M. G. Verde, M. Sakai and Y. S. Meng, *Nat. Commun.*, 2016, **7**, 1–8.
- 139 K. Lin, R. Gómez-Bombarelli, E. S. Beh, L. Tong, Q. Chen, A. Valle, A. Aspuru-Guzik, M. J. Aziz and R. G. Gordon, *Nat. Energy*, 2016, **1**, 1–8.
- 140 C. K. Zhang, Z. H. Niu, S. S. Peng, Y. Ding, L. Y. Zhang, X. L. Guo, Y. Zhao and G. H. Yu, *Adv. Mater.*, 2019, **31**, 1901052.
- 141 T. Janoschka, N. Martin, U. Martin, C. Fribe, S. Morgenthaler, H. Hiller, M. D. Hager and U. S. Schubert, *Nature*, 2015, **527**, 78–81.
- 142 T. P. Nguyen, A. D. Easley, N. Kang, S. Khan, S.-M. Lim, Y. H. Rezenom, S. Wang, D. K. Tran, J. Fan and R. A. Letteri, *Nature*, 2021, **593**, 61–66.
- 143 R. Feng, X. Zhang, V. Murugesan, A. Hollas, Y. Chen, Y. Shao, E. Walter, N. P. Wellala, L. Yan and K. M. Rosso, *Science*, 2021, **372**, 836–840.
- 144 X. Zu, L. Zhang, Y. Qian, C. Zhang and G. Yu, *Angew. Chem.*, 2020, **132**, 22347–22354.
- 145 B. Hu, C. DeBruler, Z. Rhodes and T. L. Liu, *J. Am. Chem. Soc.*, 2017, **139**, 1207–1214.
- 146 C. D. Nadell, K. Drescher and K. R. Foster, *Nat. Rev. Microbiol.*, 2016, **14**, 589–600.
- 147 Y. Liu, M.-A. Goulet, L. Tong, Y. Liu, Y. Ji, L. Wu, R. G. Gordon, M. J. Aziz, Z. Yang and T. Xu, *Chem*, 2019, **5**, 1861–1870.
- 148 C. Wang, X. Li, B. Yu, Y. Wang, Z. Yang, H. Wang, H. Lin, J. Ma, G. Li and Z. Jin, *ACS Energy Lett.*, 2020, **5**, 411–417.
- 149 S. Mahajan and R. K. Mahajan, *Adv. Colloid Interface Sci.*, 2013, **199**, 1–14.
- 150 Y. Zhang, F. Li, T. Li, M. Zhang, Z. Yuan, G. Hou, J. Fu, C. Zhang and X. Li, *Energy Environ. Sci.*, 2023, **16**, 231–240.
- 151 T. Janoschka, M. D. Hager and U. S. Schubert, *Adv. Mater.*, 2012, **24**, 6397–6409.
- 152 H. Nishide, K. Koshika and K. Oyaizu, *Pure Appl. Chem.*, 2009, **81**, 1961–1970.
- 153 J. Zhao, B.-j Gao and Y.-k Gong, *Catal. Lett.*, 2011, **141**, 1808–1813.
- 154 T. D. Gregory, M. L. Perry and P. Albertus, *J. Power Sources*, 2021, **499**, 229965.
- 155 R. M. Darling, K. G. Gallagher, J. A. Kowalski, S. Ha and F. R. Brushett, *Energy Environ. Sci.*, 2014, **7**, 3459–3477.
- 156 R. Dmello, J. D. Milshtein, F. R. Brushett and K. C. Smith, *J. Power Sources*, 2016, **330**, 261–272.
- 157 V. Dieterich, J. D. Milshtein, J. L. Barton, T. J. Carney, R. M. Darling and F. R. Brushett, *Trans. Mater. Res.*, 2018, **5**, 034001.
- 158 Y. Jing, M. Wu, A. A. Wong, E. M. Fell, S. Jin, D. A. Pollack, E. F. Kerr, R. G. Gordon and M. J. Aziz, *Green Chem.*, 2020, **22**, 6084–6092.
- 159 E. Vitaku, C. N. Gannett, K. L. Carpenter, L. Shen, H. D. Abruña and W. R. Dichtel, *J. Am. Chem. Soc.*, 2019, **142**, 16–20.
- 160 Q. Chen, Y. Li, Y. Liu, P. Sun, Z. Yang and T. Xu, *ChemSusChem*, 2021, **14**, 1295–1301.
- 161 J. Huang, S. Hu, X. Yuan, Z. Xiang, M. Huang, K. Wan, J. Piao, Z. Fu and Z. Liang, *Angew. Chem., Int. Ed.*, 2021, **60**, 20921–20925.
- 162 B. H. A. T. L. Liu, *Sci. Perspectives*, 2021, **372**, 788.
- 163 C. Zhang, L. Zhang and G. Yu, *Acc. Chem. Res.*, 2020, **53**, 1648–1659.
- 164 Y. Ding, C. Zhang, L. Zhang, H. Wei, Y. Li and G. Yu, *ACS Energy Lett.*, 2018, **3**, 2641–2648.
- 165 C. Zhang, L. Zhang, Y. Ding, X. Guo and G. Yu, *ACS Energy Lett.*, 2018, **3**, 2875–2883.
- 166 C. Zhang, H. Chen, Y. Qian, G. Dai, Y. Zhao and G. Yu, *Adv. Mater.*, 2021, **33**, 2008560.
- 167 C. Zhang, Y. Qian, Y. Ding, L. Zhang, X. Guo, Y. Zhao and G. Yu, *Angew. Chem., Int. Ed.*, 2019, **58**, 7045–7050.
- 168 K. Peng, Y. Li, G. Tang, Y. Liu, Z. Yang and T. Xu, *Energy Environ. Sci.*, 2023, **16**, 430–437.
- 169 A. Mukhopadhyay, H. Zhao, B. Li, J. Hamel, Y. Yang, D. Cao, A. Natan and H. Zhu, *ACS Appl. Energy Mater.*, 2019, **2**, 7425–7437.
- 170 W. Schlemmer, P. Nothdurft, A. Petzold, G. Riess, P. Frühwirt, M. Schmallegger, G. Gescheidt-Demner, R. Fischer, S. A. Freunberger and W. Kern, *Angew. Chem., Int. Ed.*, 2020, **59**, 22943–22946.
- 171 C. O. Wilhelmsen, S. B. Kristensen, O. Nolte, I. A. Volodin, J. V. Christiansen, T. Isbrandt, T. Sørensen, C. Petersen, T. E. Sondergaard and K. Lehmann Nielsen, *Batteries Supercaps*, 2022, **6**, e202200365.
- 172 C. K. Zhang and X. F. Li, *Curr. Opin. Electrochem.*, 2021, **30**, 100836.
- 173 C. D. Clark, J. D. Debad, E. H. Yonemoto, T. E. Mallouk and A. J. Bard, *J. Am. Chem. Soc.*, 1997, **119**, 10525–10531.
- 174 G. Levey and T. W. Ebbesen, *J. Phys. Chem.*, 1983, **87**, 829–832.
- 175 A. Brunmark and E. Cadenas, *Free Radical Biol. Med.*, 1989, **7**, 435–477.
- 176 S. Abou-Shehada, M. C. Teasdale, S. D. Bull, C. E. Wade and J. M. Williams, *ChemSusChem*, 2015, **8**, 1083–1087.
- 177 Z. M. Zhao, C. K. Zhang and X. F. Li, *J. Energy Chem.*, 2022, **67**, 621–639.
- 178 M.-A. Goulet, L. Tong, D. A. Pollack, D. P. Tabor, S. A. Odom, A. Aspuru-Guzik, E. E. Kwan, R. G. Gordon and M. J. Aziz, *J. Am. Chem. Soc.*, 2019, **141**, 8014–8019.
- 179 M. Wu, Y. Jing, A. A. Wong, E. M. Fell, S. Jin, Z. Tang, R. G. Gordon and M. J. Aziz, *Chem*, 2020, **6**, 1432–1442.

- 180 Y. Jing, E. W. Zhao, M.-A. Goulet, M. Bahari, E. M. Fell, S. Jin, A. Davoodi, E. Jónsson, M. Wu and C. P. Grey, *Nat. Chem.*, 2022, **14**, 1103–1109.
- 181 E. W. Zhao, E. Jónsson, R. B. Jethwa, D. Hey, D. Lyu, A. Brookfield, P. A. Klusener, D. Collison and C. P. Grey, *J. Am. Chem. Soc.*, 2021, **143**, 1885–1895.
- 182 E. P. Fuerst and M. A. Norman, *Weed Sci.*, 1991, **39**, 458–464.
- 183 W. J. Lu, Z. Z. Yuan, Y. Y. Zhao, H. Z. Zhang, H. M. Zhang and X. F. Li, *Chem. Soc. Rev.*, 2017, **46**, 2199–2236.
- 184 Z. Z. Yuan, Y. B. Yin, C. X. Xie, H. M. Zhang, Y. Yao and X. F. Li, *Adv. Mater.*, 2019, **31**, 1902025.
- 185 Q. Dai, Z. Zhao, M. Shi, C. Deng, H. Zhang and X. Li, *J. Membr. Sci.*, 2021, **632**, 119355.
- 186 E. Sum and M. Skyllas-Kazacos, *J. Power Sources*, 1985, **15**, 179–190.
- 187 P. Xiong, L. Zhang, Y. Chen, S. Peng and G. Yu, *Angew. Chem., Int. Ed.*, 2021, **60**, 24770–24798.
- 188 L. Su, D. Zhang, S. Peng, X. Wu, Y. Luo and G. He, *Int. J. Hydrogen Energy*, 2017, **42**, 21806–21816.
- 189 B. Li, Z. Nie, M. Vijayakumar, G. Li, J. Liu, V. Sprenkle and W. Wang, *Nat. Commun.*, 2015, **6**, 6303.
- 190 C. X. Xie, Y. Q. Duan, W. B. Xu, H. M. Zhang and X. F. Li, *Angew. Chem., Int. Ed.*, 2017, **56**, 14953–14957.
- 191 J. Hu, H. M. Zhang, W. B. Xu, Z. Z. Yuan and X. F. Li, *J. Membr. Sci.*, 2018, **566**, 8–14.
- 192 J. Q. Kim, S. So, H.-T. Kim and S. Q. Choi, *ACS Energy Lett.*, 2020, **6**, 184–192.
- 193 X. Yang, H. Zhu, F. Jiang and X. Zhou, *J. Power Sources*, 2020, **473**, 228586.
- 194 D. Zhang, Q. Wang, S. Peng, X. Yan, X. Wu and G. He, *J. Membr. Sci.*, 2019, **587**, 117189.
- 195 J. Liu, L. Yu, X. Cai, U. Khan, Z. Cai, J. Xi, B. Liu and F. Kang, *ACS Nano*, 2019, **13**, 2094–2102.
- 196 Z. Yuan, X. Li, J. Hu, W. Xu, J. Cao and H. Zhang, *Phys. Chem. Chem. Phys.*, 2014, **16**, 19841–19847.
- 197 S. Chang, J. Ye, W. Zhou, C. Wu, M. Ding, Y. Long, Y. Cheng and C. Jia, *Surf. Coat. Technol.*, 2019, **358**, 190–194.
- 198 D. De Porcellinis, B. Mecheri, A. D'Epifanio, S. Licoccia, S. Granados-Focil and M. Aziz, *J. Electrochem. Soc.*, 2018, **165**, A1137.
- 199 Z. Z. Yuan, Y. Q. Duan, T. Liu, H. M. Zhang and X. F. Li, *iScience*, 2018, **3**, 40–49.
- 200 X. L. Zhou, T. S. Zhao, L. An, L. Wei and C. Zhang, *Electrochim. Acta*, 2015, **153**, 492–498.
- 201 M. J. T. Raaijmakers and N. E. Benes, *Prog. Polym. Sci.*, 2016, **63**, 86–142.
- 202 M. S. Cha, S. W. Jo, S. H. Han, S. H. Hong, S. So, T. H. Kim, S. G. Oh, Y. T. Hong and J. Y. Lee, *J. Power Sources*, 2019, **413**, 158–166.
- 203 L. H. Yu, L. Wang, L. W. Yu, D. Mu, L. Wang and J. Y. Xi, *J. Membr. Sci.*, 2019, **572**, 119–127.
- 204 X. M. Yan, H. Q. Zhang, Z. Y. Hu, L. Li, L. Hu, Z. A. Li, L. Gao, Y. Dai, X. G. Jian and G. H. He, *ACS Appl. Mater. Interfaces*, 2019, **11**, 44315–44324.
- 205 S. Kumar, M. Bhushan and V. K. Shahi, *J. Power Sources*, 2020, **448**, 227358.
- 206 H. Z. Zhang, H. M. Zhang, X. F. Li, Z. S. Mai and J. L. Zhang, *Energy Environ. Sci.*, 2011, **4**, 1676–1679.
- 207 H. Z. Zhang, H. M. Zhang, F. X. Zhang, X. F. Li, Y. Li and I. Vankelecom, *Energy Environ. Sci.*, 2013, **6**, 776–781.
- 208 Y. Y. Zhao, M. R. Li, Z. Z. Yuan, X. F. Li, H. M. Zhang and I. F. J. Vankelecom, *Adv. Funct. Mater.*, 2016, **26**, 210–218.
- 209 W. J. Lu, Z. Z. Yuan, Y. Y. Zhao, X. F. Li, H. M. Zhang and I. F. J. Vankelecom, *Energy Environ. Sci.*, 2016, **9**, 2319–2325.
- 210 W. J. Lu, Z. Z. Yuan, Y. Y. Zhao, L. Qiao, H. M. Zhang and X. F. Li, *Energy Storage Mater.*, 2018, **10**, 40–47.
- 211 L. Qiao, H. M. Zhang, W. J. Lu, C. H. Xiao, Q. Fu, X. F. Li and I. F. J. Vankelecom, *Nano Energy*, 2018, **54**, 73–81.
- 212 L. Qiao, H. M. Zhang, W. J. Lu, Q. Dai and X. F. Li, *ACS Appl. Mater. Interfaces*, 2019, **11**, 24107–24113.
- 213 Z. Zhao, Q. Dai, X. Li, S. Zhang, S. Li and X. Li, *J. Mater. Chem. A*, 2022, **10**, 762–771.
- 214 M. R. Chapman, C. E. Willans, S. Samuelsen, N. Kapur and B. N. Nguyen, *Chemistry Open*, 2016, **5**, 351–356.
- 215 J. H. Zhou, Y. H. Liu, P. P. Zuo, Y. Y. Li, Y. Dong, L. Wu, Z. J. Yang and T. W. Xu, *J. Membr. Sci.*, 2021, **620**, 118832.
- 216 R. Tan, A. Wang, R. Malpass-Evans, R. Williams, E. W. Zhao, T. Liu, C. Ye, X. Zhou, B. P. Darwich, Z. Fan, L. Turcani, E. Jackson, L. Chen, S. Y. Chong, T. Li, K. E. Jelfs, A. I. Cooper, N. P. Brandon, C. P. Grey, N. B. McKeown and Q. Song, *Nat. Mater.*, 2020, **19**, 195–202.
- 217 Q. Dai, Z. Q. Liu, L. Huang, C. Wang, Y. Y. Zhao, Q. Fu, A. M. Zheng, H. M. Zhang and X. F. Li, *Nat. Commun.*, 2020, **11**, 13.
- 218 M. K. Petersen and G. A. Voth, *J. Phys. Chem. B*, 2006, **110**, 18594–18600.
- 219 J. Vrana, J. Charvat, P. Mazur, P. Belsky, J. Dundalek, J. Pochedic and J. Kosek, *J. Membr. Sci.*, 2018, **552**, 202–212.
- 220 K. A. Mauritz and R. B. Moore, *Chem. Rev.*, 2004, **104**, 4535–4585.
- 221 M. A. Hickner, H. Ghassemi, Y. S. Kim, B. R. Einsla and J. E. McGrath, *Chem. Rev.*, 2004, **104**, 4587–4611.
- 222 X. Li, H. Zhang, Z. Mai, H. Zhang and I. Vankelecom, *Energy Environ. Sci.*, 2011, **4**, 1147–1160.
- 223 Z. S. Mai, H. M. Zhang, X. F. Li, S. H. Xiao and H. Z. Zhang, *J. Power Sources*, 2011, **196**, 5737–5741.
- 224 S. Banerjee and D. E. Curtin, *J. Fluorine Chem.*, 2004, **125**, 1211–1216.
- 225 J. Y. Cao, H. M. Zhang, W. X. Xu and X. F. Li, *J. Power Sources*, 2014, **249**, 84–91.
- 226 W. Lu, Z. Yuan, Y. Zhao, X. Li, H. Zhang and I. F. Vankelecom, *Energy Environ. Sci.*, 2016, **9**, 2319–2325.
- 227 P. M. Budd, E. S. Elabas, B. S. Ghanem, S. Makhseed, N. B. McKeown, K. J. Msayib, C. E. Tattershall and D. Wang, *Adv. Mater.*, 2004, **16**, 456–459.
- 228 X. Zhang, T. Higashihara, M. Ueda and L. Wang, *Polym. Chem.*, 2014, **5**, 6121–6141.

- 229 D. Y. Chen and M. A. Hickner, *Phys. Chem. Chem. Phys.*, 2013, **15**, 11299–11305.
- 230 S. Kim, T. B. Tighe, B. Schwenzer, J. L. Yan, J. L. Zhang, J. Liu, Z. G. Yang and M. A. Hickner, *J. Appl. Electrochem.*, 2011, **41**, 1201–1213.
- 231 Q. Dai, F. Xing, X. Liu, D. Shi, C. Deng, Z. Zhao and X. Li, *Energy Environ. Sci.*, 2022, **15**, 1594–1600.
- 232 N. Agmon, *Chem. Phys. Lett.*, 1995, **244**, 456–462.
- 233 N. Agmon, H. J. Bakker, R. K. Campen, R. H. Henchman, P. Pohl, S. Roke, M. Thamer and A. Hassanali, *Chem. Rev.*, 2016, **116**, 7642–7672.
- 234 L. M. Ding, X. P. Song, L. H. Wang, Z. P. Zhao and G. H. He, *Electrochim. Acta*, 2018, **292**, 10–19.
- 235 K. Geng, Y. Li, Y. Xing, L. H. Wang and N. W. Li, *J. Membr. Sci.*, 2019, **586**, 231–239.
- 236 K. Geng, H. Y. Tang, Y. Li, L. Liu and N. W. Li, *J. Membr. Sci.*, 2020, **607**, 118177.
- 237 D. J. Chen, H. N. Qi, T. T. Sun, C. Yan, Y. Y. He, C. Z. Kang, Z. Z. Yuan and X. F. Li, *J. Membr. Sci.*, 2019, **586**, 202–210.
- 238 L. Hu, L. Gao, X. M. Yan, W. J. Zheng, Y. Dai, C. Hao, X. M. Wu and G. H. He, *J. Mater. Chem. A*, 2019, **7**, 15137–15144.
- 239 S. S. Peng, X. M. Wu, X. M. Yan, L. Gao, Y. Z. Zhu, D. S. Zhang, J. Li, Q. Wang and G. H. He, *J. Mater. Chem. A*, 2018, **6**, 3895–3905.
- 240 Y. Li, H. M. Zhang, H. Z. Zhang, J. Y. Cao, W. X. Xu and X. F. Li, *J. Membr. Sci.*, 2014, **454**, 478–487.
- 241 W. J. Lu, L. Qiao, Q. Dai, H. M. Zhang and X. F. Li, *J. Mater. Chem. A*, 2018, **6**, 15569–15576.
- 242 W. J. Lu, H. M. Zhang and X. F. Li, *J. Membr. Sci.*, 2019, **577**, 212–218.
- 243 G. F. Zhang, J. X. Jiang, Q. H. Zhang, X. L. Zhan and F. Q. Chen, *AICHE J.*, 2017, **63**, 739–750.
- 244 N. B. McKeown and P. M. Budd, *Chem. Soc. Rev.*, 2006, **35**, 675–683.
- 245 C. C. Ye, R. Tan, A. Q. Wang, J. Chen, B. C. Gandara, C. Breakwell, A. Alvarez-Fernandez, Z. Y. Fan, J. Q. Weng, C. G. Bezzu, S. Guldin, N. P. Brandon, A. R. Kucernak, K. E. Jelfs, N. B. McKeown and Q. L. Song, *Angew. Chem., Int. Ed.*, 2022, **61**, e202207580.
- 246 C. C. Ye, A. Q. Wang, C. Breakwell, R. Tan, C. G. Bezzu, E. Hunter-Sellars, D. R. Williams, N. P. Brandon, P. A. A. Klusener, A. R. Kucernak, K. E. Jelfs, N. B. McKeown and Q. L. Song, *Nat. Commun.*, 2022, **13**, 3184.
- 247 P. P. Zuo, Y. Y. Li, A. Q. Wang, R. Tan, Y. H. Liu, X. Liang, F. M. Sheng, G. G. Tang, L. Ge, L. Wu, Q. L. Song, N. B. McKeown, Z. J. Yang and T. W. Xu, *Angew. Chem., Int. Ed.*, 2020, **59**, 9564–9573.
- 248 O. Gronwald, N. Uematsu, N. Hosh, M. Ikeda and J. Yamaki, *J. Fluorine Chem.*, 2008, **129**, 535–540.
- 249 P. Gorgojo, S. Karan, H. C. Wong, M. F. Jimenez-Solomon, J. T. Cabral and A. G. Livingston, *Adv. Funct. Mater.*, 2014, **24**, 4729–4737.
- 250 Y. H. Chen, Y. G. Li, Y. Q. Li, J. Guo, S. H. Li and S. B. Zhang, *ACS Appl. Mater. Interfaces*, 2021, **13**, 59329–59340.
- 251 J. Hu, M. Yue, H. M. Zhang, Z. Z. Yuan and X. F. Li, *Angew. Chem., Int. Ed.*, 2020, **59**, 6715–6719.
- 252 C. Ding, H. M. Zhang, X. F. Li, T. Liu and F. Xing, *J. Phys. Chem. Lett.*, 2013, **4**, 1281–1294.
- 253 S. Zhong and M. Skyllas-Kazacos, *J. Power Sources*, 1992, **39**, 1–9.
- 254 M. Rychcik and M. Skyllas-Kazacos, *J. Power Sources*, 1987, **19**, 45–54.
- 255 Z. X. He, A. Q. Su, C. Gao, Z. Zhou, C. Y. Pan and S. Q. Liu, *Ionics*, 2013, **19**, 1021–1026.
- 256 I. Mayrhuber, C. R. Dennison, V. Kalra and E. C. Kumbur, *J. Power Sources*, 2014, **260**, 251–258.
- 257 D. S. Aaron, Q. Liu, Z. Tang, G. M. Grim, A. B. Papandrew, A. Turhan, T. A. Zawodzinski and M. M. Mench, *J. Power Sources*, 2012, **206**, 450–453.
- 258 Z. He, Z. Chen, W. Meng, Y. Jiang, G. Cheng, L. Dai and L. Wang, *J. Energy Chem.*, 2016, **25**, 720–725.
- 259 B. Sun and M. Skyllas-Kazacos, *Electrochim. Acta*, 1992, **37**, 2459–2465.
- 260 B. Sun and M. Sykllaskazacos, *Electrochim. Acta*, 1992, **37**, 1253–1260.
- 261 W. Zhang, J. Xi, Z. Li, H. Zhou, L. Liu, Z. Wu and X. Qiu, *Electrochim. Acta*, 2013, **89**, 429–435.
- 262 H. Liu, L. Yang, Q. Xu and C. Yan, *RSC Adv.*, 2014, **4**, 55666–55670.
- 263 J.-Z. Chen, W.-Y. Liao, W.-Y. Hsieh, C.-C. Hsu and Y.-S. Chen, *J. Power Sources*, 2015, **274**, 894–898.
- 264 D. Dixon, D. J. Babu, J. Langner, M. Bruns, L. Pfaffmann, A. Bhaskar, J. J. Schneider, F. Scheiba and H. Ehrenberg, *J. Power Sources*, 2016, **332**, 240–248.
- 265 K. J. Kim, Y.-J. Kim, J.-H. Kim and M.-S. Park, *Mater. Chem. Phys.*, 2011, **131**, 547–553.
- 266 Z. He, Y. Jiang, W. Meng, F. Jiang, H. Zhou, Y. Li, J. Zhu, L. Wang and L. Dai, *Appl. Surf. Sci.*, 2017, **423**, 111–118.
- 267 C. Gao, N. Wang, S. Peng, S. Liu, Y. Lei, X. Liang, S. Zeng and H. Zi, *Electrochim. Acta*, 2013, **88**, 193–202.
- 268 X. Wu, H. Xu, P. Xu, Y. Shen, L. Lu, J. Shi, J. Fu and H. Zhao, *J. Power Sources*, 2014, **263**, 104–109.
- 269 X. Wu, H. Xu, Y. Shen, P. Xu, L. Lu, J. Fu and H. Zhao, *Electrochim. Acta*, 2014, **138**, 264–269.
- 270 T. Liu, X. F. Li, H. M. Zhang and J. Z. Chen, *J. Energy Chem.*, 2018, **27**, 1292–1303.
- 271 A. Di Blasi, O. Di Blasi, N. Briguglio, A. S. Aricò, D. Sebastián, M. J. Lázaro, G. Monforte and V. Antonucci, *J. Power Sources*, 2013, **227**, 15–23.
- 272 J. Ryu, M. Park and J. Cho, *J. Electrochem. Soc.*, 2016, **163**, A5144.
- 273 C. Li, B. Xie, J. Chen, J. He and Z. He, *RSC Adv.*, 2017, **7**, 13184–13190.
- 274 M. E. Lee, H.-J. Jin and Y. S. Yun, *RSC Adv.*, 2017, **7**, 43227–43232.
- 275 C. Flox, J. Rubio-García, M. Skoumal, T. Andreu and J. R. Morante, *Carbon*, 2013, **60**, 280–288.
- 276 J. Jin, X. Fu, Q. Liu, Y. Liu, Z. Wei, K. Niu and J. Zhang, *ACS Nano*, 2013, **7**, 4764–4773.

- 277 Y. Shao, X. Wang, M. Engelhard, C. Wang, S. Dai, J. Liu, Z. Yang and Y. Lin, *J. Power Sources*, 2010, **195**, 4375–4379.
- 278 W. H. Wang and X. D. Wang, *Electrochim. Acta*, 2007, **52**, 6755–6762.
- 279 Z. González, C. Botas, C. Blanco, R. Santamaría, M. Granda, P. Álvarez and R. Menéndez, *J. Power Sources*, 2013, **241**, 349–354.
- 280 Z. González, C. Botas, C. Blanco, R. Santamaría, M. Granda, P. Álvarez and R. Menéndez, *Nano Energy*, 2013, **2**, 1322–1328.
- 281 L. Wei, T. S. Zhao, G. Zhao, L. An and L. Zeng, *Appl. Energy*, 2016, **176**, 74–79.
- 282 Z. He, L. Liu, C. Gao, Z. Zhou, X. Liang, Y. Lei, Z. He and S. Liu, *RSC Adv.*, 2013, **3**, 19774–19777.
- 283 M. Steimecke, S. Rümmler, N.-F. Schuhmacher, T. Lindenberg, M. Hartmann and M. Bron, *Electroanalysis*, 2017, **29**, 1056–1061.
- 284 M. H. Moghim, R. Eqra, M. Babaiee, M. Zarei-Jelyani and M. M. Loghavi, *J. Electroanal. Chem.*, 2017, **789**, 67–75.
- 285 M. Park, Y. J. Jung, J. Kim, H. I. Lee and J. Cho, *Nano Lett.*, 2013, **13**, 4833–4839.
- 286 M. Maharjan, A. Bhattacharai, M. Ulaganathan, N. Wai, M. O. Oo, J. Y. Wang and T. M. Lim, *J. Power Sources*, 2017, **362**, 50–56.
- 287 M. Ulaganathan, A. Jain, V. Aravindan, S. Jayaraman, W. C. Ling, T. M. Lim, M. P. Srinivasan, Q. Y. Yan and S. Madhavi, *J. Power Sources*, 2015, **274**, 846–850.
- 288 M. C. Wu, R. H. Zhang, K. Liu, J. Sun, K. Y. Chan and T. S. Zhao, *J. Power Sources*, 2019, **442**, 227255.
- 289 T. A. Zhang, Y. Zhu, Y. R. Lv, Q. Yu, S. Yao, W. J. Zhu and Z. X. He, *Ionics*, 2021, **27**, 4771–4781.
- 290 R. Wang, Y. S. Li, H. Y. Liu, Y. L. He and M. S. Hao, *J. Mater. Chem. A*, 2021, **9**, 2345–2356.
- 291 C. Minke, U. Kunz and T. Turek, *J. Power Sources*, 2017, **342**, 116–124.
- 292 L. Cao, M. Skyllas-Kazacos and D. W. Wang, *Adv. Sustainable Syst.*, 2018, **2**, 1800031.
- 293 W. Li and S. Jin, *Acc. Chem. Res.*, 2020, **53**, 2611–2621.
- 294 P. Lu, P. Leung, H. Su, W. Yang and Q. Xu, *Appl. Energy*, 2021, **282**, 116210.
- 295 E. Sanchez-Diez, E. Ventosa, M. Guarneri, A. Trovo, C. Flox, R. Marcilla, F. Soavi, P. Mazur, E. Aranzabe and R. Ferret, *J. Power Sources*, 2021, **481**, 228804.
- 296 S. C. Liao, X. Zong, B. Seger, T. Pedersen, T. T. Yao, C. M. Ding, J. Y. Shi, J. Chen and C. Li, *Nat. Commun.*, 2016, **7**, 11474.
- 297 K. Wedege, J. Azevedo, A. Khataee, A. Bentien and A. Mendes, *Angew. Chem., Int. Ed. Engl.*, 2016, **55**, 7142–7147.
- 298 K. Wedege, D. Bae, E. Drazevic, A. Mendes, P. C. K. Vesborg and A. Bentien, *RSC Adv.*, 2018, **8**, 6331–6340.
- 299 S. C. Liao, J. Y. Shi, C. M. Ding, M. Y. Liu, F. Q. Xiong, N. Wang, J. Chen and C. Li, *J. Energy Chem.*, 2018, **27**, 278–282.
- 300 Y. Liu, Y. Li, P. Zuo, Q. Chen, G. Tang, P. Sun, Z. Yang and T. Xu, *ChemSusChem*, 2020, 2245–2249, DOI: [10.1002/cscs.202000381](https://doi.org/10.1002/cscs.202000381).
- 301 N. F. Yan, G. R. Li and X. P. Gao, *J. Mater. Chem. A*, 2013, **1**, 7012.
- 302 P. Liu, Y. L. Cao, G. R. Li, X. P. Gao, X. P. Ai and H. X. Yang, *ChemSusChem*, 2013, **6**, 802–806.
- 303 N. F. Yan, G. R. Li and X. P. Gao, *J. Electrochem. Soc.*, 2014, **161**, A736–A741.
- 304 M. Yu, W. D. McCulloch, D. R. Beauchamp, Z. Huang, X. Ren and Y. Wu, *J. Am. Chem. Soc.*, 2015, **137**, 8332–8335.
- 305 W. D. McCulloch, M. Yu and Y. Wu, *ACS Energy Lett.*, 2016, **1**, 578–582.
- 306 J. Azevedo, T. Seipp, J. Burfeind, C. Sousa, A. Bentien, J. P. Araujo and A. Mendes, *Nano Energy*, 2016, **22**, 396–405.
- 307 J. R. McKone, F. J. DiSalvo and H. D. Abruna, *J. Mater. Chem. A*, 2017, **5**, 5362–5372.
- 308 Q. M. Cheng, W. Q. Fan, Y. M. He, P. Y. Ma, S. Vanka, S. Z. Fan, Z. T. Mi and D. W. Wang, *Adv. Mater.*, 2017, **29**, 1700312.
- 309 Y. Zhou, S. Zhang, Y. Ding, L. Zhang, C. Zhang, X. Zhang, Y. Zhao and G. Yu, *Adv. Mater.*, 2018, **30**, e1802294.
- 310 B. K. Durant, Y. She, P. Wang, T. Kraus and B. A. Parkinson, *J. Electrochem. Soc.*, 2018, **166**, H3001–H3008.
- 311 W. Li, H.-C. Fu, L. Li, M. Cabán-Acevedo, J.-H. He and S. Jin, *Angew. Chem.*, 2016, **128**, 13298–13302.
- 312 Z. Yuan, H. Zhang and X. Li, *Chem. Commun.*, 2018, **54**, 7570–7588.
- 313 W. Li, E. Kerr, M. A. Goulet, H. C. Fu, Y. Zhao, Y. Yang, A. Veyssal, J. H. He, R. G. Gordon, M. J. Aziz and S. Jin, *Adv. Energy Mater.*, 2019, **9**, 1900918.
- 314 F. Urbain, S. Murcia-Lopez, N. Nembhard, J. Vazquez-Galvan, C. Flox, V. Smirnov, K. Welter, T. Andreu, F. Finger and J. R. Morante, *J. Phys. D: Appl. Phys.*, 2019, **52**, 044001.
- 315 W. J. Li, J. H. Zheng, B. Hu, H. C. Fu, M. W. Hu, A. Veyssal, Y. Z. Zhao, J. H. He, T. L. Liu, A. Ho-Baillie and S. Jin, *Nat. Mater.*, 2020, **19**, 1326–1331.
- 316 S. Murcia-Lopez, M. Chakraborty, N. M. Carretero, C. Flox, J. R. Morante and T. Andreu, *Sustainable Energy Fuels*, 2020, **4**, 1135–1142.
- 317 H. C. Fu, W. Li, Y. Yang, C. H. Lin, A. Veyssal, J. H. He and S. Jin, *Nat. Commun.*, 2021, **12**, 156.
- 318 M. Duduta, B. Ho, V. C. Wood, P. Limthongkul, V. E. Brunini, W. C. Carter and Y.-M. Chiang, *Adv. Energy Mater.*, 2011, **1**, 511–516.
- 319 F. Y. Fan, W. H. Woodford, Z. Li, N. Baram, K. C. Smith, A. Helal, G. H. McKinley, W. C. Carter and Y. M. Chiang, *Nano Lett.*, 2014, **14**, 2210–2218.
- 320 E. Ventosa, D. Buchholz, S. Klink, C. Flox, L. G. Chagas, C. Vaalma, W. Schuhmann, S. Passerini and J. R. Morante, *Chem. Commun.*, 2015, **51**, 7298–7301.
- 321 W. Yan, C. Wang, J. Tian, G. Zhu, L. Ma, Y. Wang, R. Chen, Y. Hu, L. Wang, T. Chen, J. Ma and Z. Jin, *Nat. Commun.*, 2019, **10**, 2513.
- 322 Z. Li, K. C. Smith, Y. J. Dong, N. Baram, F. Y. Fan, J. Xie, P. Limthongkul, W. C. Carter and Y. M. Chiang, *Phys. Chem. Chem. Phys.*, 2013, **15**, 15833–15839.

- 323 E. Ventosa, O. Amedu and W. Schuhman, *ACS Appl. Energy Mater.*, 2018, **1**, 5158–5162.
- 324 J. Wei, P. B. Zhang, Y. Z. Liu, J. C. Liang, Y. R. Xia, A. Y. Tao, K. Q. Zhang, Z. X. Tie and Z. Jin, *ACS Energy Lett.*, 2022, **7**, 862–870.
- 325 Y. Yang, G. Y. Zheng and Y. Cui, *Energy Environ. Sci.*, 2013, **6**, 1552–1558.
- 326 L. Madec, M. Youssry, M. Cerbelaud, P. Soudan, D. Guyomard and B. Lestriez, *ChemPlusChem*, 2015, **80**, 396–401.
- 327 T. S. Wei, F. Y. Fan, A. Helal, K. C. Smith, G. H. McKinley, Y. M. Chiang and J. A. Lewis, *Adv. Energy Mater.*, 2015, **5**, 1500535.
- 328 Y. Y. Wu, D. F. Cao, X. J. Bai, H. Liu, H. Y. Hao, J. Xing, J. J. Dong and L. B. Liao, *ChemElectroChem*, 2020, **7**, 3623–3631.
- 329 K. C. Smith, Y. M. Chiang and W. C. Carter, *J. Electrochem. Soc.*, 2014, **161**, A486–A496.
- 330 S. Hamelet, T. Tzedakis, J. B. Leriche, S. Sailler, D. Larcher, P. L. Taberna, P. Simon and J. M. Tarascona, *J. Electrochem. Soc.*, 2012, **159**, A1360–A1367.
- 331 Z. X. Qi and G. M. Koenig, *J. Vac. Sci. Technol., B*, 2017, **35**, 040801.
- 332 E. Ventosa, *Curr. Opin. Chem. Eng.*, 2022, **37**, 100834.
- 333 Q. Wang, S. M. Zakeeruddin, D. Wang, I. Exnar and M. Gratzel, *Angew. Chem., Int. Ed. Engl.*, 2006, **45**, 8197–8200.
- 334 Q. Z. Huang, H. Li, M. Gratzel and Q. Wang, *Phys. Chem. Chem. Phys.*, 2013, **15**, 1793–1797.
- 335 J. R. Jennings, Q. Z. Huang and Q. Wang, *J. Phys. Chem. C*, 2015, **119**, 17522–17528.
- 336 C. Jia, F. Pan, Y. G. Zhu, Q. Huang, L. Lu and Q. Wang, *Sci. Adv.*, 2015, **1**, e150088.
- 337 J. Ye, L. Xia, C. Wu, M. Ding, C. Jia and Q. Wang, *J. Phys. D: Appl. Phys.*, 2019, **52**, 443001.
- 338 T. Paez, A. Martinez-Cuezva, J. Palma and E. Ventosa, *ACS Appl. Energy Mater.*, 2019, **2**, 8328–8336.
- 339 X. Li, *Joule*, 2019, **3**, 2066–2067.
- 340 Y. G. Zhu, Y. Du, C. Jia, M. Zhou, L. Fan, X. Wang and Q. Wang, *J. Am. Chem. Soc.*, 2017, **139**, 6286–6289.
- 341 E. Zanzola, C. R. Dennison, A. Battistel, P. Peljo, H. Vrubel, V. Amstutz and H. H. Girault, *Electrochim. Acta*, 2017, **235**, 664–671.
- 342 J. Z. Yu, L. Fan, R. T. Yan, M. Y. Zhou and Q. Wang, *ACS Energy Lett.*, 2018, **3**, 2314–2320.
- 343 E. Zanzola, S. Gentil, G. Gschwend, D. Reynard, E. Smirnov, C. R. Dennison, H. H. Girault and P. Peljo, *Electrochim. Acta*, 2019, **321**, 134704.
- 344 R. Yan and Q. Wang, *Adv. Mater.*, 2018, **30**, e1802406.
- 345 S. Gentil, D. Reynard and H. H. Girault, *Curr. Opin. Electrochem.*, 2020, **21**, 7–13.
- 346 M. Y. Zhou, Q. Z. Huang, T. N. P. Truong, J. Ghilane, Y. G. Zhu, C. K. Jia, R. T. Yan, L. Fan, H. Randriamahazaka and Q. Wang, *Chem*, 2017, **3**, 1036–1049.
- 347 E. C. Self, F. M. Delnick, R. E. Ruther, S. Allu and J. Nanda, *ACS Energy Lett.*, 2019, **4**, 2593–2600.
- 348 Y. Kim, A. Varzi, A. Mariani, G. T. Kim, Y. Kim and S. Passerini, *Adv. Energy Mater.*, 2021, **11**, 2102061.
- 349 Y. Zhou, G. Cong, H. Chen, N.-C. Lai and Y.-C. Lu, *ACS Energy Lett.*, 2020, **5**, 1732–1740.
- 350 M. L. Meyerson, S. G. Rosenberg and L. J. Small, *ACS Appl. Energy Mater.*, 2022, **5**, 4202–4211.
- 351 P. Navalpotro, J. Palma, M. Anderson and R. Marcilla, *Angew. Chem., Int. Ed. Engl.*, 2017, **56**, 12460–12465.
- 352 P. Navalpotro, J. Palma, M. Anderson and R. Marcilla, *Angew. Chem.*, 2017, **129**, 12634–12639.
- 353 P. Navalpotro, N. Sierra, C. Trujillo, I. Montes, J. Palma and R. Marcilla, *ACS Appl. Mater. Interfaces*, 2018, **10**, 41246–41256.
- 354 M. O. Bamgbopa, Y. Shao-Horn, R. Hashaikeh and S. Almheiri, *Electrochim. Acta*, 2018, **267**, 41–50.
- 355 S. Hou, L. Chen, X. Fan, X. Fan, X. Ji, B. Wang, C. Cui, J. Chen, C. Yang, W. Wang, C. Li and C. Wang, *Nat. Commun.*, 2022, **13**, 1281.
- 356 P. Navalpotro, C. M. S. S. Neves, J. Palma, M. G. Freire, J. A. P. Coutinho and R. Marcilla, *Adv. Sci.*, 2018, **5**, 1800576.
- 357 P. Navalpotro, C. Trujillo, I. Montes, C. M. S. S. Neves, J. Palma, M. G. Freire, J. A. P. Coutinho and R. Marcilla, *Energy Storage Mater.*, 2020, **26**, 400–407.
- 358 A. F. Molina-Osorio, A. Gamero-Quijano, P. Peljo and M. D. Scanlon, *Curr. Opin. Electrochem.*, 2020, **21**, 100–108.